Continuum Modelling and Analysis of a Class of One and Two Dimensional Elastic Metamaterials with Local Rotation

by

Antonio Schiavone

A thesis submitted in partial fulfillment of the requirements for the degree

of

Master of Science

Department of Mechanical Engineering

University of Alberta

Abstract

The group of materials classified as "metamaterials" have accrued great interest in the scientific community as of late for their potential to revolutionize several multidisciplinary applications. Metamaterials are defined as synthetic/man-made materials which have been engineered to possess a number of desired unusual, and often counterintuitive properties which do not occur naturally. The inception of metamaterials into engineering science was in the field of optics when a material exhibiting an apparent negative index of refraction was designed. Following this, so-called "optical metamaterials" were researched and implemented in the field of electromagnetic cloaking, as well as utilized to design superlenses with sub-wavelength resolution. Recently a subclass of metamaterials known as elastic metamaterials has become of great interest to engineering scientists. This is a large class of materials which exhibits one or more unusual elastic properties such as negative Poisson's ratio, negative effective stiffness, negative shear modulus, and many more. Elastic metamaterials have potential for application in the fields of impact mitigation, shock absorption, wave attenuation, energy shielding, and wave guiding, to name a few.

In order to facilitate the use of this new class of materials, it is of paramount importance to possess the ability to predict the behaviour of these materials under specific, as well as sufficiently general loading conditions. There are two main ways to do this; the first of which is experimentally, through trial and error, and the second is analytically by creating a mathematical model

capable of predicting both material behaviour and effective properties under specific loading conditions. This thesis will focus on the latter method.

There exists a myriad of mathematical techniques for material characterization, some of these techniques include homogenization methods, unit cell design, discrete modelling, and continuum modelling. This thesis will focus on the continuum modelling of a class of elastic metamaterials with local rotational effects. Typically, when local effects need to be considered in the framework of a continuum, the micropolar continuum model is the first avenue people explore. In this thesis it will be shown that this model is incapable of capturing all of the salient features present in both one, and two dimensional elastic metamaterials belonging to this class.

In this thesis a series of continuum models are developed with increasing generality. First, in the third chapter, a micropolar-type continuum model is derived for a specific one-dimensional double negative metamaterial capable of exhibiting negative mass and/or negative modulus under certain loading frequencies when subject to harmonic loads. This is done by analyzing a discrete structure, obtaining the equations of motion, and then making a continuous approximation to bring the discrete model to the continuum framework. This model is used to evaluate the transient response of a specific one-dimensional semi-infinite elastic metamaterial when subject to an axial impact. In the fourth chapter, a higher order continuum model is developed in a manner very similar to the methodology presented in the third chapter, but with a higher order derivative of the rotational variable θ. This

model is then generalized to an entire class of materials, even though it is developed using a representative discrete structure. Harmonic wave propagation is then studied in the same one-dimensional elastic metamaterial that was modelled in the third chapter using this new model, leading to the determination of the stop and passing bands, as well as the determination of the dispersion relation governing the wave propagation. This new model is then compared to both the model in the third chapter, as well as the discrete model to determine the range of suitability. In the fifth chapter a model for a two-dimensional class of elastic metamaterials with local rotation is developed in a slightly different way than in the previous two chapters. In this chapter a set of constitutive laws for the relevant class of materials is proposed, and then a representative discrete metamaterial is modelled, and approximated as a continuum to prove suitability of the model. This model is then used to study harmonic longitudinal (P) and transverse (S) wave propagation in the material, which covers all cases of general two-dimensional wave propagation. The stop and passing bands, as well as the dispersion relations were determined for both wave propagation schemes and the effect of local rotation was analyzed. The sixth chapter uses the model developed in the fifth chapter to study surface wave propagation in a new continuum with local rotation. The dispersion relation of the surface wave is obtained, as well as expressions for the decay parameters, b_1 and b_2. The behaviour of the general dispersion relation, as well as some simplified cases are investigated. It is found that surface waves propagating through a continuum with

local rotation are dispersive even when the local rotational effects are small compared to the translational ones. Two parameters governing general wave propagation, f and g are identified. The parameter f controls the height of frequency peaks in the dispersion relation, and the parameter g controls the location of the second peak. Furthermore, for values of $f \approx 1$ or greater, surface waves are found to propagate with wavespeeds significantly lower than c_R, a phenomenon unique to this continuum. Finally, the motion of the particles residing on the surface of this continuum is determined to be elliptical when subject to surface wave propagation, similar to classical Rayleigh wave propagation.

Preface

Chapter 1 of this thesis has been previously published as:
A. Schiavone, Z.W. Li, X.D. Wang. 2021, Modeling and Analysis of the Transient Behaviour of an Elastic Metamaterial as a Generalized Cosserat Continuum, ASME J. Appl. Mechs. Vol. 88. Issue 9. 091003.

Chapter 2 of this thesis has, in part, previously been published as:
A. Schiavone, X.D. Wang. 2021, Continuous Modelling of a Class of Periodic Elastic Metamaterials with Local Rotation, Z. Angew. Math. Phys., Vol. 72, Article Number 29,

Chapter 4 of this thesis has been accepted for publication in Mathematics and Mechanics of Solids as: A. Schiavone, X.D. Wang. 2022. Dispersive Surface Waves Propagating Through a Continuous Elastic Medium with Local Rotation, Accepted July 29th, 2022

Chapter 3 of this thesis has been submitted as: A. Schiavone, X.D. Wang. 2022. Development and Analysis of a New Continuum Model of a Class of Elastic Metamaterials with Local Rotational Effects, submitted April 5th, 2022

Parts of this thesis will be presented as: A. Schiavone, Z. Li, X.D. Wang, Continuum Modelling and Analysis of Periodic Elastic Metamaterials with Local Rotation, Proceedings of the ASME 2022 International Mechanical Engineering Congress and Exposition, Colombus, Ohio, October 2022

Dedication

I would like to express the highest degree of gratitude to my supervisor Professor Xiaodong Wang for his constant mentorship and guidance over the entirety of my Master's degree, and for enabling my tremendous growth as a researcher and academic. I have greatly enjoyed working closely with you over these past two years, and I sincerely hope that we can continue to do research together in the future. I would like to thank Ethan Proctor, Justin Adames, Dustin Adams, Michael Huang, Henry Huang, Eric Papagiannis, Lara Percival and many more of my closest friends for their love and friendship.

Most importantly I would like to thank my family. I would like to thank my mother for always loving and supporting me through every stage of my life, even when I so vehemently refused to be supported.

Saving the most important for last, I would like to thank my father; for not only teaching me as my instructor in both graduate and undergraduate courses, but also for all the advice (appreciated or not!) throughout the years, especially in the years following my undergrad. Above all else, you have imparted upon me your love and passion for mathematical research, and ignited that same passion within me, the flames of which I will carry for the rest of my life and career. The body of work that follows this dedication is in large part due to your influence as an educator and a mentor, so it only seems right to dedicate it to you.

"It is not knowledge, but the act of learning, not possession but the act of getting there, which grants the greatest enjoyment." - Carl Freidrich Gauss

Acknowledgements

The work contained within this thesis was made possible by funding from the Natural Sciences and Engineering Research Council (NSERC), Alberta Innovates (AI), NOVA Chemicals Corporation, and a generous scholarship funded by distinguished Professor, Dr. William Youdelis.

Contents

List of Tables

List of Figures

1. Background and Introduction

The term "metamaterial" refers to a synthetic material with unusual, and often counterintuitive material properties. The inception of metamaterials into material science, and subsequently engineering science, began in the field of optics in the form of a material engineered to possess a negative index of refraction [1]. These optical metamaterials have pioneered advancements in the field of electromagnetic cloaking [2, 3], as well as greatly aided in the design of superlenses with sub-wavelength resolution [4, 5]. Typically metamaterials are organized into sub-classes based on the nature of the atypical material properties they possess. For example, optical metamaterials are termed as such due to the inherent unusual optical properties they possess, such as a negative index of refraction (as previously mentioned). Elastic metamaterials are a relatively new classification of metamaterials which, as the name would suggest, possess unusual bulk elastic properties. Some of these aforementioned unusual bulk elastic properties can include a negative Poisson's ratio [6], negative dynamic stiffness [7, 8, 9], negative dynamic mass density [10], negative shear modulus [11, 12], rarefaction waves, or many of these properties [13, 14, 15, 16]. These elastic metamaterials, if successfully utilized, may enable advancements in applications such as wave attenuation [17, 18, 19], energy shielding [20, 21], impact mitigation/shock absorption [22, 23, 24], and sound absorption [26, 27, 28]. For this reason, this sub-group of elastic metamaterials has accrued a large amount of attention in the scientific community. Tantamount to the creation of these materials is the ability to optimize their performance in specific applications. Optimization of material properties is typically achieved in one of two ways; experimentally, through trial and error, or analytically, through a process known as mathematical modelling, where physical principles are used along with the requisite mathematics to create a series of mathematical expressions which, when solved provide a plethora of information about material behaviour under arbitrary loading, as well as general material properties agnostic of loading conditions. This thesis will focus on the latter method. The difficulty with mathematical modelling arises in the balancing of mathematical complexity with real world accuracy. If one makes the model too simple, although easy to solve and highly tractable, the information that one can glean out of such a model is useless, as it does not represent reality closely enough. On the other hand, if the model is made to be too complicated, although highly accurate, it may become intractable, rendering it useless as well. The art of mathematical

modelling lies in building the precise amount of mathematical complexity into the model which provides the greatest amount of accuracy while retaining the highest degree of tractability possible.
Recently, there has been a large body of research dedicated to the modelling of elastic metamaterials due to their immense potential for application. One of the most common ways researchers attempt to model these materials is through the use of a mathematical procedure known as a homogenization technique. Homogenization techniques seek to obtain the macro-scale bulk elastic properties agnostic of material micro-structure. This method, originating in the mechanics and analysis of composite materials [29], has recently been extended to three-dimensional elastic metamaterials with very complicated microstructure and achieved moderate levels of success [30, 31]. The most common technique used for metamaterial modelling is known colloquially as unit cell design. This is a technique in which a metamaterial's substructure is decomposed to a point where it can be described as the periodic repetition of a fundamental element called a unit cell. This is extremely useful to simplify the task of modelling a three-dimensional metamaterial [6] as well as for designing new metamaterials to exhibit specific properties, as it grants microlevel control over the structure with much less complication, and through the avenue of numerical methods the desired quantities can then be approximately obtained. A downside to this method is that the material must be periodic, and discrete methods are frequently required to extract desired quantities. The third method commonly used in modelling a material is known as continuum modelling, a method which draws from a branch of mathematical models called continuum field theories. Continuum field theories were developed throughout hundreds of years, by scientific and mathematical giants such as Augustin-Louis Cauchy and Leonhard Euler, however the man that should be regarded as the "godfather" of modern continuum mechanics is Clifford Ambrose Truesdell III who, along with Walter Noll published some of the most seminal pieces of work unifying continuum theories [32]. This model/methodology describes a material as a continuum body, meaning each point in the material is in 1-1 correspondence with a mathematical point in Euclidean 3-space ($\mathbb{R}^3$). In this model each mathematical point has no size and has ascribed to it a motion, which uniquely maps a point in the reference configuration to a point in the current configuration. From this motion, displacement, velocity and acceleration fields can be determined, as well as important engineering properties such as stress, strain, yield stress, and deflection to name a few. This theory is typically

linearized for small deformations to yield some of the most common and frequently used equations in engineering science. The major shortfall of classical continuum theory is the absence of mathematical structure with which to quantify a material's intrinsic granular structure. This is particularly important when describing materials like sand, or when modelling nanomaterials and fibre reinforced composites. When these more complicated materials need to be modelled, a more sophisticated mathematical model must be used. The solution to this problem in the 1900s was a set of field theories known as microcontinuum field theories. The main point of dissonance between these theories and traditional continuum theories is the constituent parts of a continuum body. In microcontinuum field theories, a continuum consists of smaller deformable bodies termed microcontinuua, and one can describe the behaviour of a point within a material by the superposition of the motion of the relevant microcontinuum's centroid, and the motion of the particular material point with respect to that centroid. This is more conceptually difficult to understand, and much more mathematically difficult to analyze than rational continuum mechanics, often requiring a more holistic knowledge of abstract mathematical topics. However, this framework allows material scientists to capture material behaviour outside of that captured by classical continuum theory. The most widely used of these theories is known as micropolar continuum mechanics, a simplification of the general micromorphic continuum theory in which each microcontinuum is considered rigid (i.e. can only undergo rigid translation and rotation). This is an excellent model for biomaterials such as bone or blood, as well as composite materials such as fibre reinforced composites. The micropolar continuum model recently been used to create a continuum model of a fibrous elastic metamaterial with a cubic lattice substructure [33], which was subsequently extended [34] to study acoustic metamaterials with local rotation. Micropolar continuum mechanics has also been used to moderate success to describe metamaterials with chiral geometry [35]. However, the micropolar continuum framework has been proven inadequate in capturing all salient features of metamaterials with strong coupling between the local rotational motion, and macro translational motion [36, 37]. This necessitates the development of new continuum models for these materials.

1.1. Statement of Purpose

In this thesis several new continuum models will be developed capable of modelling these materials in both one, and two dimensions. The next chap-

ter will be dedicated to preliminaries and notation, so that in the discussion to follow, everything is clear. In the third chapter a simple model capable of capturing transient behaviour of a particular one-dimensional elastic metamaterial possessing strong local rotational-macro translational coupling effects is developed, and used to analyze an impact problem. The fourth chapter will introduce a more refined one-dimensional model with higher order derivatives of the local rotational variable θ, for not only one specific metamaterial, but the entire class of materials. This model will also be used to investigate harmonic wave propagation in the specific metamaterial investigated in the previous chapter. A comparison will be made between this model, the model from the previous chapter, and a corresponding discrete model in order to determine the range of suitability. The fifth chapter will generalize the model developed in the fourth chapter to two dimensions, and study general 2-D wave propagation using this new model. The sixth chapter will focus on surface wave propagation in a new two-dimensional continuum given by the model developed in Chapter 5. The seventh and final chapter is dedicated to conclusions and suggestions for future work.

2. Preliminaries and Notation

2.1. Symbols

Symbol	Meaning
$\mathbf{1}$	The "shifter"
∂	Partial derivative
$\wedge$	Vector Product
$\mathbf{C}$	The classical elasticity tensor
C_{KL}	Components of the Right Cauchy-Green deformation tensor
f_i	The components of the body force vector
E_{KL}	The components of the Lagrange strain tensor
i^v	The volumetric moment of inertia in micropolar theory
m_i	The components of the body moment vector
P_{KL}	A new strain tensor for microcontinuum theory
R_k	The components of the rotation vector in classical continuum mechanics
S	Arclength in the reference configuration
s	Arclength in the current configuration
t	Time
u_i	The components of the displacement vector
$\mathbf{u}$	The displacement vector
x	One of the in-plane Cartesian directions
$\mathbf{x}$	The position vector of a point in the current configuration or the motion
$\mathbf{x}'$	The position vector of a point in the current configuration in microcontinuum theory
$\mathbf{X}$	The position vector of a point in the reference configuration
α	A micropolar material constant or the grade of a micromorphic continuum
β	A micropolar material constant
$\boldsymbol{\chi}$	The motion or micromotion
δ_{ij}	The components of the Kroneker Delta
Δ	The Laplacian operator
$\boldsymbol{\varepsilon}$	The linear small strain tensor
ϵ_{ijk}	The components of the Levi-Civita permutation tensor
Γ_{KLM}	Components of a candidate for a strain measure in micropolar theory
γ	A micropolar material constant
κ	A micropolar material constant
λ	A micropolar material constant
μ	A micropolar material constant
ψ_{KL}	Components of a candidate for a strain measure in micropolar theory

ϕ_{LK}	The components of a microdisplacement tensor in referential coordinates
ϕ_{lk}	The components of a microdisplacement tensor in eulerian coordinates
ϕ_M	The components of the axial vector of ϕ_{LK}
ρ^v	The volumetric mass density in micropolar theory
$\boldsymbol{\sigma}$	The Cauchy stress tensor
τ_{ji}	The components of the twist tensor
θ_j	The components of the microrotation vector
$\boldsymbol{\Xi}$	Vectors relating to the deformable directors in the reference configuration
$\boldsymbol{\xi}$	Vectors relating to the deformable directors in the current configuration

Before beginning with the main content of this thesis, it is important to establish notation that will be pervasive throughout, as well as some ideas and requisite background knowledge. In this section some important notation will be presented, as well as a general overview of 3-D micropolar theory, including the reduction of this theory to one and two dimensions, as well the formal linearization process.

2.2. Notation

This thesis will make use of the Einstein summation notation, where a repeated index represents summation over that index. (For example, $x_{ii} = x_{11} + x_{22} + x_{33}$ for $i = 1, 2, 3$) Standard Newtonian notation will be employed, wherein a first order time derivative is denoted by a dot on top of a variable, with multiple dots signifying higher order derivatives. Partial derivatives will be represented using the following notation $(...)_{,i} = \frac{\partial(...)}{\partial x_i}$. Tensor and vector variables will be distinguished by the bolding of the variable, whereas scalar variables will not be bolded. (Ex. a is a scalar and $\mathbf{a}$ is a vector or tensor) The vector product of two vectors will be represented using the following symbol: $\wedge$. The Levi-Civita permutation tensor will be denoted by ϵ_{ijk}, and the Kroneker delta by δ_{ij}. The "shifter" will be denoted by $\mathbf{1}$. In this thesis, "big O" notation will be used to represent higher order terms and their growth rates.

2.3. An Overview of Continuum Theories

Since the inception of rational continuum mechanics into the field of engineering science in the mid 1900s, describing materials with significant granular structure has been a challenge. Rational continuum mechanics is a theory based on the idea that a material is itself a continuous medium consisting of an infinity of infinitely small mathematical points, leaving no room for the idea of microstructure. A visual representation of the typical continuum framework is shown in Fig. 1. The motion, $\boldsymbol{\chi}$, as shown in Fig. 1 is defined by:

$$\boldsymbol{\chi}(\mathbf{X}, t) = \mathbf{x}(\mathbf{X}, t) \tag{1}$$

where t is time, $\mathbf{X}$ is a material point in the reference configuration and $\mathbf{x}$ is a point in the current configuration. This definition of the motion gives rise to a constitutive law using the framework of linear continuum mechanics for classical solids [38]:

$$\boldsymbol{\sigma} = \mathbf{C}\boldsymbol{\varepsilon} \tag{2}$$

where $\mathbf{C}$ is the classical elasticity tensor, $\boldsymbol{\sigma}$ is the Cauchy stress tensor, and $\boldsymbol{\varepsilon}$ is the linear small strain tensor. This constitutive law is known colloquially as Hooke's law in most undergraduate engineering programs, and is one of the most widely used and famous equations in all of solid mechanics. This relation is very accurate when describing isotropic elastic simple solid materials, however when significant microstructure is involved, it loses some accuracy.

In order to account for the effect of microstructure, microcontinuum field theories were developed. The basic idea of these theories is to have two motions, one which describes the motion of a microcontinuum's centroid, and one which describes the motion of a point within the microcontinuum with respect to its centroid. This framework is shown visually in Fig. 2, where the relationship between the current and reference configuration is given by the following equation:

$$\mathbf{x}' = \mathbf{x}(\mathbf{X}, t) + \boldsymbol{\chi}(\mathbf{X}, t)\boldsymbol{\Xi} \tag{3}$$

where $\mathbf{x}$ is the motion from classical continuum mechanics, $\boldsymbol{\chi}$ is now what is defined as the micromotion, $\boldsymbol{\Xi}$ are the vectors representing the deformable directors, t is time, $\mathbf{X}$ is a material point in the reference configuration and $\mathbf{x}'$ is a point in the current configuration. The most commonly used and theoretically developed microcontinuum scheme is known as micropolar continuum mechanics. This is a modelling framework in which every continuum body consists of smaller rigid subcontinuua, capable only of rigid translations and rotations.

2.4. Micropolar Continuum Mechanics

The governing equations of a traditional finite strain micropolar continuum are presented below in component form [40]:

$$\sigma_{ji,j} + f_i^v = \rho^v \ddot{u}_i \tag{4}$$

$$\epsilon_{ijk}\sigma_{jk} + \chi_{ji,j} + m_i^v = i^v \ddot{\theta}_i \tag{5}$$

where $i, j = 1, 2, 3$, σ_{ji} are the Cartesian components of the Cauchy stress tensor, f_i^v are the components of the body force per unit volume, rho^v is the density per unit volume, u_i is the displacement vector in the standard Cartesian basis, e_i, χ_{ji} are the Cartesian components of the couple stress tensor, m_i^v are the components of the body moment per unit volume, i^v is

the inertia per unit volume, and θ_i is the microrotation in the same Cartesian basis. These equations can be related to displacements and microrotations using the following constitutive relations [40]:

$$(\mu + \kappa)\varepsilon_{ij} + (\mu - \kappa)\varepsilon_{ji} + \lambda\varepsilon_{kk}\delta_{ij} \tag{6}$$

$$\chi_{ij} = (\gamma + \beta)\tau_{ij} + (\gamma - \beta)\tau_{ji} + \alpha\tau_{kk}\delta_{ij} \tag{7}$$

where $\gamma, \alpha, \mu, \lambda, \kappa$ and β are micropolar material constants, ε_{ij} are the Cartesian components of the strain tensor, and τ_{ij} are the Cartesian components of the twist tensor. It is important to note here that contrary to popular belief, and many erroneous statements in literature, μ and λ are not the Lamé constants from classical linear elasticity, although they use the same symbols [40].

Up until this point, the theory presented on micropolar continuum mechanics has been finite deformation theory, which is not the theory we wish to use. The passage from finite deformation to linear theory is challenging, but proceeds in a similar way as traditional continuum mechanics. Presented below, without derivation, are the linear expressions for the strain tensor and the twist tensor [39]:

$$\varepsilon_{ij} = u_{j,i} - \epsilon_{ijk}\theta_k = \varepsilon_{ij}^{traditional} - \epsilon_{ijk}(R_k - \theta_k) \tag{8}$$

$$\tau_{ij} = \theta_{j,i} \tag{9}$$

Plugging in Eqs. 8 and 9 into Eqs. 6 and 7, we obtain the following alternative form of the constitutive laws:

$$(\mu + \kappa)(u_{j,i} - \epsilon_{ijk}\theta_k) + (\mu - \kappa)(u_{i,j} - \epsilon_{jik}\theta_k) + \lambda(u_{k,k} - \epsilon_{kkm}\theta_m)\delta_{ij} \tag{10}$$

$$\chi_{ij} = (\gamma + \beta)\theta_{j,i} + (\gamma - \beta)\theta_{i,j} + \alpha\theta_{k,k}\delta_{ij} \tag{11}$$

Plugging in Eqs. 10 and 11 into Eqs. 4 and 5, the following equations of motion can be obtained for a small displacement micropolar continuum:

$$(\mu + \kappa)\, u_{i,jj} + (\mu - \kappa + \lambda)\, u_{j,ji} - 2\kappa\epsilon_{ijk}\theta_{j,k} + f_i^v = \rho^v \ddot{u}_i, \tag{12}$$

$$(\gamma + \beta)\, \theta_{i,jj} - 4\kappa\theta_i + (\gamma - \beta + \alpha)\, \theta_{j,ji} - 2\kappa\epsilon_{ijk}u_{j,k} + m_i^v = i^v \ddot{\theta}_i, \tag{13}$$

2.5. Micropolar Equations in Lower Dimensions

In this thesis of particular interest are not the small strain 3-D micropolar equations, but the one and two dimensional reductions of these equations. In this subsection the one and two dimensional reductions will be derived from the small strain 3-D micropolar equations to reference later in the thesis.

2.5.1. Micropolar Equations in Two Dimensions

In order to reduce the 3-D micropolar equations to two dimensions, simply set $i, j = 1, 2$, and assume that only θ_3 exists (rotation about the z-axis). With these assumptions, replacing 1 with x and 2 with y, as well as dropping the subscript on the θ (as only one direction of θ is being considered) the following equations can be obtained:

$$(2\mu + \lambda)u_{,xx} + (\mu + \kappa)u_{,yy} + (\mu - \kappa + \lambda)v_{,yx} + 2\kappa\theta_{,y} = \rho^v \ddot{u} \tag{14}$$

$$(2\mu + \lambda)v_{,yy} + (\mu + \kappa)v_{,xx} + (\mu - \kappa + \lambda)u_{,xy} - 2\kappa\theta_{,x} = \rho^v \ddot{v} \tag{15}$$

$$(\gamma + \beta)\Delta\theta - 4\kappa\theta + 2\kappa(v_{,x} - u_{,y}) = i^v \ddot{\theta} \tag{16}$$

where u is the displacement in the x-direction, and v is the displacement in the y-direction.

2.5.2. Micropolar Equations in One Dimension

To reduce the equations to 1-D, only one displacement u_1 is considered, and the field is assumed uniform in the 2 and 3-directions. i.e. $u_2 = u_3 = 0$, $\partial/\partial x_2 = \partial/\partial x_3 = 0$ Applying these conditions to Eq. 12 yields the following simplifications for $i = 1$:

$$u_{i,jj} = u_{j,ji} = u_{1,11} \qquad \epsilon_{ijk}\theta_{j,k} = 0 \tag{17}$$

Without body forces, Eq. 12 becomes

$$(2\mu + \lambda)u_{1,11} = \rho^v \ddot{u}_1 \tag{18}$$

Furthermore, we consider rotation in all 3 directions with the following restrictions given:

$$\theta_{3,jj} = \theta_{3,11} \qquad \theta_{j,j3} = 0 \qquad \epsilon_{3jk}u_{j,k} = 0 \tag{19}$$

Without body moment, Eq. 13 can be rewritten as:

$$(\gamma + \beta)\theta_{3,11} - 4\kappa\theta_3 = i^v\ddot{\theta}_3 \tag{20}$$

Replacing 1 with x and dropping the subscript on θ as well as u, the following equations are obtained:

$$(2\mu + \lambda)u_{,xx} = \rho^v\ddot{u} \tag{21}$$

$$(\gamma + \beta)\theta_{,xx} - 4\kappa\theta = i^v\ddot{\theta} \tag{22}$$

2.6. Decoupling of Micropolar Equations in Linear Theory

A keen eye would notice in the previous section that the displacement, u and the microrotation, θ, become entirely decoupled in the 1-D micropolar model. This will be quite significant in the coming chapters, as it eludes to the fact that the micropolar model is unable to capture the salient features that arise due to rotational-translational coupling in one dimension, and possibly higher dimensions. In this subsection the decoupling of the microrotation from the translation in linear theory will be demonstrated by following the transformation from finite deformation micropolar theory to linear micropolar theory.

The decoupling of the displacement and microrotation is mainly due to the linearizing approximations for the strain tensors in micropolar theory. In order to better understand why this happens, it is helpful to derive the strain measures from first principles. Consider a material point in a general microcontinuua of grade α in both the reference and current configurations. Considering only homogeneous deformations, the relationship between a material point and a point in the current configuration is the following for a micromorphic continuum of grade α:

$$\mathbf{x}^{(\alpha)} = \mathbf{x}(\mathbf{X}, t) + \boldsymbol{\chi}_K(\mathbf{X}, t)\boldsymbol{\Xi}_K^{(\alpha)} \tag{23}$$

$$\mathbf{X}^{(\alpha)} = \mathbf{X}(\mathbf{x}, t) + \boldsymbol{\chi}_k^{-1}(\mathbf{x}, t)\xi_k^{(\alpha)} \tag{24}$$

This furnishes the following arclength expression when we set $\alpha = 1$ (a micromorphic continuum of grade 1) in the current configuration:

$$\begin{aligned}(ds)^2 = d\mathbf{x}\cdot d\mathbf{x} = (\mathbf{x}_{,K}\cdot\mathbf{x}_{,L} + 2(\mathbf{x}_{,K}\cdot\boldsymbol{\chi}_{.L} + \mathbf{x}_{,L}\cdot\boldsymbol{\chi}_{M,K})\Xi_M + \\ \boldsymbol{\chi}_{M,K}\cdot\boldsymbol{\chi}_{N,L}\Xi_M\Xi_N)dX_K dX_L + 2(\mathbf{x}_{,L}\cdot\boldsymbol{\chi}_L + \boldsymbol{\chi}_L\cdot\boldsymbol{\chi}_{M,K}\Xi_M)dX_K d\Xi_L + \\ \boldsymbol{\chi}_K\cdot\boldsymbol{\chi}_L d\Xi_K d\Xi_L\end{aligned} \tag{25}$$

Similarly, the arclength in the reference configuration can be defined as:

$$(dS)^2 = dX_K dX_K + 2dX_K d\Xi_K + d\Xi_K d\Xi_K \tag{26}$$

From Eq. 25, 3 good candidates for strain measures can be defined:

$$C_{KL} = x_{k,K} x_{k,L} \qquad \psi_{KL} = x_{k,K}\chi_{kL} \qquad \Gamma_{KLM} = x_{k,K}\chi_{kL,M} \tag{27}$$

Writing Eq. 25 in terms of the expressions given in Eq. 27 the following form of the arclength is obtained:

$$\begin{aligned}(ds)^2 = (C_{KL} + 2\Gamma_{KML}\Xi_M + \chi_{kM,K}\chi_{kN,L}\Xi_M\Xi_N)dX_K dX_L + \\ 2(\psi + \chi_{kL}\chi_{kM,K}\Xi_M)dX_K d\Xi_L + \chi_{kK}\chi_{kL}d\Xi_K d\Xi_L\end{aligned} \tag{28}$$

From Eq. 28 it can be seen that if:

$$C_{KL} = \psi_{KL} = \delta_{KL} \qquad \Gamma_{KLM} = 0 \tag{29}$$

then Eq. 28 is exactly equal to Eq. 26 and there is no change in arclength between the reference and current configurations, and hence no strain. This ratifies the assertion that the expressions given in Eq. 27 are indeed good candidates for strain measures. Defining a displacement vector $\mathbf{u}$:

$$\mathbf{u} = \mathbf{x} - \mathbf{1X} \tag{30}$$

this expression has the following component representations in referential and spatial coordinates respectively:

$$U_K = x_k\delta_{kK} - X_K \tag{31}$$

$$u_K = x_k - X_K\delta_{Kk}. \tag{32}$$

Equations 31 and 32 can be differentiated and rearranged to obtain the following expressions:

$$x_{k,K} = (\delta_{LK} + U_{L,K})\delta_{kL} \tag{33}$$

$$X_{K,k} = (\delta_{lk} - u_{l,k})\delta_{Kl}. \tag{34}$$

Introducing microdisplacement tensors ϕ_{LK} and ϕ_{lk}:

$$\chi_{kK} = (\delta_{LK} + \phi_{LK})\delta_{kL} \tag{35}$$

$$\chi_{kK}^{-1} = (\delta_{lk} - \phi_{lk})\delta_{Kl} \tag{36}$$

and utilizing the expressions given in Eqs. 30-36 the potential strain measures defined in Eq. 27 can be written in the following way:

$$C_{KL} = \delta_{KL} + U_{K,L} + U_{L,K} + U_{M,K}U_{M,L} \tag{37}$$

$$\psi_{KL} = \delta_{KL} + \phi_{KL} + U_{L,K} + U_{M,K}\phi_{ML} \tag{38}$$

$$\Gamma_{KLM} = \phi_{KL,M} + U_{N,K}\phi_{NL,M} \tag{39}$$

When linearizing these strain tensors for small deformation gradients, we neglect the higher order terms. When linearized, the following expressions are obtained:

$$C_{KL} = \delta_{KL} + U_{K,L} + U_{L,K} + O(x^2) \tag{40}$$

$$\psi_{KL} = \delta_{KL} + \phi_{KL} + U_{L,K} + O(x^2) \tag{41}$$

$$\Gamma_{KLM} = \phi_{KL,M} + O(x^2) \tag{42}$$

These are the linear forms of the potential strain measures introduced in Eq. 27, when the higher order terms are neglected. As is clear in Eq. 29, only one of these measures of strain is actually zero when there is no u or ϕ, making them unsuitable to be strain tensors. To fix this, we introduce two alternative strain tensors which will be zero under these conditions, one of which is the classical Lagrange strain tensor:

$$E_{KL} = \frac{1}{2}(C_{KL} - \delta_{KL}) = \frac{1}{2}(U_{K,L} + U_{L,K}) \tag{43}$$

$$P_{KL} = \psi_{KL} - \delta_{KL} = \phi_{KL} + U_{L,K} \tag{44}$$

$$\Gamma_{KLM} = \phi_{KL,M} \tag{45}$$

These equations hold for general micromorphic media subject to small deformation gradients. In order to specialize to micropolar theory we must impose the restriction that only rigid motions of the microcontinuua are permitted. This will be imposed by restricting the form of the microdisplacement tensor, specifically we will require that the microdisplacement tensor is skew-symmetric. This means it can be represented by an axial vector in the following way:

$$\phi_{KL} = -\epsilon_{KLM}\phi_M \tag{46}$$

where ϕ_M is the axial vector of ϕ_{KL}. An interesting parallel can be drawn here between the microdisplacement tensor $\boldsymbol{\phi}$ and the macro-rotation tensor $\mathbf{R}$ from classical continuum mechanics. In classical theory, $\mathbf{R}$ is also skew symmetric, admitting the representation:

$$R_{KL} = \frac{1}{2}(U_{K,L} - U_{L,K}) = -\epsilon_{KLM} R_M \tag{47}$$

where R_M is the axial vector of R_{KL}. With Eqs. 46 and 47 in mind, the following expressions for strain tensors from Eqs. 43-45 can be rewritten for micropolar theory specifically as:

$$E_{KL} = \frac{1}{2}(C_{KL} - \delta_{KL}) = \frac{1}{2}(U_{K,L} + U_{L,K}) \tag{48}$$

$$P_{KL} = E_{KL} + \epsilon_{KLM}(R_M - \phi_M) \tag{49}$$

$$\Gamma_{KLM} == -\epsilon_{KLB}\phi_{B,M} \tag{50}$$

From these equations, it is clear that for one-dimensional theory ($K = L = 1$) we have no coupling between rotational and translational motion; i.e. rotational and translational motion completely decouple in one dimension. This is a drawback of linear micropolar theory, and a point the new models developed in this thesis will improve upon.

2.7. Figures

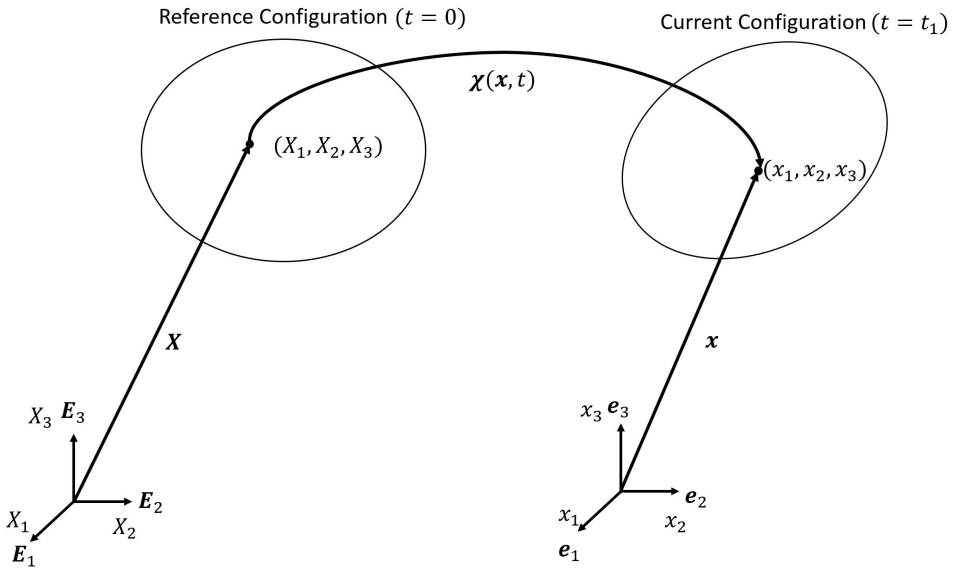

Figure 1: The framework used to describe two states in classical continuum mechanics

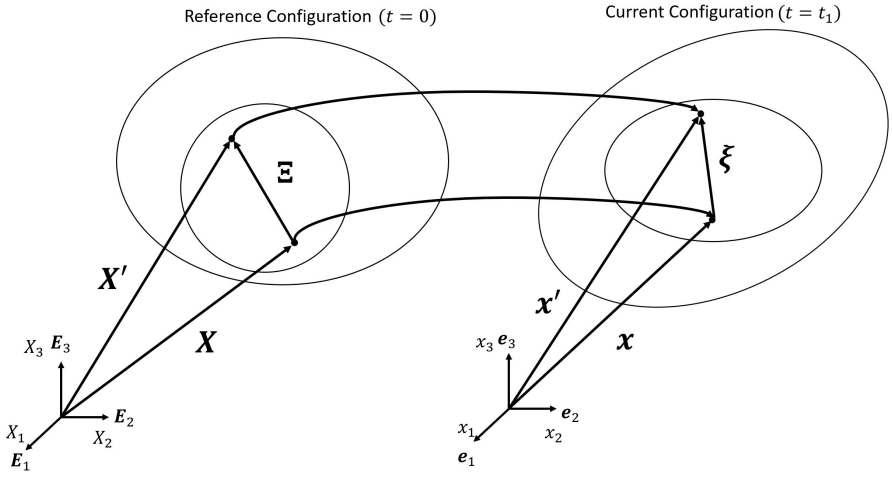

Figure 2: The framework used to describe two states in classical microcontinuum theories

3. A One-Dimensional Model of the Transient Behaviour of a Particular Double Negative Elastic Metamaterial

3.1. Symbols

Symbol	Meaning
∂	Partial derivative
$H(t)$	The Heaviside step function
π	A mathematical constant approximately equal to 3.14159...
e	Euler's number
A	Area
$A(p)$	A coefficient in the general solution of the transient problem
$B(p)$	A term in the general solution of the transient problem
c	Wavespeed
E	Effective elastic modulus of the metamaterial and bar
F_i	The force exerted by the side spring attached to disk i
F_i^0	The force exerted by the central spring attached to disk i
F_0	The impact force
f_0	The magnitude of the impact force
I	The moment of inertia of a disk or the metamaterial system
i^v	The volumetric moment of inertia in micropolar continuum mechanics
i	The imaginary unit
k	The spring constant of a side spring
k_0	The spring constant of a central spring
$\overline{k}$	Spring constant per unit length and per unit cross sectional area of the bar
L	The length of one unit cell
m	The mass of one disk or the metamaterial system
p	Angular frequency (rad/s)
R	The radius associated with a side spring
T	Normalized time
t	Time
t_0	Initial time
U	The frequency domain displacement field
u_i	The displacement of disk i
$\ddot{u}_i$	The acceleration of disk i
u	The pointwise displacement field
$\ddot{u}$	The acceleration field
$\overline{u}$	The normalized displacement field

X	The normalized position coordinate
x	One of the planar Cartesian directions
α	The ratio between the stiffness of a central spring and a side spring
β	A micropolar material constant and a parameter in the frequency domain
Δ	An integral term in the analytic solution to the transient problem
ε	The strain field
$\overline{\varepsilon}$	The normalized strain field
ε_0	The initial strain field
κ	A micropolar material constant
λ	A micropolar material constant or a material constant in the bar model
$\overline{\lambda}$	One of the governing parameters for the transient problem
μ	A micropolar material constant
ρ	The volumetric mass density of the metamaterial
ρ^v	The volumetric mass density in micropolar continuum mechanics
σ	The Cauchy stress field
σ_0	The initial Cauchy stress
θ_i	The local rotation of disk i
$\ddot{\theta}_i$	The second time derivative of the local rotation of disk i
θ	The pointwise local rotation field
$\ddot{\theta}$	The second time derivative of the local rotation field
ξ	The radius of gyration of a rigid disk

In this chapter a micropolar-type continuum model suitable for representing a double negative elastic metamaterial with strong coupling between local rotational motion and large scale macro translational motion capable of exhibiting negative effective mass and/or modulus when subject to certain harmonic loads is developed. The most successful models of such a material have been created using the framework of micropolar continuum mechanics. Although this modelling framework can provide a reasonable description of the behaviour of this material it will be shown in this chapter that when the micropolar field equations are reduced to one dimension, the model is unable to capture all of the salient features of this material. To create a new continuum model, a rather novel methodology will be used; instead of starting at a continuum model, and trying to apply the equations to a discrete structure, the model is generated from a discrete structure and then made continuous by a series of approximations. Classically, when continuum modelling is done, one typically starts from a mathematical structure, and attempts to fit physical structures within that framework. This unconventional method of continuum modelling will provide the opportunity for more salient features to be expressed in the model. After this conversion is done, it will be shown that the new continuum model should be classified as a micropolar-type continuum model due to inherent structural similarities, despite differences in the modelling methodologies. This is an important piece of work, as it connects physically viable structures to the somewhat nebulous field of micropolar continuum mechanics, as well as extends the revered theory to the more complicated materials we are currently moving towards.

3.2. Statement and Formulation of the Problem

In the development of elastic metamaterials, it has been demonstrated that periodic unit cells capable of exhibiting both translational and rotational resonance can generate desired single or double negative properties, i.e. negative effective mass and/or modulus [14, 15]. The local rotation present in each unit cell plays an important role in the generation of the aforementioned negative effective properties and can be viewed as an effect akin to the microrotation present in traditional micropolar continuum theory. In this chapter, a small strain micropolar-type model is developed from a discrete elastic metamaterial, and subsequently compared with the classical small strain micropolar model. The new model is then used to study the transient behaviour of the discrete metamaterial, and the range of suitability of the new continuum model is explored.

3.2.1. The Discrete Model of the Metamaterial

The metamaterial of interest is a metamaterial system consisting of unit cells which support both local translational and rotational deformation. This metamaterial can exhibit negative mass and/or negative modulus under certain loading frequencies when subjected to harmonic loads [14, 15] These properties indicate that this type of metamaterial has the potential to be used in dynamic loading applications, such as vibration isolation and wave attenuation. The discrete model of the metamaterial as a series of identical rigid disks and linear Hookean springs is shown in Fig. 3 and a unit cell of this metamaterial system is shown in Fig. 4.

The governing equations immediately follow from the kinetics of rigid disk i, as shown in Fig. 4,

$$F_{i+1} + F_{i+1}^0 - F_i - F_i^0 = m\ddot{u}_i, \tag{51}$$

$$R\left(F_{i+1} + F_i\right) = I\ddot{\theta}_i, \tag{52}$$

with the forces being defined as:

$$F_{i+1} = k\left(u_{i+1} - u_i - R\theta_{i+1} - R\theta_i\right) \tag{53}$$

$$F_i = k\left(u_i - u_{i-1} - R\theta_i - R\theta_{i-1}\right) \tag{54}$$

$$F_{i+1}^0 = k_0\left(u_{i+1} - u_i\right) \tag{55}$$

$$F_i^0 = k_0\left(u_i - u_{i-1}\right) \tag{56}$$

Here, F_i and F_{i+1} represent the force exerted by the side springs attached to the ith disk, F_i^0 and F_{i+1}^0 represent the force exerted by the central springs, u_i represents the linear displacement corresponding to the ith disk and θ_i is the rotational displacement of the ith disk, k_0 is the spring constant of the central springs, and k is the spring constant of the side springs, assumed equal in every unit cell. R, m and I represent the radius associated with the side spring, mass and moment of inertia of each identical disk, respectively.

Substituting Eqs. (53), (54), (55), and (56) into Eqs. (51) and (52), the following two coupled ordinary differential equations (ODEs) are obtained

$$\left(k + k_0\right)\left(u_{i+1} - 2u_i + u_{i-1}\right) - kR\left(\theta_{i+1} - \theta_{i-1}\right) = m\ddot{u}_i, \tag{57}$$

$$kR\left(u_{i+1} - u_{i-1}\right) - kR^2\left(\theta_{i+1} + 2\theta_i + \theta_{i-1}\right) = I\ddot{\theta}_i, \tag{58}$$

which govern the general dynamic response of the discrete metamaterial system.

3.2.2. First Order Continuum Approximation

The discrete metamaterial can be modelled using a continuum model when the length scale of the phenomena of interest is larger than the size of a unit cell. In order to convert this discrete model to a continuum model, the following approximations were used:

$$u_{i+1} - 2u_i + u_{i-1} = L^2 \frac{\left(\frac{u_{i+1} - u_i}{L} - \frac{u_i - u_{i-1}}{L}\right)}{L} \approx L^2 \frac{\partial^2 u}{\partial x^2} \tag{59}$$

$$u_{i+1} - u_{i-1} = L\left(\frac{u_{i+1} - u_i}{L} + \frac{u_i - u_{i-1}}{L}\right) \approx 2L\frac{\partial u}{\partial x} \tag{60}$$

$$\theta_{i+1} + 2\theta_i + \theta_{i-1} \approx 4\theta \tag{61}$$

$$\theta_{i+1} - \theta_{i-1} \approx 2L\frac{\partial \theta}{\partial x} \tag{62}$$

where L is the length of the unit cell. These approximations give rise to the following governing equations:

$$(k + k_0)\, L^2 \frac{\partial^2 u}{\partial x^2} - 2kRL\frac{\partial \theta}{\partial x} = m\ddot{u} \tag{63}$$

$$2kRL\frac{\partial u}{\partial x} - 4kR^2\theta = I\ddot{\theta} \tag{64}$$

Eqs. (63) and (64) represent a new elastic continuum containing local rotational displacement θ in addition to the linear displacement u. Generally speaking, this continuum can be described as a micropolar-type medium.

3.2.3. Comparison with the Classical Micropolar Model

When comparing Eqs. 63 and 64 to the one-dimensional micropolar equations developed in the preliminaries section, a simlitude becomes apparent between the aforementioned sets of equations. It should be noted that the one-dimensional micropolar equations are per unit volume, whereas Eqs. (63) and (64) are not. The constants can be related as follows:

$$2\mu + \lambda = \frac{(k + k_0)\, L}{A}, \quad \rho^v = \frac{m}{AL}, \quad \gamma + \beta = 0, \quad \kappa = \frac{kR^2}{AL}, \quad i^v = \frac{I}{AL}. \tag{65}$$

Clearly, since the coefficient of the θ_{xx} term is zero, this metamaterial represents a micropolar-type metamaterial possessing zero dynamic rotational stiffness. In addition to this, it can also be seen that the continuum model developed from the discrete model shows a strong coupling between the linear and rotational displacements and contains additional terms related to the local rotation in the unit cell. These terms make for a more accurate description of the rotational effects on metamaterial behaviour.

The main objective of the current chapter is to utilize the newly developed micropolar-type continuum model to represent the effects of the local rotational motion in the unit cells in order to accurately predict the behaviour of the metamterial. These local rotational effects dominate the behaviour of the metamaterial, which can be represented in the discrete model by setting the stiffness of the central springs to be much lower than that of the side springs. Therefore, in the following discussion it is assumed that the stiffness of the central springs are negligible ($k_0 \approx 0$). Eqs. (63) and (64) can be simplified into one partial differential equation (PDE) by first taking the partial derivative of Eq. (64) with respect to x and then subbing in the expression for $\partial\theta/\partial x$ obtained from Eq. (63) into Eq. (64). The governing equation of the metamaterial becomes:

$$kL\frac{\partial^2 u}{\partial x^2} - \frac{4kR^2}{IL}mu = \frac{m}{L}\ddot{u} \tag{66}$$

Where zero initial displacements and velocities have been assumed.

Defining the effective elastic modulus E and mass density ρ of the metamaterial as

$$E = \frac{kL}{A}, \quad \rho = \frac{m}{AL}, \tag{67}$$

with A being the cross-sectional area of the unit cell, Eq. (66) can be rewritten as:

$$E\frac{\partial^2 u}{\partial x^2} - \frac{4E}{L^2}\left(\frac{R}{\xi}\right)^2 u = \rho\ddot{u} \tag{68}$$

where u is the longitudinal displacement and ξ is the radius of gyration of the rigid disk of the unit cell.

3.3. Semi-Infinite Bar Model With an Elastic Spring Support

The dynamic response of an elastic bar with a continuous elastic spring support along the axial direction, as shown in Fig. 5, is governed by the

following equation of motion

$$E\frac{\partial^2 u}{\partial x^2} - \overline{k}u = \rho\ddot{u}, \tag{69}$$

where $\overline{k}$ is the spring constant per unit length and per unit cross section area of the bar, E is the elastic modulus, ρ is the mass density and u is the axial displacement of the bar. Upon comparison of Eqs. (69) and (68), a resounding similitude becomes apparent between the two equations, with the spring constant $\overline{k}$ being given by

$$\overline{k} = 4E\left(\frac{R}{\xi}\right)^2\left(\frac{1}{L^2}\right). \tag{70}$$

Interestingly, this means that the current metamaterial system will exhibit some of the same typical transient behaviour expected from an elastic bar with a continuous elastic support loaded.

3.3.1. Solution of the Semi-Infinite Bar Problem

Consider now the transient response of the metamaterial subjected to an impact at its boundary. A boundary force $F_0 = f_0 H(t)$ is applied to the left boundary ($x = 0$) of a semi-infinite metamaterial to simulate a compressive impact, where $H(t)$ is the Heaviside step function, and f_0 is the magnitude of the impact force. The boundary condition can be described in terms of stress as

$$\sigma\left(0,t\right) = -\sigma_0 H\left(t\right), \tag{71}$$

where $\sigma_0 = f_0/A$ is the magnitude of the stress at the left end, $x = 0$, of the bar.

Redefine Eq. (69) as

$$\frac{\partial^2 u}{\partial x^2} - \lambda u = \frac{1}{c^2}\ddot{u}, \tag{72}$$

where

$$c = \sqrt{\frac{E}{\rho}}, \quad \lambda = 4\left(\frac{R}{\xi}\right)^2\frac{1}{L^2}. \tag{73}$$

Applying Fourier transform defined by

$$U\left(x,p\right) = \frac{1}{2\pi}\int_{-\infty}^{\infty} u\left(x,t\right)e^{ipt}dt, \tag{74}$$

Eq. (72) can be transformed into the Fourier domain by imposing the condition that $u(x,t) = 0$ for all $t < 0$, to give the following equation:

$$\frac{\partial^2 U}{\partial x^2} + \frac{\beta^2}{c^2} U = 0, \tag{75}$$

where

$$\beta = \sqrt{p^2 - \lambda c^2}. \tag{76}$$

Eq. (75) has a general solution of the form:

$$U(x,p) = A(p)\, e^{i\frac{\beta}{c}x} + B(p)\, e^{-i\frac{\beta}{c}x}. \tag{77}$$

For the semi-infinite bar, it is required that the solution stays bounded as $x \to \infty$, which indicates that $B(p) = 0$, if $\mathrm{Im}(\beta) > 0$ is assumed in the general Fourier domain. The general solution of $u(x,t)$ can then be expressed as

$$u(x,t) = \int_{-\infty}^{\infty} A(p)\, e^{i\frac{\beta}{c}x} e^{-ipt} dp. \tag{78}$$

Applying the boundary condition

$$E\frac{\partial u}{\partial x}|_{x=0} = -\sigma_0 H(t) \tag{79}$$

to Eq. (78), $A(p)$ is found to be

$$A(p) = -\frac{\sigma_0 c}{2\pi E p \beta}. \tag{80}$$

This means that the transient displacement field in the metamaterial is

$$u(x,t) = -\int_{-\infty}^{\infty} \frac{\sigma_0 c}{2\pi E p \beta} e^{i\frac{\beta}{c}x} e^{-ipt} dp, \tag{81}$$

and the transient strain field is given by:

$$\varepsilon(x,t) = -\frac{i\sigma_0}{2\pi E} \int_{-\infty}^{\infty} \frac{1}{p} e^{i\frac{\beta}{c}x} e^{-ipt} dp. \tag{82}$$

The integration shown in Eq. (82), after a tedious bit of mathematical manipulation of the inverse Fourier transform, admits the following analytical

solution:

$$\varepsilon(x,t) = -\frac{\sigma_0}{E} H\left(t - \frac{x}{c}\right) + \frac{\sigma_0}{2\pi E}\Delta - \frac{\sigma_0}{2E}\left(e^{-\sqrt{\lambda}x} - 1\right), \tag{83}$$

where:

$$\begin{aligned}\Delta \equiv & 2\int_{\sqrt{\lambda}c}^{\infty} \frac{1}{p}\left[\sin\left(\frac{\sqrt{p^2-\lambda c^2}}{c}x - pt\right) - \sin\left(p\left(\frac{x}{c} - t\right)\right)\right] dp \\ & - 2\int_{\varepsilon}^{\sqrt{\lambda}c} \frac{1}{p}\left[e^{-\frac{\sqrt{\lambda c^2 - p^2}}{c}x}\sin(pt) + \sin\left(p\left(\frac{x}{c} - t\right)\right)\right] dp.\end{aligned} \tag{84}$$

This solution satisfies the original governing equations, the initial conditions, as well as the boundary conditions.

3.4. Numerical Results and Discussion

In this section, the dynamic behaviour of the metamaterial is simulated using the newly developed micropolar-type continuum model. The resulting wave propagation in response to the applied impact at the end of the metamaterial is studied to evaluate the accuracy of the new continuum model. This section was done in collaboration with Dr. Zhengwei Li, and is taken directly from our publication [36].

The following normalized parameters are used in the evaluation of the dynamic behaviour of the metamaterial,

$$\overline{u} = \frac{u}{ct_0}, \quad \overline{\varepsilon} = \frac{\varepsilon}{\varepsilon_0}, \quad \varepsilon_0 = \frac{\sigma_0}{E}, \quad T = \frac{t}{t_0}, \quad X = \frac{x}{t_0 c}, \tag{85}$$

where $\overline{u}$, $\overline{\varepsilon}$, T and X are the normalized displacement, strain, time and coordinate, respectively, with

$$c = \sqrt{\frac{E}{\rho}} = \frac{kL^2}{m}. \tag{86}$$

The equation of motion of the bar model, Eq. (72), can then be normalized as

$$\frac{\partial^2 \overline{u}}{\partial X^2} - \overline{\lambda}\overline{u} = \frac{\partial^2 \overline{u}}{\partial T^2}, \tag{87}$$

with

$$\overline{\lambda} = \lambda \left(ct_0\right)^2 = 4 \left(\frac{R}{\xi}\right)^2 \left(\frac{ct_0}{L}\right)^2 . \tag{88}$$

It should be mentioned that with the normalization, the elastically supported bar model is controlled by a single parameter $\overline{\lambda}$, which contains R/ξ and ct_0/L. But for the original discrete model, three parameters, R/ξ, R/L and ct_0/L, affect the behaviour of the metamaterial independently.

In the following discussion, the analytical solution of the continuum model given by Eqs. (83) and (84) is analyzed and compared with the solution of the discrete metamaterial model, Eqs. (57) and (58), and the finite element analysis of the semi-infinite elastically-supported bar model. The solution of the discrete model is obtained using the standard solver ODE45 in MATLAB and the details can be found in Appendix B. For the finite element analysis, COMSOL Multiphysics 5.5a is used with the bar being modelled in 2-D with a height-to-length ratio of 1/500 to ensure that the length will contain the range of wave propagation. The material used is aluminum with the density, Young's modulus and Poisson's ratio being 2700 kg/m^3, 70 GPa and 0.33, respectively. The spring foundations are applied on the upper and lower edges of the bar, and a compressive force pulse is applied at the left end of the bar. Free triangular elements in COMSOL are used to mesh the bar model and the convergence analysis has been conducted to ensure the accuracy of the numerical results. The strains along the middle line of the bar are then extracted for comparison.

3.5. Effects of Low-Stiffness Central Springs

As discussed in previously, the metamaterial studied can be modelled as a micropolar-type continuum. The rotational effects of the metamaterial system are primarily due to the local rotational motion of the disks, which is generated by the side springs in the metamaterial. In the following discussion, the effect of removing the low-stiffness central springs in the metamaterial will be evaluated.

Comparisons were made between the strain distributions corresponding to different stiffness ratios, $\alpha = k_0/k$, in response to the applied impact forces at the end of the metamaterial. $\alpha = 0$ indicates that the central springs are removed. The results for $\alpha = 0.00, 0.05, 0.10, 0.20$ are shown in Fig. 6 for the case where $\overline{\lambda} = 1.037$, $R/\xi = 0.05$, and $R/L = 0.1$ at the moment of $t/t_0 = 2.5$. The results indicate that even for $\alpha = 0.2$, the central spring

shows very limited effects on the waveform. For all values of α considered, the pulse shape of the normalized strain of the discrete model agrees well with those of the bar model. Following the compression pulse, it mainly endures tensile strains, which is especially evident for the bar model. The effect of α in this case becomes less significant. Similar phenomenon is observed in Fig. 7, which illustrates the case with $\overline{\lambda} = 1.037$, $R/\xi = 0.10$, and $R/L = 0.10$ at the moment of $t/t_0 = 2.5$. These results demonstrate that low stiffness central springs have limited effect on the dynamic behaviour of the micropolar-type continuum. In the following discussion, α is assumed to be zero, indicating that the central springs are removed.

3.6. Comparison Between Continuum and Discrete Models

To evaluate the accuracy of the continuum model in describing the dynamic behaviour of the discrete model, comparisons are made between the two models. Figs. 8 and 9 show the response of the metamaterial at the instant $t/t_0 = 2.5$ for $\overline{\lambda} = 1.037 \times 10^{-2}$, and $\overline{\lambda} = 1.037 \times 10^{-1}$, respectively. The comparison between the continuum model and the discrete model shows a very good agreement. The elastically supported bar is also simulated using FEA and compared to the analytical solution. A discrepancy in the predicted speeds of waves from analytical and numerical results is observed, which is consistent with the well-known fact that a thick bar (non-negligible transverse deformation) will exhibit a higher wavespeed than a thin bar (negligible transverse deformation).

3.7. Effect of Parameter $\overline{\lambda}$

$\overline{\lambda}$ dominates the continuum bar model and plays a critically important role in the dynamic response of the metamaterial system. To evaluate the effect of $\overline{\lambda}$, the strain distributions for $\overline{\lambda} = 1.037 \times 10^{-2}$, 0.5185, and 1.037 are shown in Figs. 10, 11, and 12, respectively, at $t_0/t = 2.5$ with $ct_0/L = 5.1$ and $R/L = 0.10$. As expected, for lower values of $\overline{\lambda}$, the results from the continuum model exhibit a higher degree of agreement with the discrete model. With the increase of $\overline{\lambda}$, the shape of the pulse propagating in the metamaterial predicted by the continuum model starts to diverge from that predicted by the discrete model. This comparison clearly shows the suitability and limitations of the continuum model in simulating the dynamic response of the metamaterial system. It is interesting to mention that even for relatively high $\overline{\lambda}$ values, the continuum model can still accurately predict the speed at which the pulse propagates in the metamaterial.

3.8. Effect of the Ratio R/ξ

The ratio R/ξ plays an important role in the dynamic response of the discrete model. Even for a given $\overline{\lambda}$, R/ξ will change the rotational behaviour of the discrete metamaterial system. Fig. 13 shows the strain distributions for $R/\xi = 0.200$, 0.100, 0.050 and 0.025 with $\overline{\lambda} = 0.5185$ and $R/L = 0.10$ at $t/t_0 = 2.5$. The corresponding results for $\overline{\lambda} = 1.037$ are shown in Fig. 14. For a fixed $\overline{\lambda}$, t_0 increases when R/ξ decreases and there are less data points shown in the results of the discrete model, as expected. The main trends of the normalized strain distribution remain similar for all of these cases, indicating consistency within the solution even with variation of this important ratio.

3.9. Effect of Impact Duration

An impact with a short duration will generate more significant variation in the wave field, and hence challenge the suitability of the continuum model in describing the discrete metamaterials. Figs. 15, 16 and 17 show the wave fields for different t_0 with $R/\xi = 0.05$ at the instant $t = 2.5t_0$, for the cases where ct_0/L equals to 3.2, 7.2 and 10.2, respectively. It is observed that a shorter impact duration makes the strain distribution from the discrete model less smooth. But the overall strain distribution remains in good agreement with that of the bar model for all different impact durations considered.

3.10. Effect of the Ratios R/L

The ratio R/L represents the vertical distance of the side springs to the centre of mass of the corresponding disk relative to the length of the unit cell. Figs. 18 and 19 show the strain distributions associated with different R/L values, $0.01, 0.05, 0.10$ and 0.50 for $\overline{\lambda} = 0.5185$ and 1.037, respectively, with $R/\xi = 0.10$ and $ct_0/L = 5.1$. The results show that the effect of R/L is limited to low values of R/L only ($R/L = 0.01$). For the cases considered, the normalized strain distributions for $R/L = 0.05$, 0.10 and 0.50 are almost identical.

3.11. Conclusions

- The traditional micropolar model is insufficient to describe this particular double negative elastic metamaterial with strong local rotational-translational coupling
- A new micropolar-type continuum model was generated from a discrete structure

- The new continuum model showed good agreement with both finite element analysis of an equivalent bar model, and numerical analysis of the original discrete model for values of the governing parameter $\lambda < 1$
- For larger values of λ although the waveform predicted by the continuum model diverges from that predicted by the finite element model, as well as the discrete model, the wave speed and pulse length remain accurately predicted by the continuum model

3.12. Figures

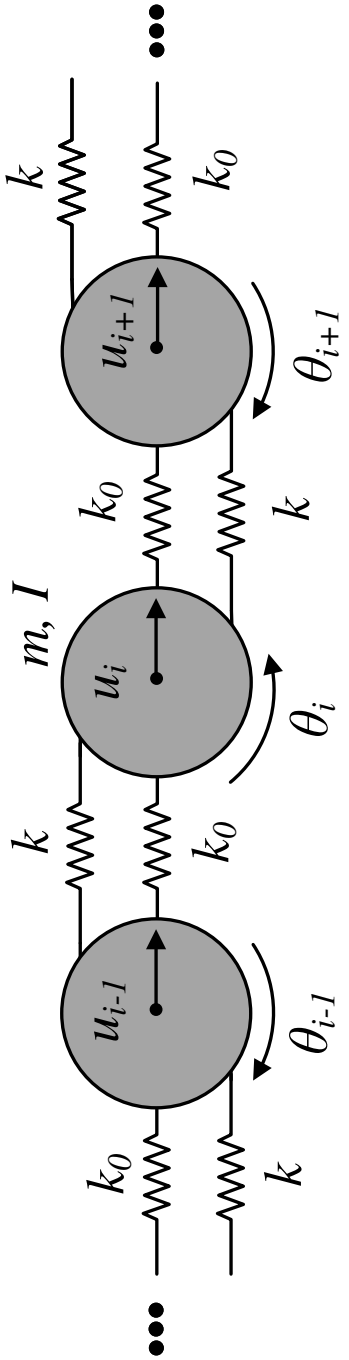

Figure 3: The discrete one-dimensional metamaterial model.

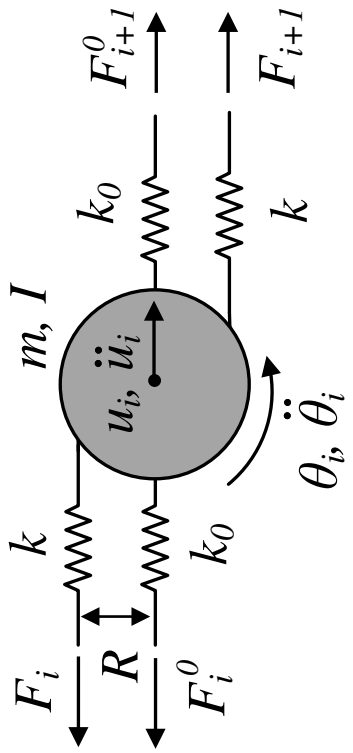

Figure 4: The i^{th} unit cell of the metamaterial.

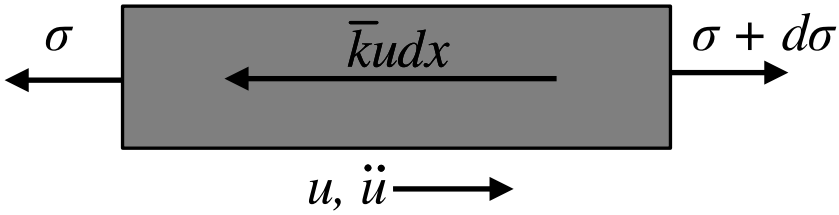

Figure 5: An infinitesimal element of an elastic bar with an axial spring support.

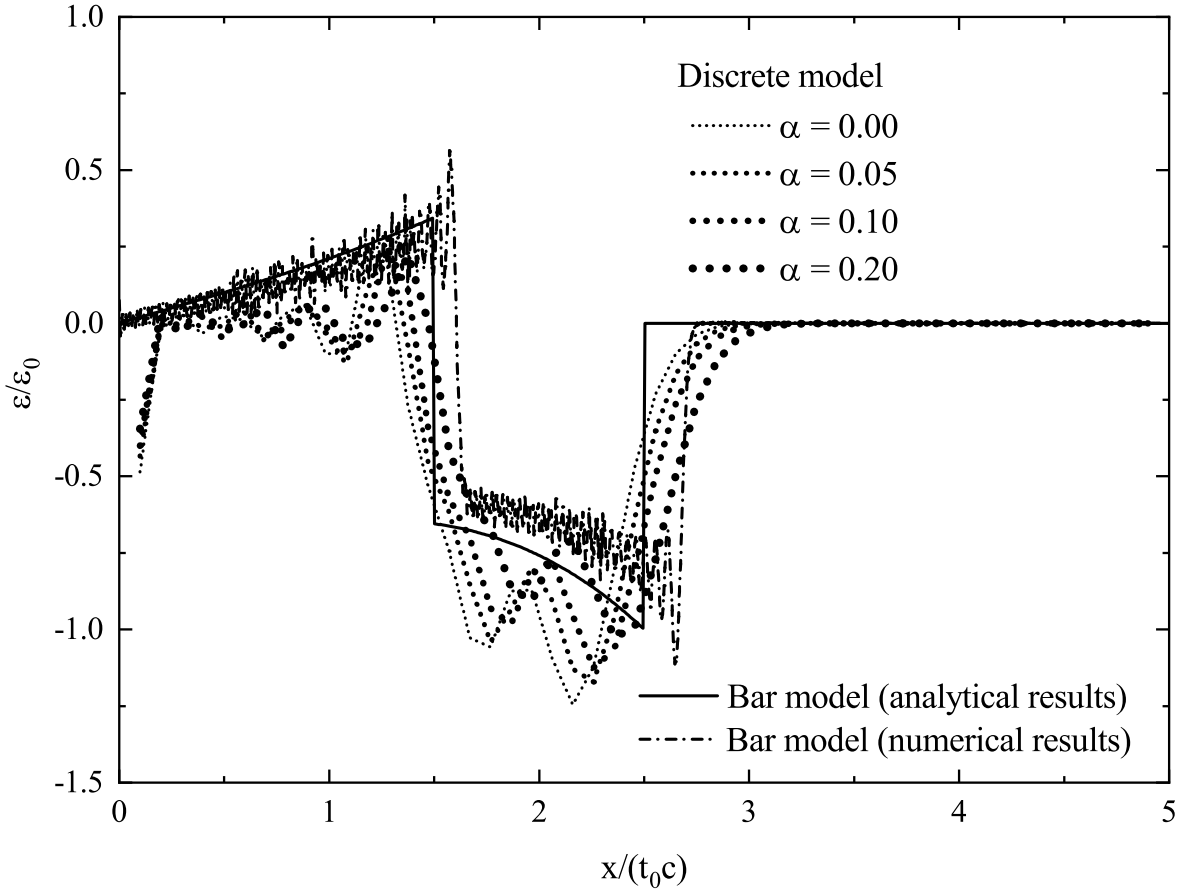

Figure 6: The normalized strain distribution for $R/\xi = 0.05$, $R/L = 0.10$, and $ct_0/L = 10.2$, at $t/t_0 = 2.5$ $\left(\overline{\lambda} = 1.037\right)$.

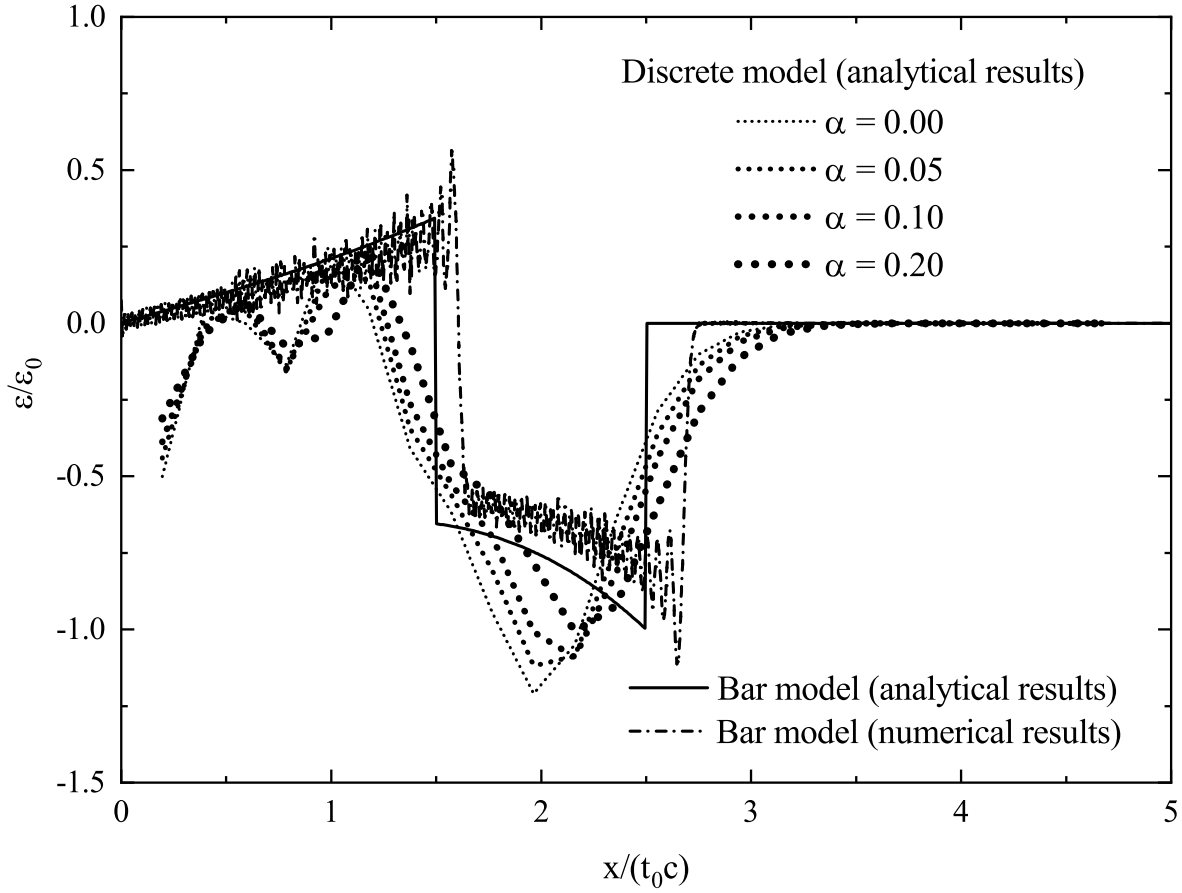

Figure 7: The normalized strain distribution for $R/\xi = 0.10$, $R/L = 0.10$, and $ct_0/L = 5.1$, at $t/t_0 = 2.5$ $\left(\overline{\lambda} = 1.037\right)$.

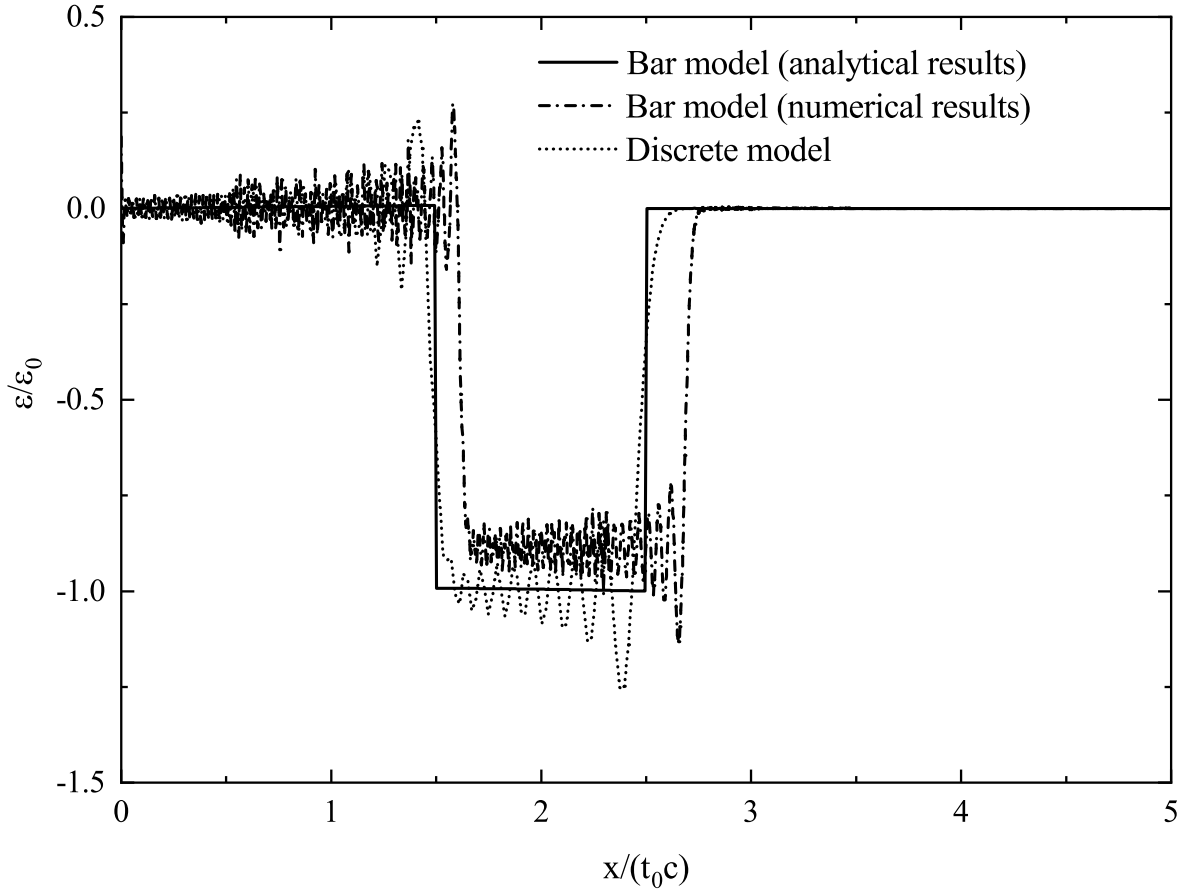

Figure 8: The normalized strain distribution for $R/\xi = 0.001$, $R/L = 0.10$, and $ct_0/L = 101.8$, at $t/t_0 = 2.5$ $\left(\overline{\lambda} = 1.037 \times 10^{-2}\right)$.

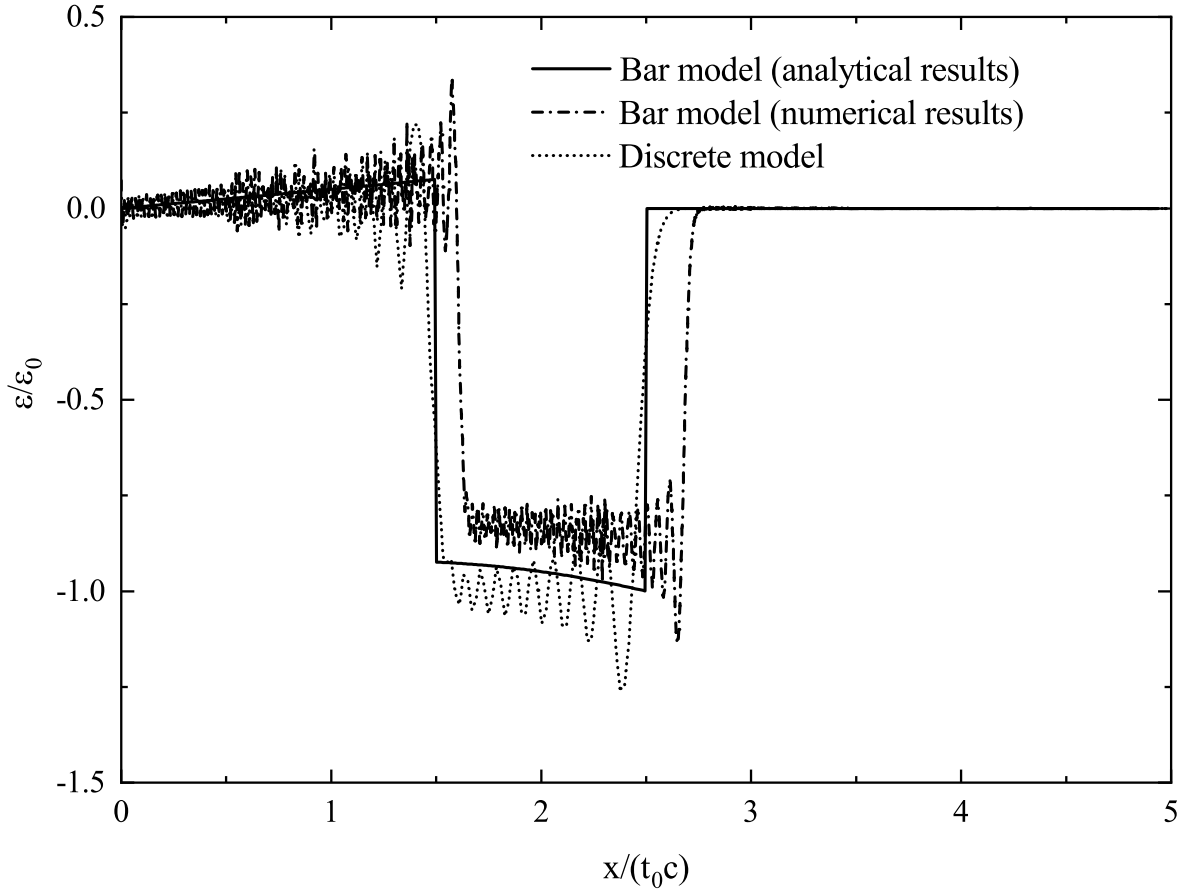

Figure 9: The normalized strain distribution for $R/\xi = 0.0032$, $R/L = 0.10$, and $ct_0/L = 50.9$, at $t/t_0 = 2.5$ $\left(\overline{\lambda} = 0.1037\right)$.

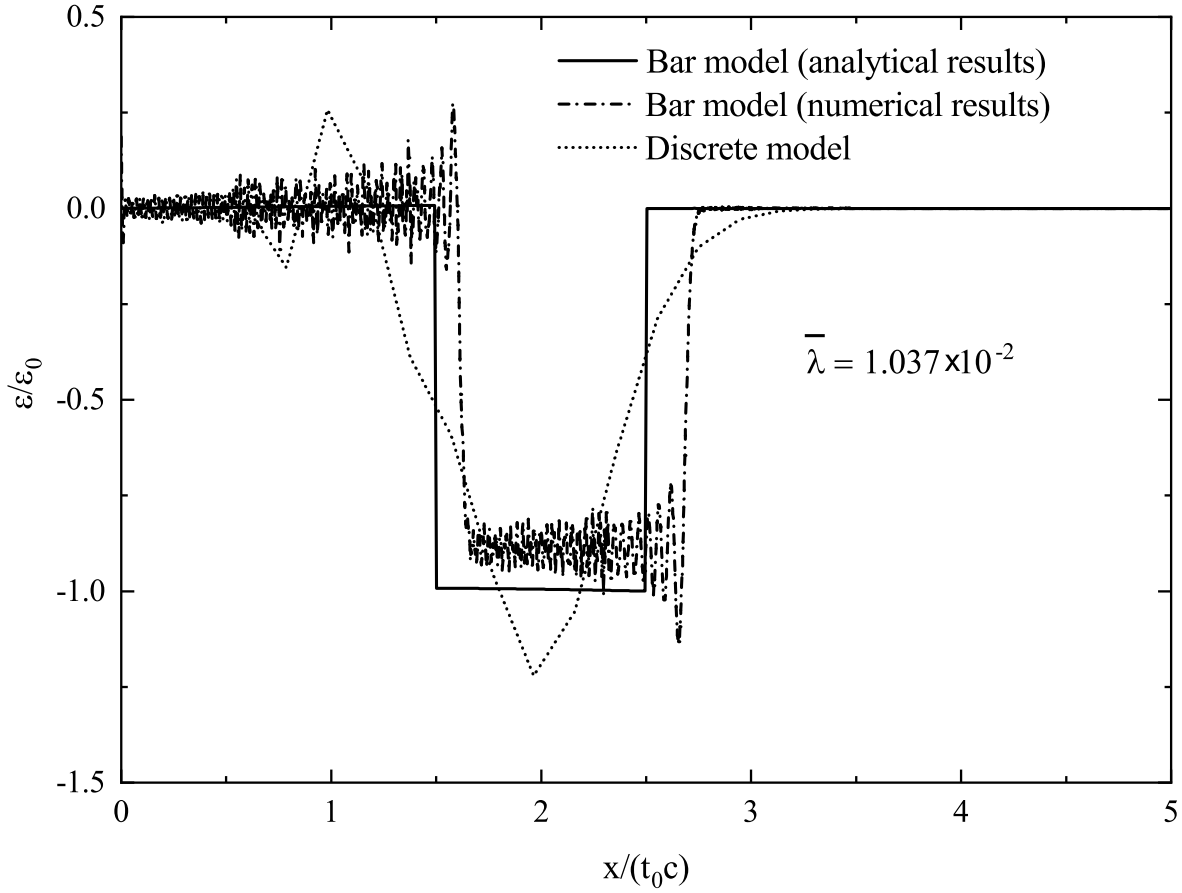

Figure 10: The normalized strain distribution for $R/\xi = 0.01$, $R/L = 0.10$, and $ct_0/L = 5.1$, at $t/t_0 = 2.5$ $\left(\overline{\lambda} = 1.037 \times 10^{-2}\right)$.

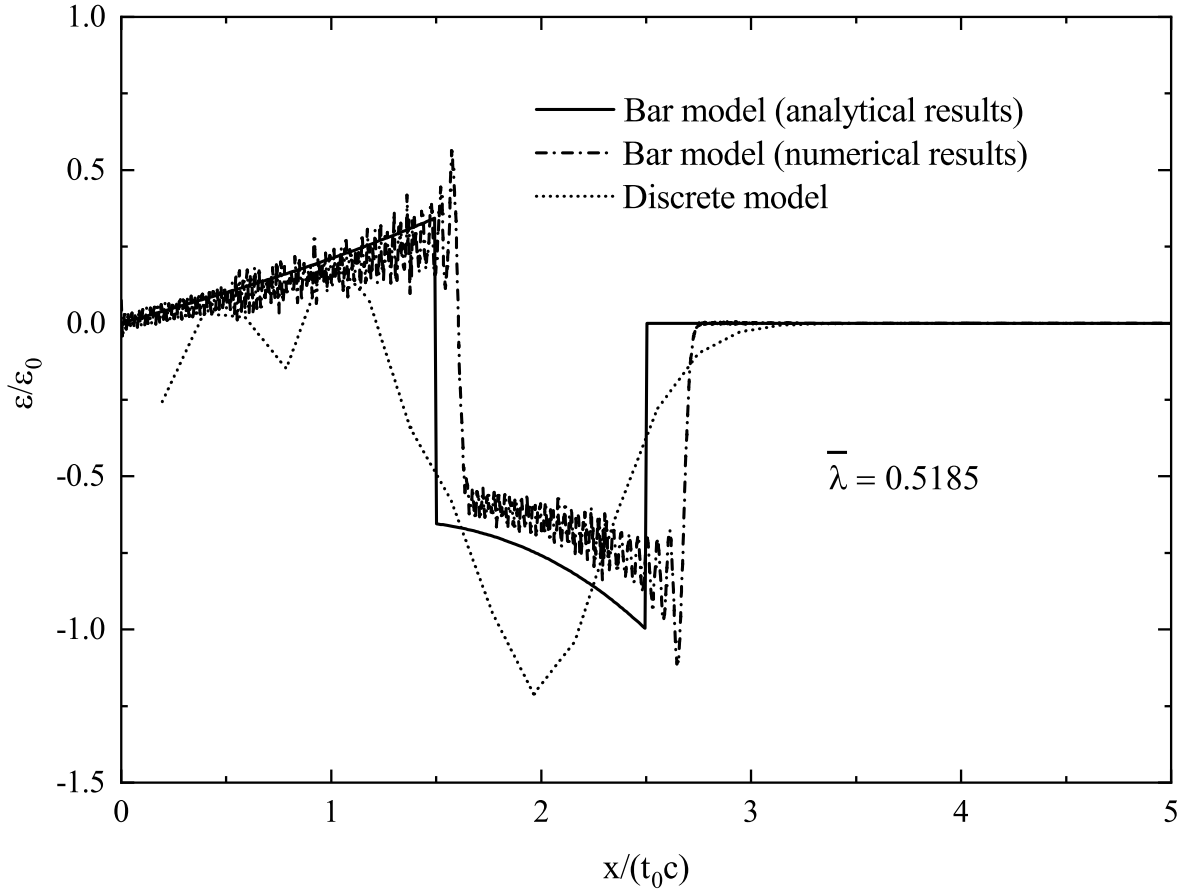

Figure 11: The normalized strain distribution for $R/\xi = 7.07 \times 10^{-2}$, $R/L = 0.10$, and $ct_0/L = 5.1$, at $t/t_0 = 2.5$ $\left(\overline{\lambda} = 0.5185\right)$.

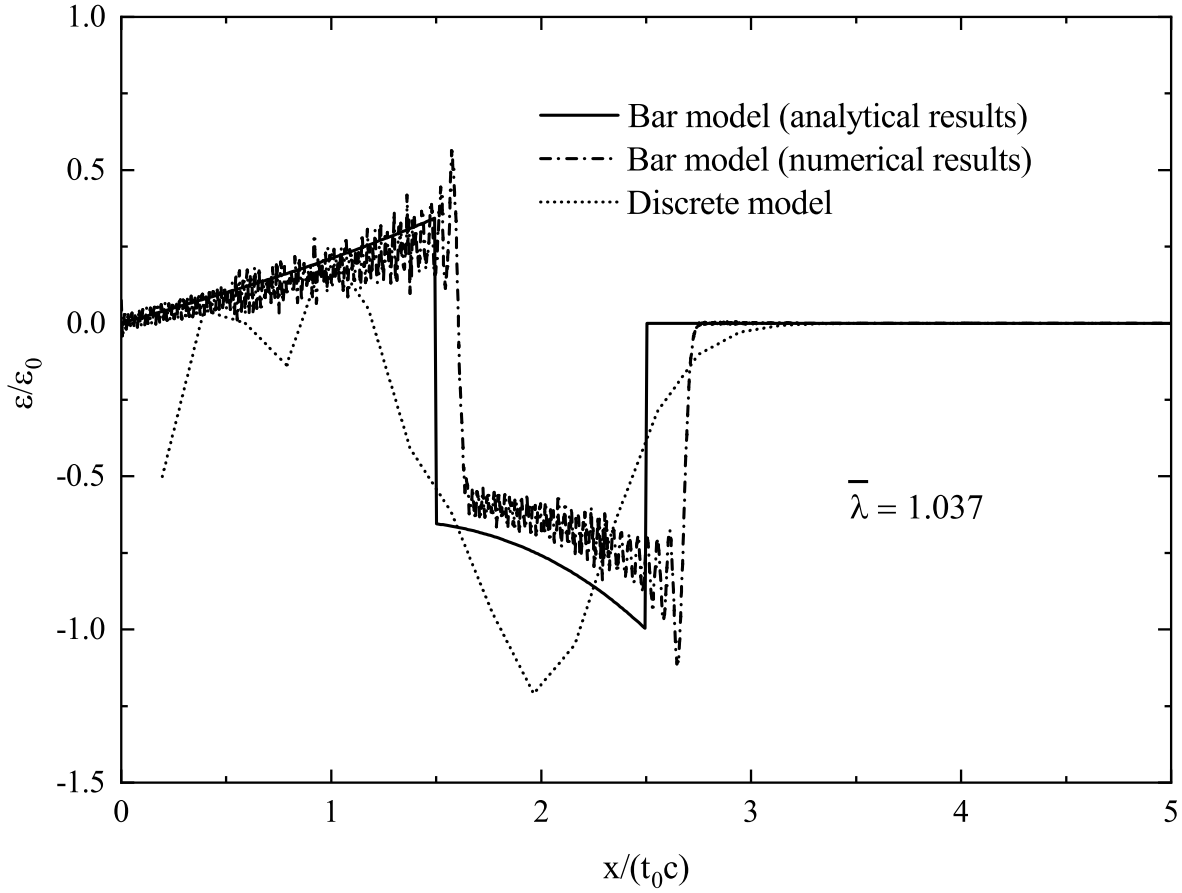

Figure 12: The normalized strain distribution for $R/\xi = 0.10$, $R/L = 0.10$, and $ct_0/L = 5.1$, at $t/t_0 = 2.5$ $\left(\overline{\lambda} = 1.037\right)$.

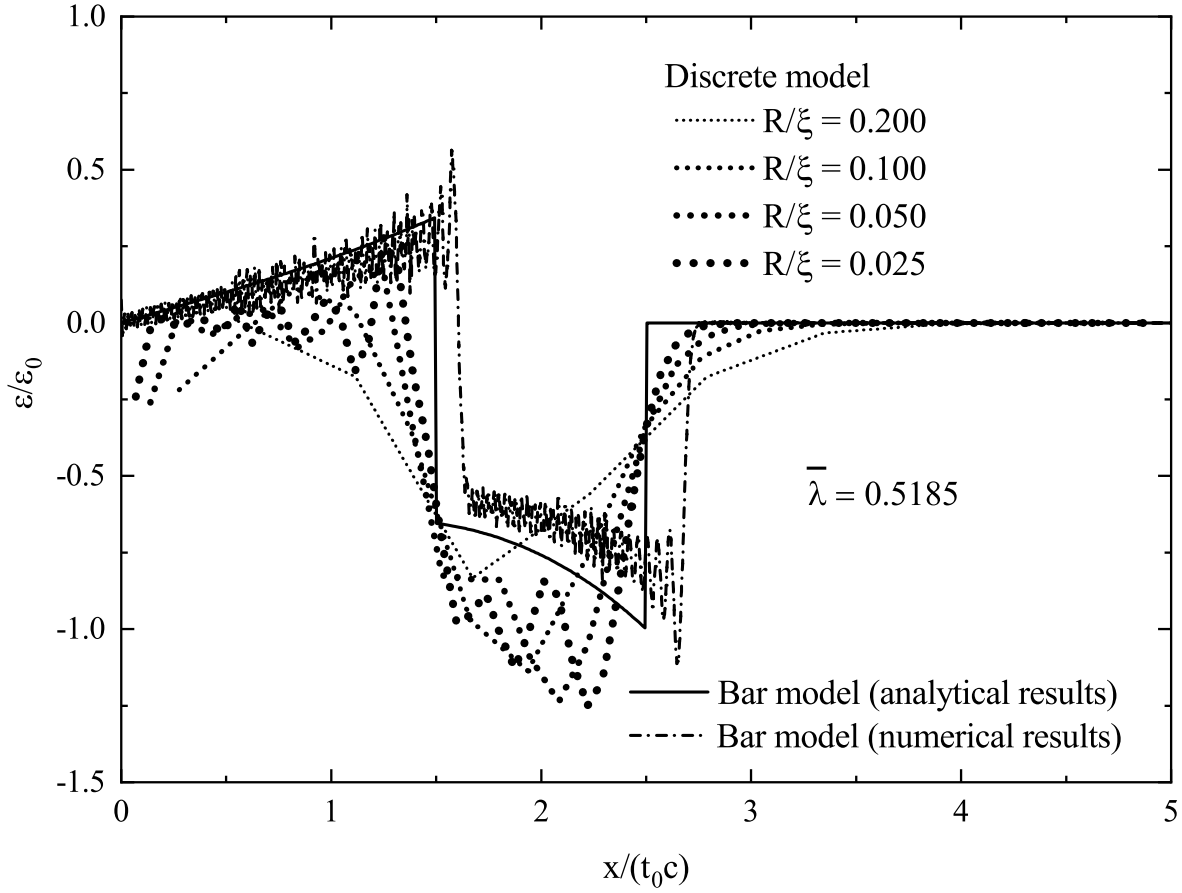

Figure 13: The normalized strain distribution for $\overline{\lambda} = 0.5185$, $R/L = 0.10$, at $t/t_0 = 2.5$.

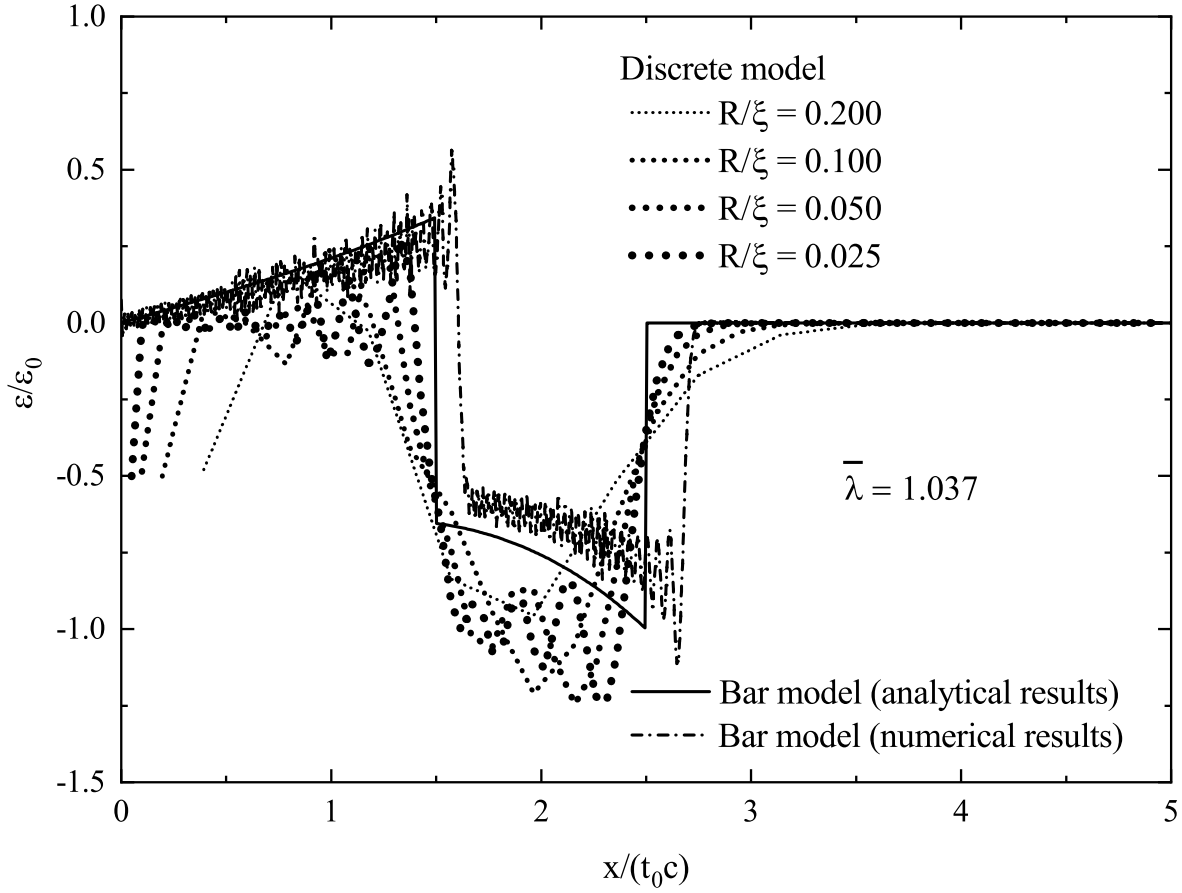

Figure 14: The normalized strain distribution for $\overline{\lambda} = 1.037$, $R/L = 0.10$, at $t/t_0 = 2.5$.

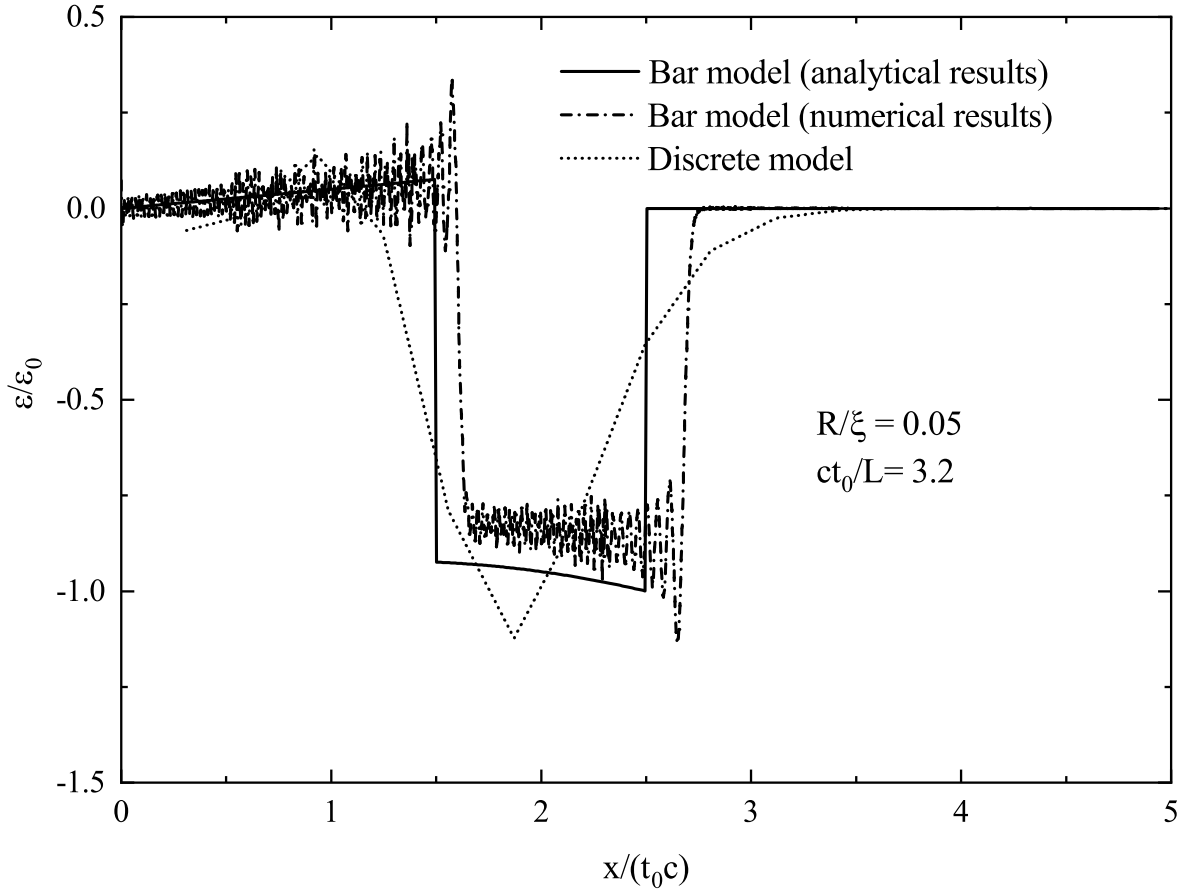

Figure 15: The normalized strain distribution for $R/\xi = 0.05$, $R/L = 0.10$, and $ct_0/L = 3.2$, at $t/t_0 = 2.5$ $\left(\overline{\lambda} = 0.1037\right)$.

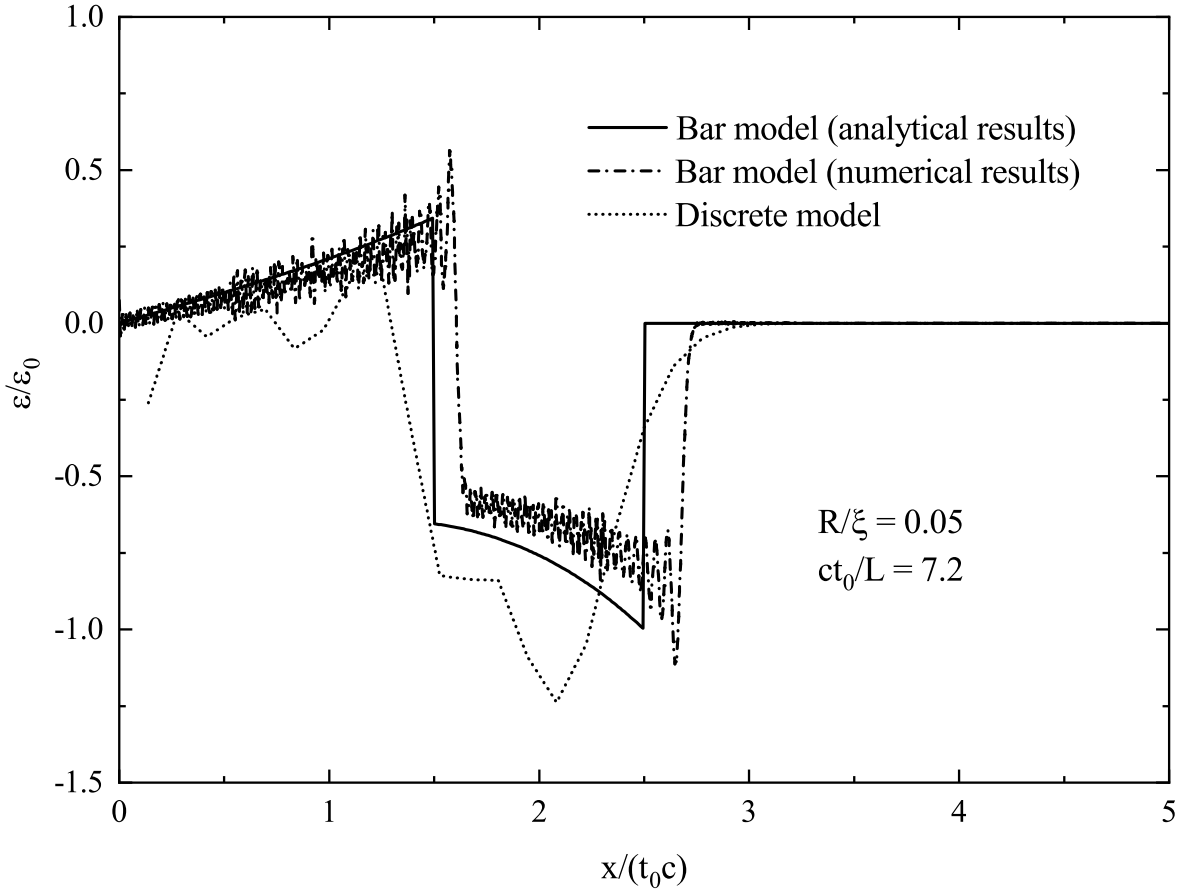

Figure 16: The normalized strain distribution for $R/\xi = 0.05$, $R/L = 0.10$, and $ct_0/L = 7.2$, at $t/t_0 = 2.5$ $\left(\overline{\lambda} = 0.5185\right)$.

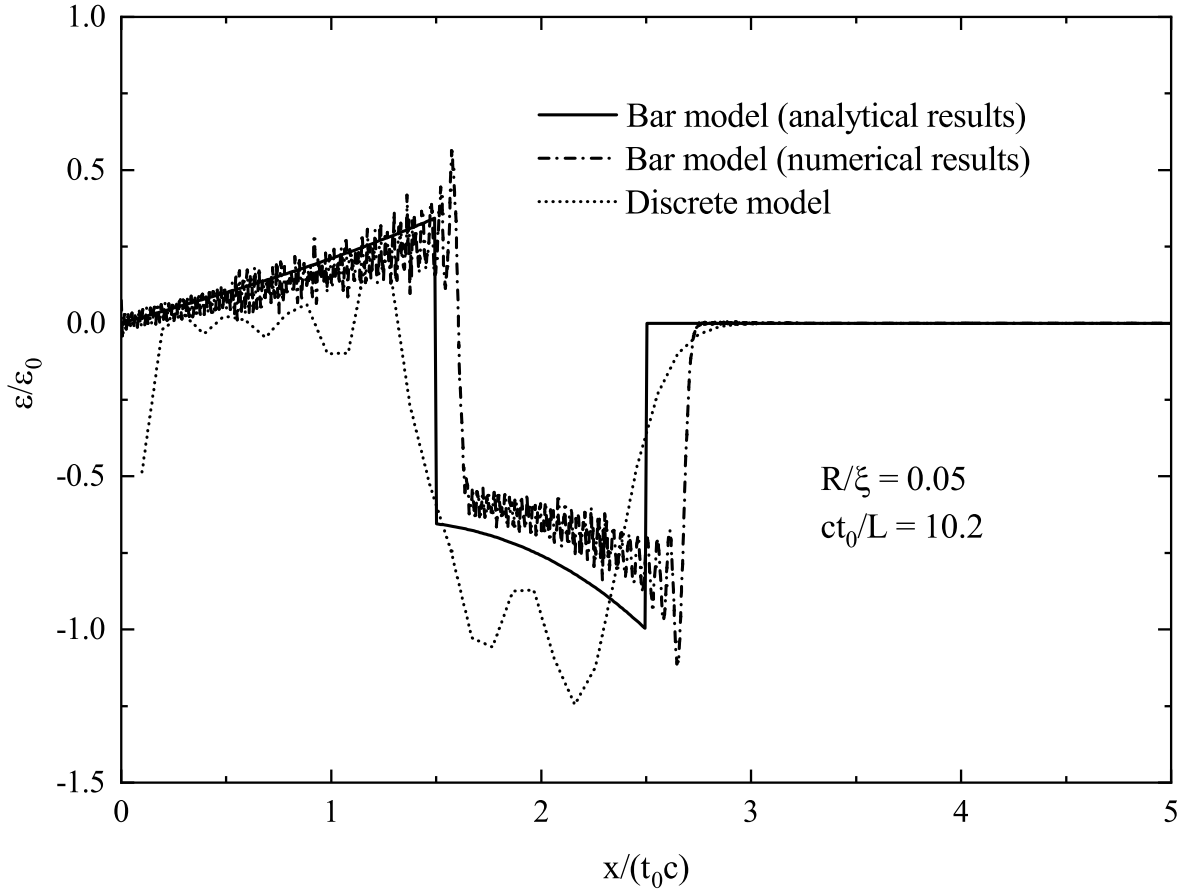

Figure 17: The normalized strain distribution for $R/\xi = 0.05$, $R/L = 0.10$, and $ct_0/L = 10.2$, at $t/t_0 = 2.5$ $\left(\overline{\lambda} = 1.037\right)$.

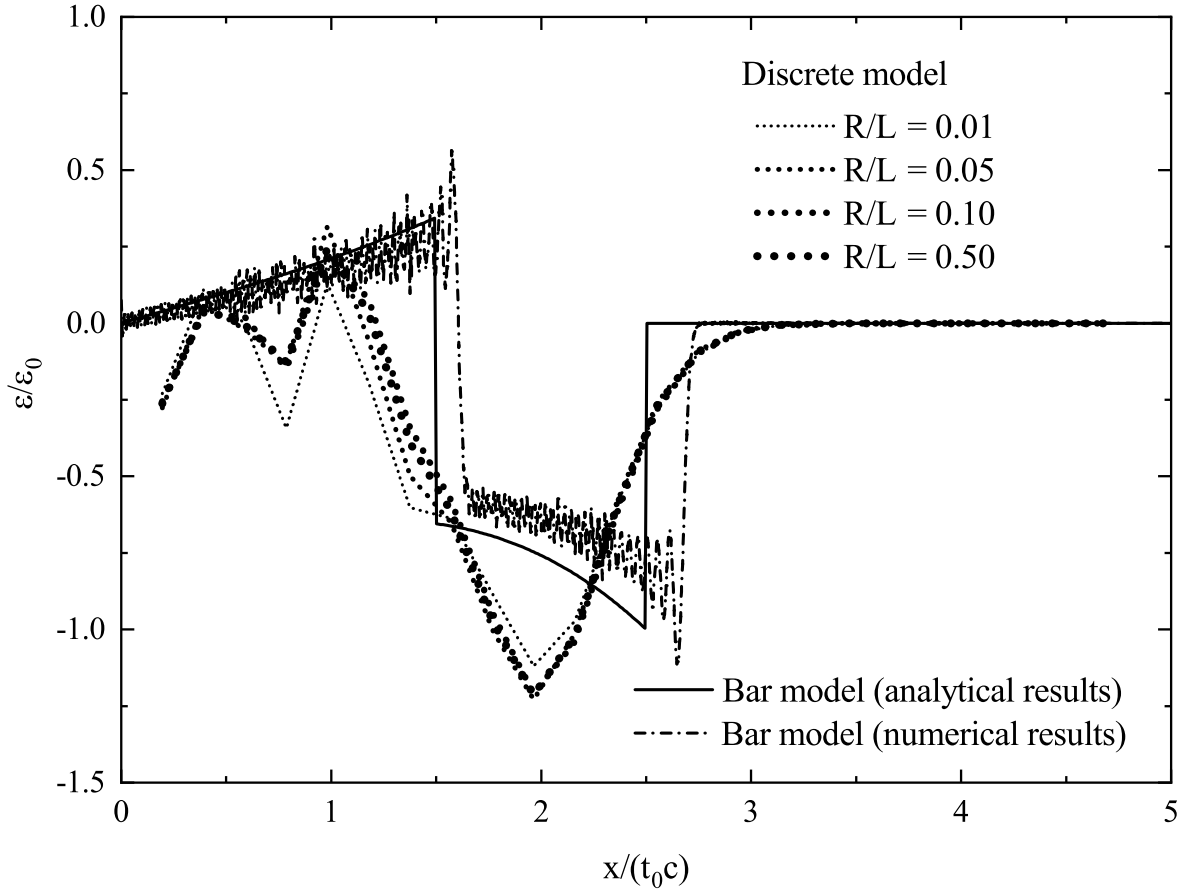

Figure 18: The normalized strain distribution for $R/\xi = 7.07 \times 10^{-2}$, and $ct_0/L = 5.1$, at $t/t_0 = 2.5$ with different R/L $\left(\overline{\lambda} = 0.5185\right)$.

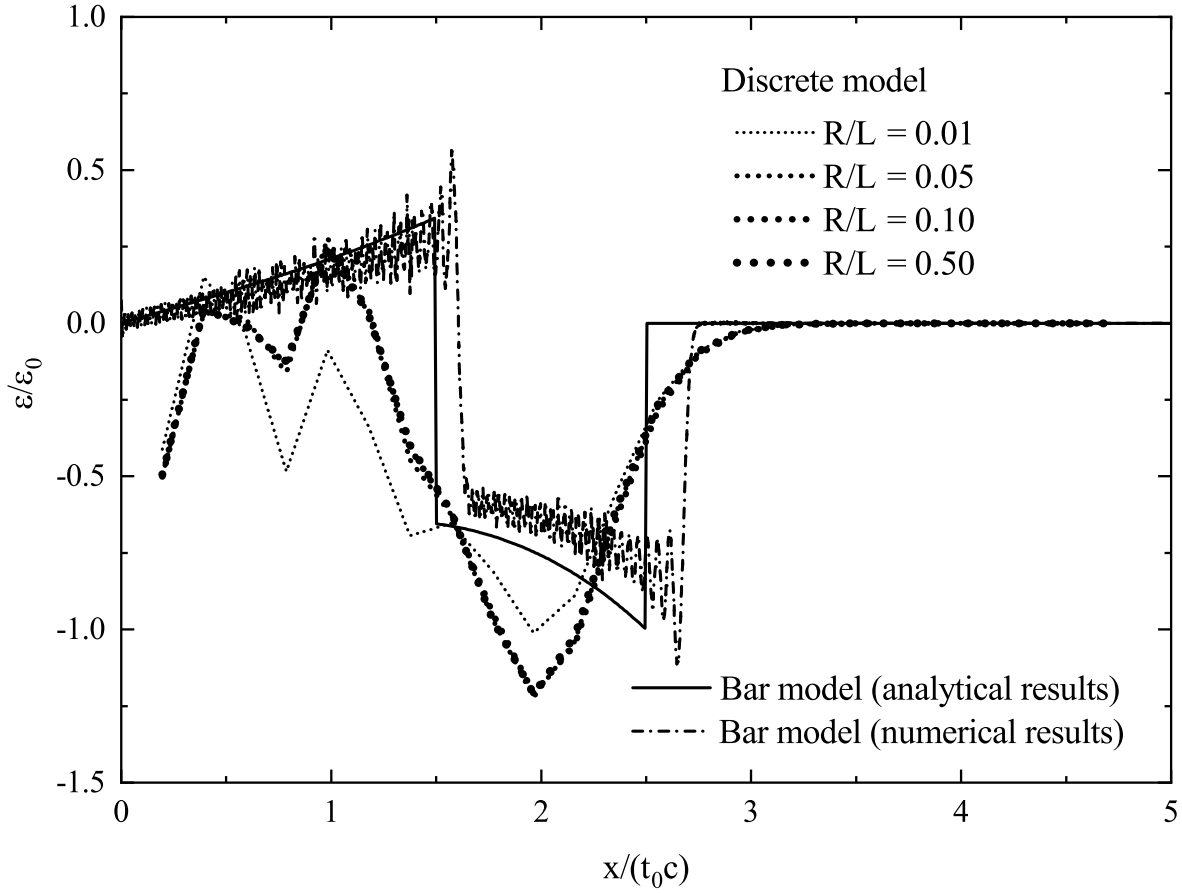

Figure 19: The normalized strain distribution for $R/\xi = 0.10$, and $ct_0/L = 5.1$, at $t/t_0 = 2.5$ with different R/L $\left(\overline{\lambda} = 1.037\right)$.

4. A New Continuum Model of a Class of One-Dimensional Metamaterials Subject to Harmonic Loading

4.1. Symbols

Symbol	Meaning
e	Euler's number
A	Area
a	An important term in the dispersion relation
$\overline{A}$	A constant related to the amplitude of the waves
$\mathbf{a}$	The acceleration vector field
$\mathbf{b}$	The body force vector
b	An important term in the dispersion relation
c	An important term in the dispersion relation
E_0	Young's modulus
F_j	The magnitude of the force exerted by the left spring attached to disk j
F_{j+1}	The magnitude of the force exerted by the right spring attached to disk j
G_1	The magnitude of u
G_2	The magnitude of θ
I	The moment of inertia of a disk or the metamaterial system
i	The imaginary unit
i^v	The volumetric moment of inertia of a micropolar continuum
k	The stiffness of the springs
$\overline{k}$	A new rotational elastic constant
$\overline{\overline{k}}$	A new rotational elastic constant
K	Wavenumber
L	The length of a unit cell
M	Local moment
m	Mass
p	Angular frequency
p^*	Normalized angular frequency
p_1	The first critical frequency
p_2	The second critical frequency
R	The radial position of a radial spring
R_{mag}	A constant relevant to the behaviour of the eigenvalues
u	The linear displacement field
$\tilde{u}$	The linear displacement profile for 1-D wave propagation
u_j	The displacement of disk j

x	Position
α	Part of the phase angle of the eigenvalues
β	A micropolar material constant
η	A new rotational coupling constant
ε	Strain
γ	A micropolar material constant
κ	A micropolar material constant
λ	A micropolar material constant and a complex constant related to the wavenumber
λ_1	The first branch of λ
λ_2	The second branch of λ
Ω	A parameter representing inertial effects
ω_0	A critical frequency predicted by the discrete model
ω_1	A critical frequency predicted by the discrete model
ϕ	An important parameter in the dispersion relation of the discrete model
ρ^v	The volumetric mass density of a micropolar continuum
ρ	Volumetric mass density
$\boldsymbol{\sigma}$	The Cauchy stress tensor
θ	The local rotation field
$\tilde{\theta}$	The local rotational displacement profile for 1-D wave propagation
θ_j	The local rotation of disk j
μ	A micropolar material constant
ζ	The radius of gyration of a rigid disk

In this chapter we expand on the ideas presented in the third chapter, and generalize them to an entire class of one-dimensional materials. To this end, a representative discrete structure for the class of one-dimensional metamaterials of interest is used to develop a suitable continuum model, for which new set of new constitutive laws are derived. The dispersion relation of the representative material subject to harmonic wave propagation, as well as the stop and passing bands are determined, and compared to those generated by both a discrete model, and the model developed in Chapter 3.

4.2. Development of the Model

Consider a simple structure formed by a series of identical unit cells consisting of linear Hookean springs and rigid disks [36]. This model allows for the incorporation of local elements which are free to rotate within the unit cells, while maintaining coupling with the macro-scale translation of each unit cell. The details of this one-dimensional metamaterial system are shown in Figs. 20 and 21.

Since the focus of this work is on the coupling between local-rotational and translational motion, the effect of the central springs can be ignored. If a harmonic motion of frequency p (rad/s) is considered, the governing equations can be formulated by balancing both linear and angular momentum of a single unit cell:

$$F_{j+1} - F_j = -p^2 m u_j \tag{89}$$

$$R(F_{j+1} + F_j) = -p^2 I \theta_j 2 \tag{90}$$

with the forces being defined as:

$$F_{j+1} = k(u_{j+1} - u_j - R(\theta_{j+1} + \theta_j)) \tag{91}$$

$$F_j = k(u_j - u_{j-1} - R(\theta_{j-1} + \theta_j)). \tag{92}$$

Here, F_j and F_{j+1} represent the magnitudes of the forces exerted by the left and right springs attached to the jth disk, u_j and θ_j represent the linear and rotational displacements corresponding to the jth disk, k is the spring constant, assumed equal in every spring, R, m, and I represent the radial position of the spring, mass, and moment of inertia of each identical disk, respectively. Substituting Eqs. (91) and (92) into Eqs. (89) and (90), the following coupled equations of motion for the discrete metamaterial are obtained:

$$k(u_{j+1} - 2u_j + u_{j-1}) - kR(\theta_{j+1} - \theta_{j-1}) = -p^2 m u_j \tag{93}$$

$$kR(u_{j+1} - u_{j-1}) - kR^2(\theta_{j+1} + 2\theta_j + \theta_{j-1}) = -p^2 I\theta_j. \tag{94}$$

4.2.1. Continuous Modelling of the Dynamic Behaviour of the Metamaterial

If treated as a continuous function of coordinate x, the displacement $u(x)$ can be expanded as a Taylor series at x_j:

$$u(x) = u_j + u'(x_j)(x - x_j) + \frac{1}{2}u''(x_j)(x - x_j)^2 + O(x^3). \tag{95}$$

Since at x_{j-1} and x_{j+1} the displacements are u_{j-1} and u_{j+1} respectively, making use of these values in Eq. (95) and assuming that all unit cells have the same length L, the derivatives in Eq. (95) can be expressed as:

$$u'(x_j) = \frac{u_{j+1} - u_{j-1}}{2L} \tag{96}$$

$$u''(x_j) = \frac{u_{j+1} + u_{j-1} - 2u_j}{L^2}. \tag{97}$$

Similar relations for θ can be obtained. From these unique representations, the following relations can be established:

$$u_{j+1} - 2u_j + u_{j-1} \approx L^2\frac{\partial^2 u}{\partial x^2} \tag{98}$$

$$u_{j+1} - u_{j-1} \approx 2L\frac{\partial u}{\partial x} \tag{99}$$

$$\theta_{j+1} + 2\theta_j + \theta_{j-1} \approx L^2\frac{\partial^2 \theta}{\partial x^2} + 4\theta \tag{100}$$

$$\theta_{j+1} - \theta_{j-1} \approx 2L\frac{\partial \theta}{\partial x}. \tag{101}$$

This gives rise to the following system of coupled partial differential equations (PDEs) governing the properties of the original metamaterial:

$$kL^2\frac{\partial^2 u}{\partial x^2} - 2kRL\frac{\partial \theta}{\partial x} + p^2 mu = 0 \tag{102}$$

$$2kRL\frac{\partial u}{\partial x} - kR^2L^2\frac{\partial^2 \theta}{\partial x^2} - 4kR^2\theta + p^2 I\theta = 0. \tag{103}$$

This system of coupled PDEs represents the new continuum model obtained from the continuous modelling of the harmonic response of the metamaterial with strong local-rotational-translational coupling. Note that this model can be used for non-harmonic loading as well by simply replacing the p^2mu term with $-m\ddot{u}$ and the $p^2I\theta$ term with $-I\ddot{\theta}$. Clearly, the strong local-rotational-translational coupling mentioned previously is present in these equations.

4.2.2. Comparison With the Classical Micropolar Continuum Model

One may notice that there is remarkable similitude between the equations of the developed continuum model and those of a classical micropolar continuum. We will now contrast the classical micropolar continuum equations with these new equations derived for this specific class of materials. The micropolar equations for a one-dimensional material are given in the first chapter by Eqs. 21 and 22. When comparing Eqs. 21 and 22 with Eqs. 102 and 103 respectively, a similitude becomes apparent between the aforementioned sets of equations, noting that Eqs. 21 and 22 are per unit volume, whereas Eq. 102 and Eq. 103 are not. Largely important is the fact that in the current one-dimensional case, the micro-rotation and linear displacement completely decouple in the micropolar model, indicating the degeneration of the coupling effect. A direct comparison between the models yields the following relations for the material constants:

$$2\mu + \lambda = \frac{k}{L}, \quad \rho^v = \frac{m}{AL}, \quad \gamma + \beta = -\frac{2kR^2}{L}, \quad \kappa = \frac{kR^2}{AL}, \quad i^v = \frac{I}{AL},$$

where A is the cross-sectional area of the metamaterial. Upon comparison it becomes evident that in Eqs. (102) and (103) there are extra terms that are not present within the governing equations of the traditional micropolar continuum, indicating that the traditional micropolar model is not suitable for modelling this representative metamaterial, and thus unable to completely describe some salient features of this class of metamaterials. A new continuum model will be developed for this class of metamaterials and a new constitutive relation will be presented in the following section.

4.3. Generalization of the Continuous Model and Development of a New Constitutive Law

To develop a continuous model of the metamaterial, starting from Eqs. (102) and (103) we first define the following material constants:

$$E_0 = \frac{kL}{A} \quad \eta = \frac{2RE_0}{L}.$$

For this new class of materials the balance of linear momentum should be satisfied:

$$div(\boldsymbol{\sigma}) + \rho\mathbf{b} = -p^2\rho\mathbf{a} \tag{104}$$

where $\mathbf{b}$ is the body force vector per unit volume, $\mathbf{a}$ is the magnitude of the acceleration per unit volume, and $\boldsymbol{\sigma}$ is the Cauchy stress tensor. For the current situation (1-D, small displacement gradient, no body force), Eq. (104) reduces to the following:

$$\frac{\partial\sigma}{\partial x} = -p^2\rho u. \tag{105}$$

Comparing Eq. (105) with Eq. (102), and considering the parameters defined above, we can make the following equivalency:

$$\sigma = E_0\varepsilon - \eta\theta \tag{106}$$

where ε is the classical linear Hookean strain, $\varepsilon = u_{,x}$. This result clearly shows that the stress is directly affected by the local rotation inside the unit cell, represented by θ.

As previously shown, the local rotation θ within the unit cell is controlled by Eq. (103), with its left-hand side representing the local moment M which dominates the local rotation inside the unit cell. Naturally, this local moment can be obtained directly from Eq. (103) and the equation governing the local rotation has the form:

$$M = -p^2 i^v \theta \tag{107}$$

with the local moment being

$$M = \overline{k}\theta + \overline{\overline{k}}\theta'' + \eta u'. \tag{108}$$

Defining:

$$\overline{k} = -\tfrac{4R^2k}{AL} \quad \overline{\overline{k}} = -\tfrac{kLR^2}{A}. \tag{109}$$

The relation between the local moment M and the displacements u and θ will in general depend on the local structure of the unit cell of the metamaterial. Eq. (108) represents only the specific local moment for the current metamaterial system. It is interesting to note that the coefficients $\overline{k}$ and $\overline{\overline{k}}$ are always negative for this material, suggesting a negative rotational stiffness.

4.4. One-Dimensional Harmonic Wave Propagation in the Metamaterial

In order to demonstrate the application of the new continuum model, harmonic wave propagation in the metamaterial will be analyzed. The harmonic displacements are assumed to be in the following general form:

$$\tilde{u} = u(x)e^{-ipt} \qquad \tilde{\theta} = \theta(x)e^{-ipt} \tag{110}$$

where p is the circular frequency and t is time.

4.4.1. General Dispersion Relation

Under the harmonic excitation defined by Eq. (110), the system of equations (102) and (103) can be written in matrix form:

$$\begin{bmatrix} kL^2 & 0 \\ 0 & -kR^2L^2 \end{bmatrix} \begin{bmatrix} u'' \\ \theta'' \end{bmatrix} + \begin{bmatrix} 0 & -2kRL \\ -2kRL & 0 \end{bmatrix} \begin{bmatrix} u' \\ \theta' \end{bmatrix} + \begin{bmatrix} mp^2 & 0 \\ 0 & Ip^2 - 4kR^2 \end{bmatrix} \begin{bmatrix} u \\ \theta \end{bmatrix} = \begin{bmatrix} 0 \\ 0 \end{bmatrix} \tag{111}$$

where $'$ represents a derivative with respect to x. For a general wave, assuming a waveform:

$$\begin{bmatrix} u \\ \theta \end{bmatrix} = \begin{bmatrix} G_1 \\ G_2 \end{bmatrix} e^{\lambda x} \tag{112}$$

where λ is an unknown complex constant related to the wavenumber and G_1, G_2 are the magnitudes of u and θ respectively, the following eigenvalue problem is generated:

$$\begin{bmatrix} kL^2\lambda^2 + mp^2 & -2kRL\lambda \\ 2kRL\lambda & -kR^2L^2\lambda^2 + Ip^2 - 4kR^2 \end{bmatrix} \begin{bmatrix} G_1 \\ G_2 \end{bmatrix} = \begin{bmatrix} 0 \\ 0 \end{bmatrix} \tag{113}$$

which leads to the following characteristic equation:

$$\lambda^4 + \frac{p^2}{kL^2}\left(m - \frac{I}{R^2}\right)\lambda^2 - \frac{m}{kL^4}\left(\frac{I}{kR^2}p^4 - 4p^2\right) = 0. \tag{114}$$

The eigenvalue λ can be solved from Eq. (114):

$$\lambda = \pm\frac{p}{L\sqrt{2k}}\sqrt{-\left(m-\frac{I}{R^2}\right) \pm \sqrt{\left(m-\frac{I}{R^2}\right)^2 + \frac{4mI}{R^2} - \frac{16km}{p^2}}}. \quad (115)$$

As a result, Eq. (115) is obtained, which represents the relation between λ and p, the dispersion relation for the harmonic wave. Lastly, with λ given by Eq. (115), G_1 and G_2 can easily be obtained by plugging the solution back into Eq. (113) to get:

$$G_1 = \overline{A}(2kRL\lambda) \quad G_2 = \overline{A}(kL^2\lambda^2 + mp^2). \quad (116)$$

Where $\overline{A}$ is a constant. An eigenvector or waveform for each eigenvalue can be determined through G_1 and G_2 using Eq. (113). Yielding expressions for either of these quantities however, is challenging, as G_1 and G_2 are functions of both λ and p, and hence will change with frequency p. Simple, analytic expressions can, however, be obtained for the wavenumbers.

4.4.2. Determination of Wavenumbers

Wavenumber K is related to the harmonic solution of the form $e^{\lambda x - ipt}$, meaning it should satisfy:

$$iK = \lambda. \quad (117)$$

It is clear from Eq. (115) that λ is controlled by several critical values of the frequency p at which the behaviour of the eigenvalues changes. Defining:

$$a = m - \frac{I}{R^2}, \quad b = \frac{4mI}{R^2}, \quad c = 16km \quad (118)$$

the following expression for λ is obtained:

$$\lambda = \pm\frac{p}{L\sqrt{2k}}\sqrt{-a \pm \sqrt{a^2 + b - \frac{c}{p^2}}}. \quad (119)$$

The critical frequencies will be the roots of the terms under each square root, satisfying the following equations:

$$a^2 + b - \frac{c}{p^2} = 0 \quad (120)$$

$$-a \pm \sqrt{a^2 + b - \frac{c}{p^2}} = 0. \tag{121}$$

Eqs. (120) and (121) yield two critical frequencies p_1 and p_2 with:

$$p_1 = \sqrt{\frac{c}{a^2 + b}}, \quad p_2 = \sqrt{\frac{c}{b}}. \tag{122}$$

It is also evident that the eigenvalues λ given in Eq. (119) possess different branches, which change not only based on the two critical values of p, but also the sign of the parameter a. Because of this, the eigenvalue must be chosen separately for both positive and negative values of a in each interval $[0, p_1]$,$[p_1, p_2]$,$[p_2, \infty)$. Defining the branches of λ as:

$$\lambda_1 = \pm \frac{p}{L\sqrt{2k}} \sqrt{-a + \sqrt{a^2 + b - \frac{c}{p^2}}}, \quad \lambda_2 = \pm \frac{p}{L\sqrt{2k}} \sqrt{-a - \sqrt{a^2 + b - \frac{c}{p^2}}} \tag{123}$$

the behaviour of the eigenvalue in different frequency ranges can then be classified and their expressions can be determined, as shown in Tables 4 and 5.

Table 4: A tabulation of the solutions of the eigenvalues in each range of p

Eigenvalue	sign of a	$0 < p < p_1$	$p_1 < p < p_2$	$p_2 < p < \infty$
λ_1	$a > 0$	$\frac{-i}{L\sqrt{2k}} p \lvert R_{mag} \rvert e^{\frac{-i\alpha}{2}}$	$\frac{-ip}{L\sqrt{2k}} \sqrt{a - \sqrt{a^2 + b - \frac{c}{p^2}}}$	$\frac{-p}{L\sqrt{2k}} \sqrt{-a + \sqrt{a^2 + b - \frac{c}{p^2}}}$
λ_1	$a < 0$	$\frac{-1}{L\sqrt{2k}} p \lvert R_{mag} \rvert e^{i\frac{\alpha}{2}}$	$\frac{-p}{L\sqrt{2k}} \sqrt{a - \sqrt{a^2 + b - \frac{c}{p^2}}}$	$\frac{-p}{L\sqrt{2k}} \sqrt{-a + \sqrt{a^2 + b - \frac{c}{p^2}}}$
λ_2	$a > 0$	$\frac{i}{L\sqrt{2k}} p \lvert R_{mag} \rvert e^{i\frac{\alpha}{2}}$	$\frac{-ip}{L\sqrt{2k}} \sqrt{a + \sqrt{a^2 + b - \frac{c}{p^2}}}$	$\frac{-ip}{L\sqrt{2k}} \sqrt{a + \sqrt{a^2 + b - \frac{c}{p^2}}}$
λ_2	$a < 0$	$\frac{-1}{L\sqrt{2k}} p \lvert R_{mag} \rvert e^{-i\frac{\alpha}{2}}$	$\frac{-p}{L\sqrt{2k}} \sqrt{-a - \sqrt{a^2 + b - \frac{c}{p^2}}}$	$\frac{-ip}{L\sqrt{2k}} \sqrt{a + \sqrt{a^2 + b - \frac{c}{p^2}}}$

where:

$$\alpha = \arctan\left(\sqrt{\frac{\frac{c}{p^2} - a^2 - b}{|a|}}\right), \qquad |R_{mag}| = \left|\frac{c}{p^2} - b\right|^{1/4} \tag{124}$$

Table 5: A tabulation of the behaviour of the eigenvalues in each range of p

Eigenvalue	sign of a	$0 < p < p_1$	$p_1 < p < p_2$	$p_2 < p < \infty$
λ_1	$a > 0$	Real + Imaginary	Purely Imaginary	Purely Real
λ_1	$a < 0$	Real + Imaginary	Purely Real	Purely Real
λ_2	$a > 0$	Real + Imaginary	Purely Imaginary	Purely Imaginary
λ_2	$a < 0$	Real + Imaginary	Purely Real	Purely Imaginary

The corresponding waveform as defined by Eq. (111) can then be determined:

$$\begin{bmatrix} u \\ \theta \end{bmatrix} = \overline{A}_1 \begin{bmatrix} 2kRL\lambda_1 \\ kL^2\lambda_1^2 + mp^2 \end{bmatrix}^{(1)} e^{\lambda_1 x} + \overline{A}_2 \begin{bmatrix} 2kRL\lambda_2 \\ kL^2\lambda_2^2 + mp^2 \end{bmatrix}^{(2)} e^{\lambda_2 x}. \tag{125}$$

where $\overline{A}_1$ and $\overline{A}_2$ are constants representing the amplitudes of the wave, and λ_1 and λ_2 being defined appropriately using the expressions given in Table (4).

4.5. General Behaviour of the Dispersion Relation

The imaginary parts of the eigenvalues λ_1 and λ_2 drive the propagation of the harmonic wave propagating through this specific continuous metamaterial. The real parts of these eigenvalues represent the spatially varying amplitude of the displacement. When the eigenvalue is purely imaginary we have wave propagation, when the eigenvalue is purely real we have no wave propagation, and therefore a "stop-band" is formed.

As shown in Tables (4) and (5) these properties are closely related to the parameter a defined in Eq. (118), which represents the relative significance between the mass and rotational inertia (moment of inertia) of a unit cell. Introducing the radius of gyration ζ of the local disk with the moment of inertia being given by $I = m\zeta^2$, a can be expressed as:

$$a = m(1 - (\zeta/R)^2) = m(1 - \Omega^2) \tag{126}$$

with $\Omega = \zeta/R$. If $\zeta/R < 1$, the parameter a will be positive, and if the converse is true, a will be negative. In terms of Ω, the critical frequencies p_1 and p_2 become:

$$p_1^2 = \frac{16\frac{k}{m}}{(1+\Omega^2)^2}, \quad p_2^2 = 4\frac{k}{m}\frac{1}{\Omega^2}. \tag{127}$$

These results show that the critical frequencies are entirely controlled by k/m and Ω. For the case where $a > 0$ ($\Omega < 1$) it is clear from the solution of λ given by Eq. (115) that the first wavenumber (λ_1) has a stop-band at $p > p_2$, and a passing band for $p < p_2$, and the second wavenumber (λ_2) has no stop-bands. For the case that $a < 0$ ($\Omega > 1$), the first wavenumber does not allow wave propagation except for $p < p_1$. The second wavenumber shows a stop-band for $p_1 < p < p_2$, and predicts wave propagation without decay for $p > p_2$.

4.6. Comparison With Other Models

4.6.1. Dispersion Relation From The Discrete Model

The dispersion relation for the current discrete metamaterial system can be obtained directly by solving an eigenvalue problem using Eqs. (93) and (94), which results in the following dispersion curve:

$$\left(\frac{e^{\lambda L}-1}{e^{\lambda L}+1}\right)^2 = \frac{1}{\Omega^2}\frac{1-p^2/\omega_0^2}{1-p^2/\omega_1^2} \tag{128}$$

with L being the length of the unit cell and

$$\omega_0^2 = \frac{4R^2k}{m\zeta^2} = 4\frac{k}{m}\frac{1}{\Omega^2}, \qquad \omega_1^2 = \frac{4k}{m}. \tag{129}$$

For $\omega_0 < p < \omega_1$ or $\omega_1 < p < \omega_0$:

$$LK = arccos\left(\frac{1-\phi^2}{1+\phi^2}\right) \tag{130}$$

where ϕ is defined as:

$$\phi = \frac{1}{\Omega}\sqrt{\left|\frac{1-p^2/\omega_0^2}{1-p^2/\omega_1^2}\right|}. \tag{131}$$

For $\omega_0 < \omega_1 < p$ ($a < 0$) or $p < \omega_1 < \omega_0$ ($a > 0$)

$$\lambda L = \pm i\pi + ln\left|\frac{1+\phi}{1-\phi}\right|. \tag{132}$$

For $p < \omega_0 < \omega_1$ $(a < 0)$ or $\omega_1 < \omega_0 < p$ $(a > 0)$

$$\lambda L = ln \left| \frac{1+\phi}{1-\phi} \right|. \tag{133}$$

These results show that in addition to the passing band between ω_0 and ω_1, propagating waves also exist from ω_1 to infinity $(a < 0)$ or from ω_1 to zero $(a > 0)$.

4.6.2. Dispersion Relation From a Lower Order Model

In the study of the transient response of the metamaterial system an elastically supported bar is used [36], which represents a lower order version of the model presented in this paper without considering the higher order term θ'' in the local rotational motion of the unit cell. When similar analysis is conducted on the bar model, the following dispersion curve is obtained:

$$L\lambda = \sqrt{\frac{m}{k}(p_2^2 - p^2)}. \tag{134}$$

This dispersion relation predicts the range $p < p_2$ as a stop-band where no wave propagation is obtained, and the range $p > p_2$ as the passing band where wave propagation will occur.

4.6.3. Comparison Between the Models

To compare the dispersion relations obtained from the discrete model, the current continuous model and the lower order continuous model, first rewrite ω_0, p_1 and p_2 in terms of ω_1 as:

$$p_2^2 = \omega_0^2 = \frac{\omega_1^2}{\Omega^2} \qquad p_1^2 = \frac{4\omega_1^2}{(1+\Omega^2)^2}. \tag{135}$$

with:

$$\omega_1^2 = \frac{4k}{m}. \tag{136}$$

It is interesting to observe that all three models predict a unique critical frequency $p = p_2 = \omega_0$, indicating a good agreement between these models around $p = p_2$. The variations of these critical frequencies with Ω are shown in Fig. 22. The discrete model predicts passing bands in $(0, p_2)$ for $a > 0$ or (p_2, ∞) for $a < 0$. The lower order continuum model predicts a passing band

for $p > p_2$ and a stop band for $p < p_2$, which matches the behaviour of the discrete model for only the case where $a < 0$. In comparison, as shown by the behaviour of the wavenumbers given in Table 4, the current higher order continuum model predicts both passing bands in $(0, p_2)$ for $a > 0$ (λ_1) and (p_2, ∞) for $a < 0$ (λ_2), in agreement with the discrete model.
The normalized wavenumber $KL = Im(L\lambda)$ under different normalized frequencies $p^* = p/\sqrt{\frac{k}{m}}$ from these three models is compared in Figs. 23 and 24 for $\zeta/R > 1$ and $\zeta/R > 1$ respectively. It is observed that the lower order continuum model perfectly matches the discrete model near $p = p_2$ when $\zeta/R > 1$, however it is not capable of capturing the behaviour present in the discrete model for the case where $\zeta/R < 1$. The current higher order continuum model also accurately predicts the wavenumber near $p = p_2$ (λ_2) for $\zeta/R > 1$, as shown in Fig. 23. For $\zeta/R < 1$, as shown in Fig. 24, the current higher order model is capable of predicting the same passing band through a branch λ_1 as the discrete model and providing the wavenumber near p_2 $(p > p_2)$, which is in good agreement with that predicted using the discrete model.

Figures 25, 26, 27, and 28 provide detailed comparisons of the wavenumbers between the models for ζ/R= 100, 20, 5 and 2 respectively. The results show excellent agreement between the new continuum model and the discrete model for large values of ζ/R near $p = p_2$. Figures 29, 30, and 31 illustrate the comparisons of the wavenumbers (λ_1) between models for $\zeta/R = 0.5, 0.2$ and 0.125 respectively, showing passing bands in $p < p_2$. It is interesting to observe that the new continuum model is in an excellent agreement with the discrete model in the range $p_1 < p < p_2$ for small ζ/R values. This shows clearly that even for $\zeta/R < 1$ in which the lower order continuum model is incapable of representing wave propagation, the new continuum model can predict behaviour extremely close to that predicted by the discrete model.

When ζ/R is close to 1, the original discrete metamaterial system experiences a strong resonance and its dispersion curve becomes $e^{\lambda L} = 0, \infty$, indicating no wave propagation. The current model shows significant discrepancy at this point, and therefore is not suitable for cases where ζ/R is around 1.

4.7. Behaviour of Wavenumbers of the Current Continuum Media

The continuum model itself represents a class of materials with internal/local rotation, as given in Eqs. 105-109. Its behaviour under wave

propagation is further illustrated in figures 32 and 33, directly comparing the effect of the parameters ζ/R for $\zeta/R \geq 1$ and $\zeta/R < 1$, respectively. These figures show clearly that, the location of the passing and stop band are significantly affected by ζ/R and dominated by p_1 and/or p_2.

4.8. Conclusions

- A new model was developed to encompass an entire class of elastic metamaterials which cannot be modelled by classical micropolar continuum mechanics
- Stop and passing bands for harmonic wave propagation in a representative elastic metamaterial belonging to the general group were obtained
- The location of the stop and passing bands in the frequency spectrum for this class of materials are influenced mainly by the parameter ζ/R
- The new continuum model predicts the same critical frequency p_2 and the same stop bands as the discrete model
- The new continuum model captures wave propagation in the frequency range $p > p_2$ for $\zeta/R < 1$, which the lower order model in the previous chapter could not predict

4.9. Figures

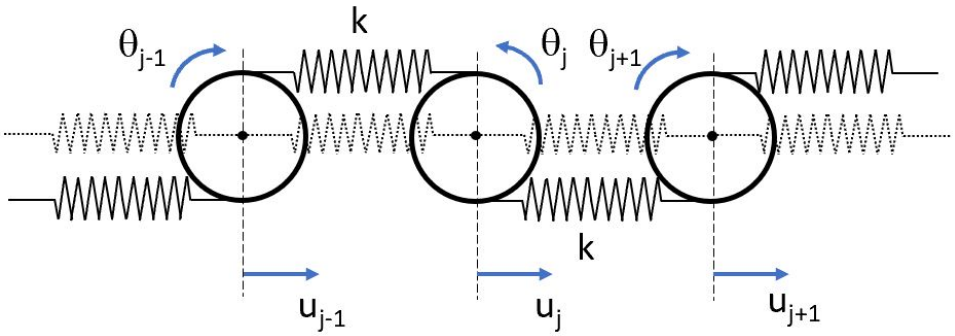

Figure 20: A representative discrete model of the periodic metamaterial consisting of rigid disks and linear Hookean springs

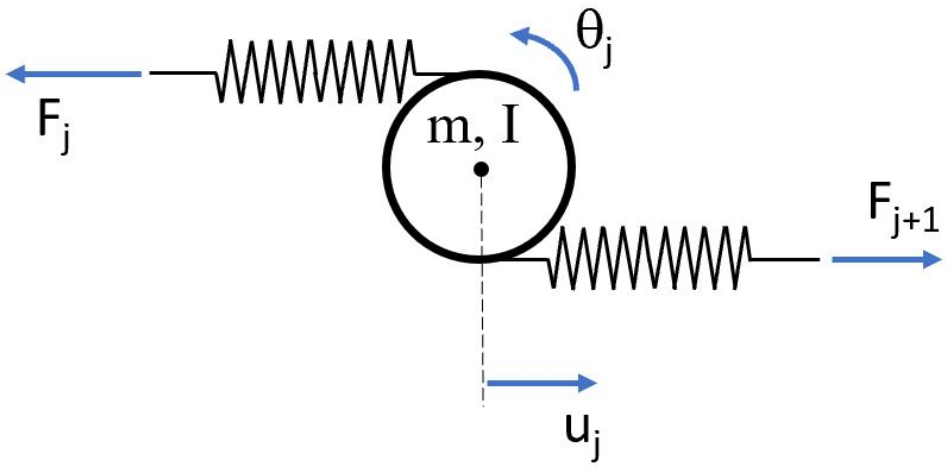

Figure 21: A unit cell of the discrete periodic metamaterial

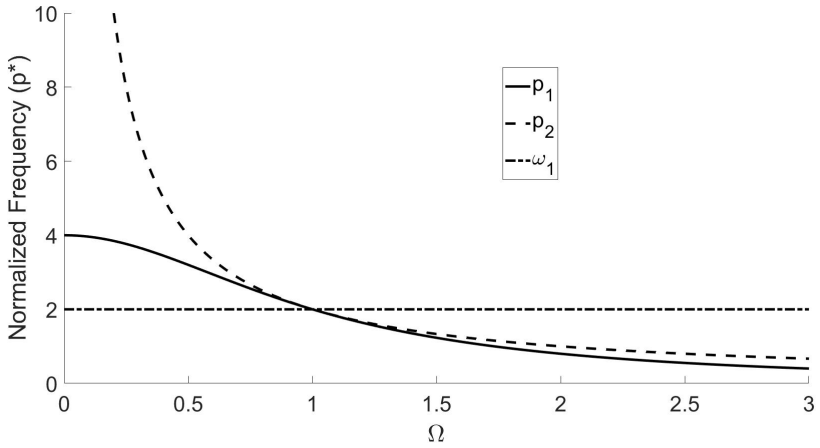

Figure 22: The variation of critical frequencies with respect to $\Omega = \zeta/R$

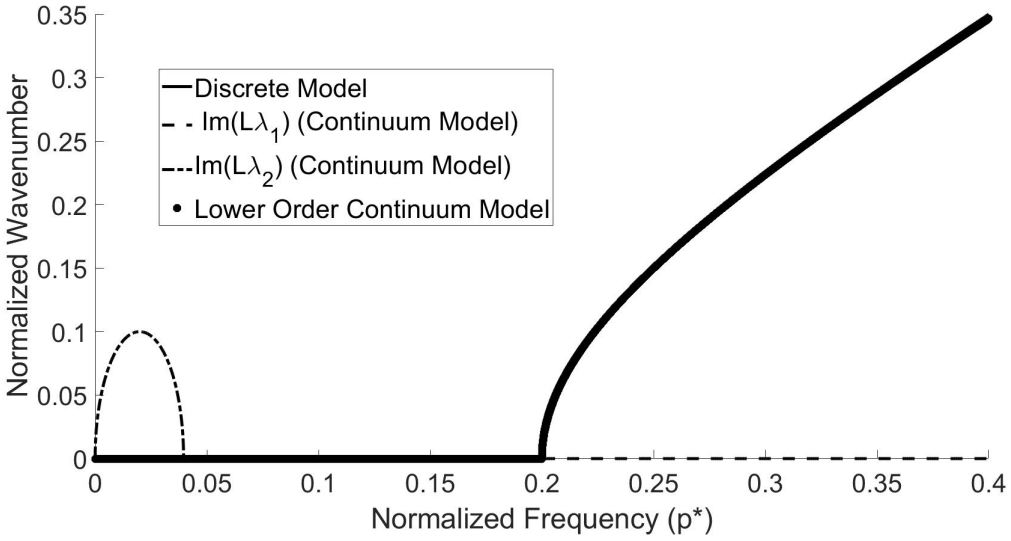

Figure 23: A comparison between the three different models for $\zeta/R = 10$

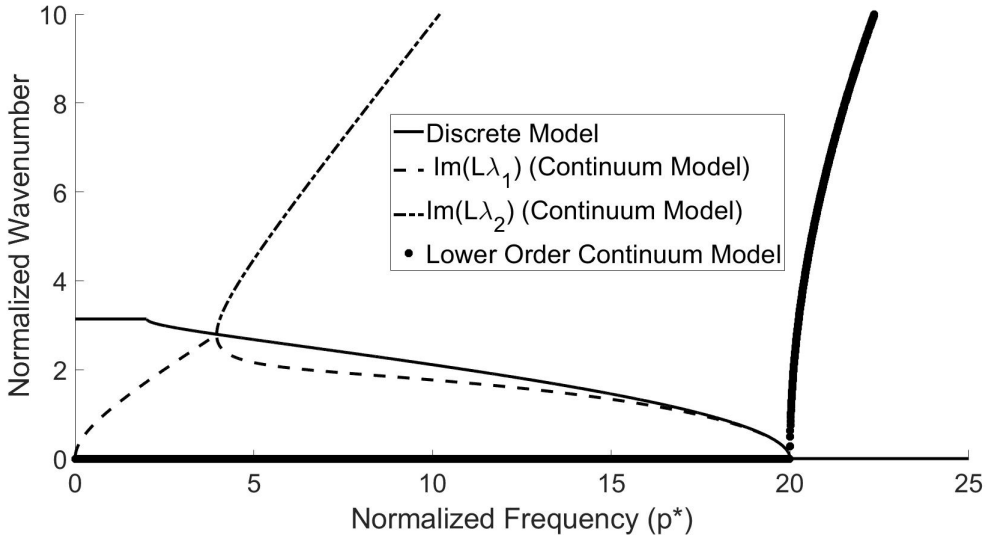

Figure 24: A comparison between the three different models for $\zeta/R = 0.1$

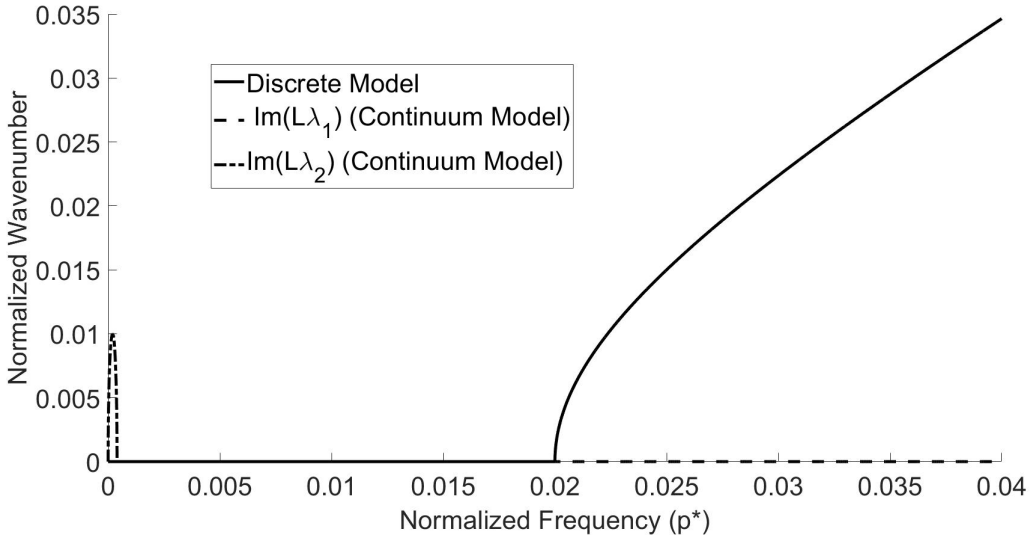

Figure 25: A comparison between the discrete model and the new continuum model for $\zeta/R = 100$

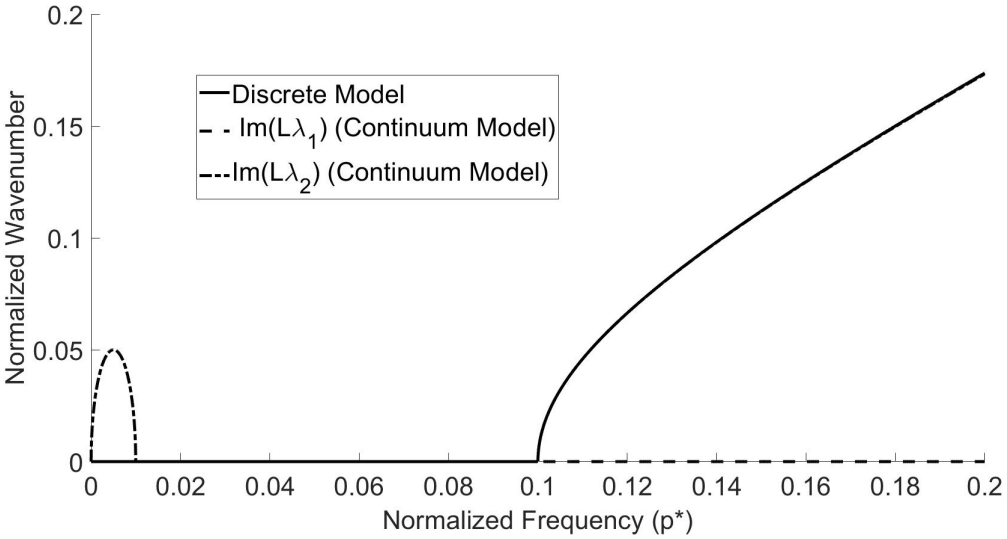

Figure 26: A comparison between the discrete model and the new continuum model for $\zeta/R = 20$

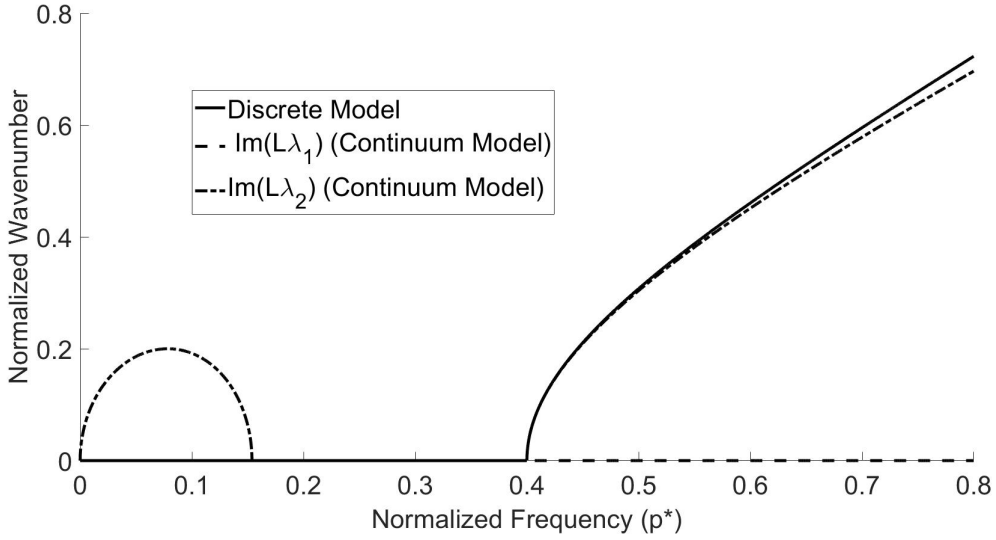

Figure 27: A comparison between the discrete model and the new continuum model for $\zeta/R = 5$

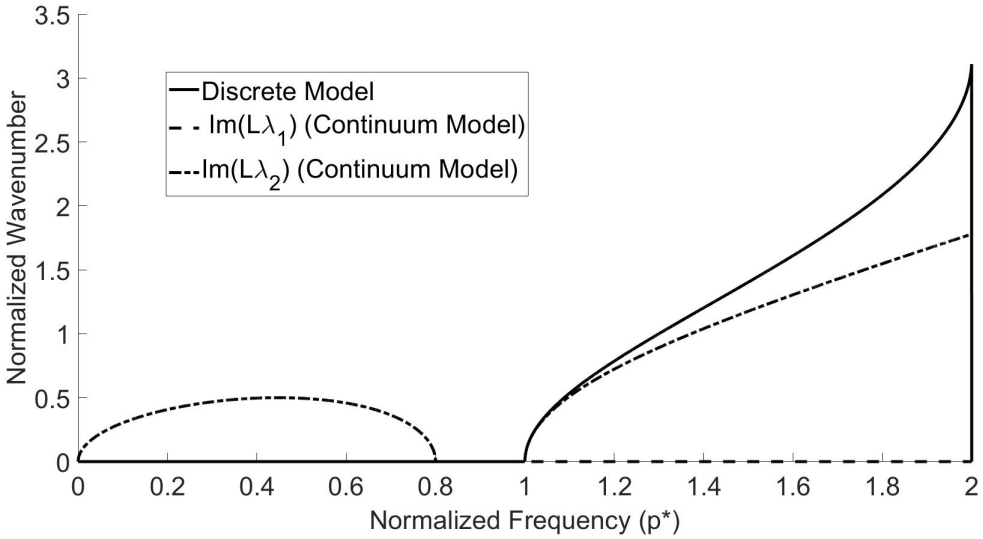

Figure 28: A comparison between the discrete model and the new continuum model for $\zeta/R = 2$

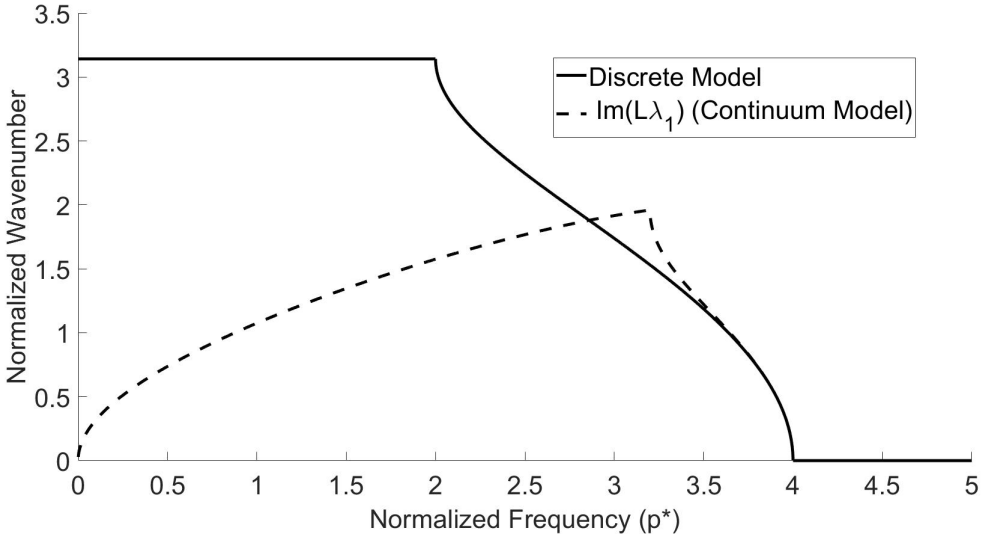

Figure 29: A comparison between the discrete model and the new continuum model for $\zeta/R = 0.5$

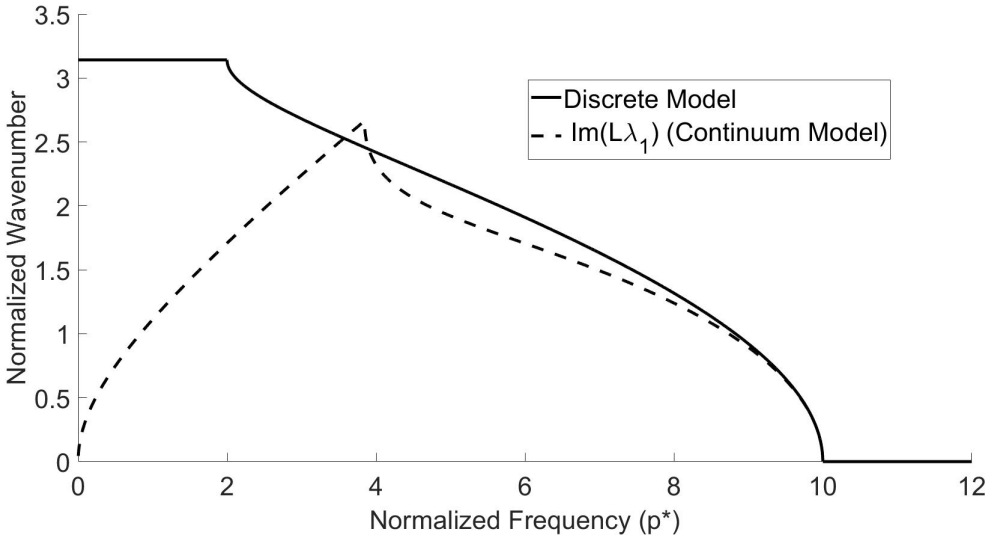

Figure 30: A comparison between the discrete model and the new continuum model for $\zeta/R = 0.2$

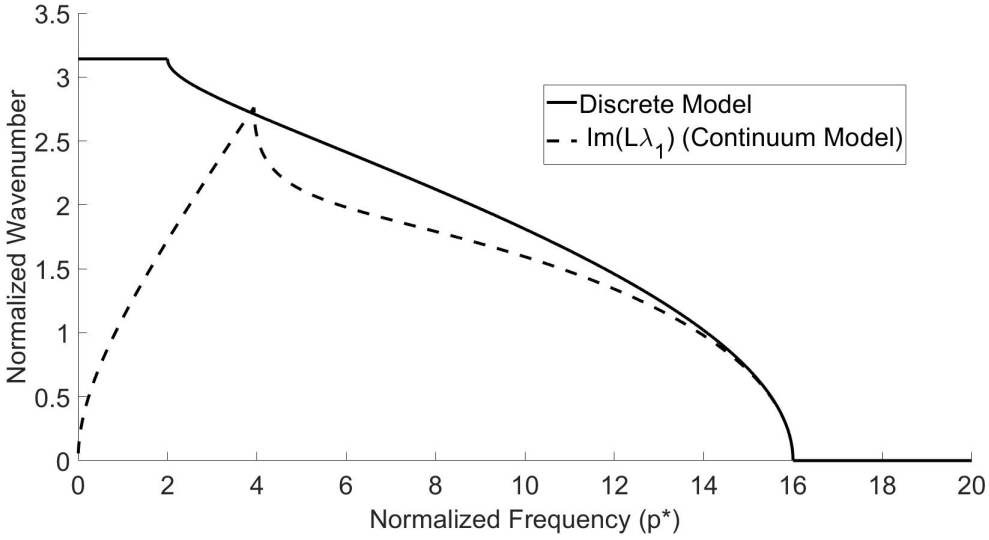

Figure 31: A comparison between the discrete model and the new continuum model for $\zeta/R = 0.125$

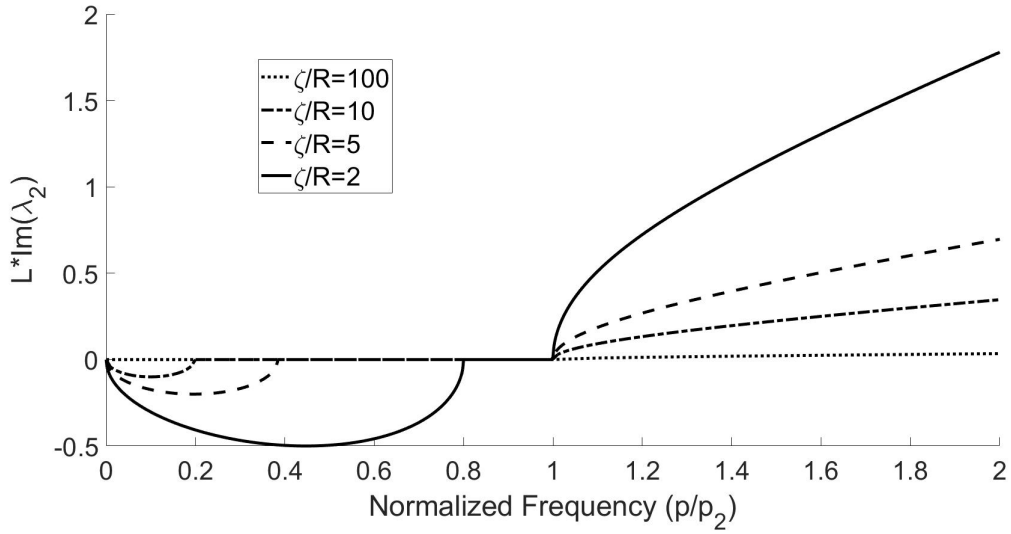

Figure 32: The variation of the second wavenumber with respect to the normalized frequency for different values of the parameter ζ/R

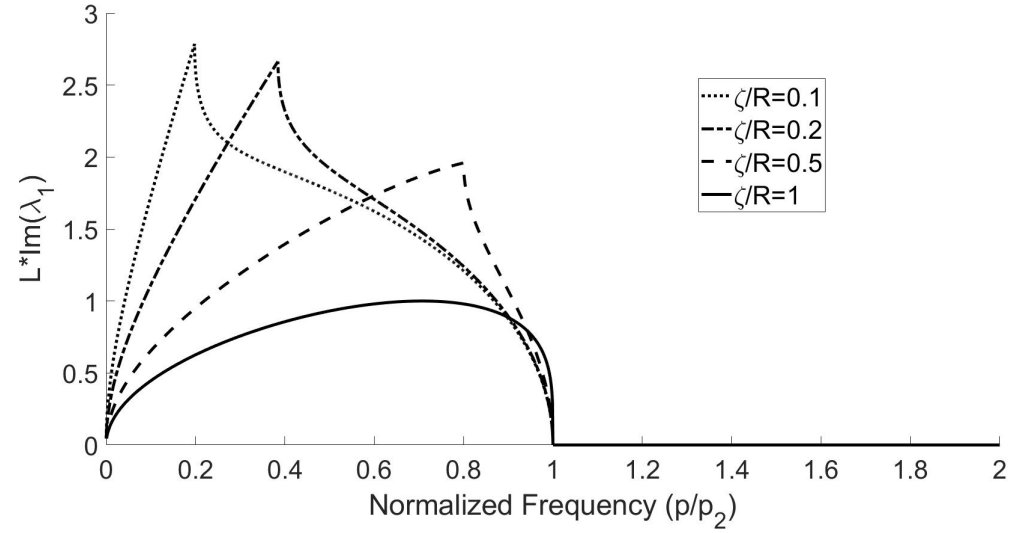

Figure 33: The variation of first wavenumber with respect to the normalized frequency for different values of the parameter ζ/R

5. A New Continuum Model for a Class of Two-Dimensional Elastic Metamaterials

5.1. Symbols

Symbol	Meaning
e	Euler's number
ΔL	The change in central spring length
Δd	The change of length of a tangential spring
Δd_{rigid}	The rigid length released during deformation
Δd_{spring}	The stretch of a tangential spring
$\Delta\alpha$	The change in the angle α caused by deformation
A_0	The cross-sectional area of the central bars
A_1	The cross-sectional area of the tangential bars
a	A characteristic length
b	The into-the-page thickness of the RVE
$\mathbf{C}$	The classical elasticity tensor
C_{ijkl}	The components of the elasticity tensor
c	Wavespeed
E	Young's Modulus
E_0	The stiffness of the central bars or Young's Modulus for the 1-D model
E_1	The stiffness of the tangential bars
E'	A normalized Young's Modulus
F	A force corresponding to a central spring
F'	A force corresponding to a tangential spring
G	The shear modulus
I	The moment of inertia of a disk or the metamaterial system
i	The imaginary unit
i^*	The inertia per unit volume
K	Wavenumber
k	The stiffness of a central spring
k'	The stiffness of a tangential spring
$\overline{k}$	Normalized wavenumber
L	A characteristic length for the previously developed 1-D model
L'	The length of the central spring when the neighbouring disk is moved
L_0	The initial length of the central spring
M	The local moment
m	The mass of a disk or the metamaterial system

p	A new proposed rotational coupling constant
q	A new rotational coupling constant
q_1	A new proposed rotational coupling constant
q_2	A new proposed rotational coupling constant
R	The radius of a rigid disk
R_{ij}	The components of a new rotational coupling tensor
t	Time
U_0	The amplitude of the u displacement profile for longitudinal wave propagation
$\ddot{u}_i$	The components of the pointwise acceleration field
$\ddot{u}$	The x-component of the acceleration field
$\ddot{v}$	The y-component of the acceleration field
V	Volume
V_0	The amplitude of the harmonic transverse wave
x	One of the planar Cartesian directions
y	The planar Cartesian directions perpendicular to x
α	The angle formed between a central spring and a tangential spring
β	The angle the central spring makes with the x-axis
$\boldsymbol{\varepsilon}$	The linear small strain tensor
ε_{kl}	The components of the small strain tensor
ε_{AB}	The strain on a plane with a normal in the A direction in the direction of B
Δ	The 2-D Laplacian operator
η	A rotational coupling constant for a previously developed 1-D model
η^0	A dimensionless governing parameter for longitudinal wave propagation
λ	A new rotational coupling constant
ν	Poisson's Ratio
$\overline{\Omega}$	Normalized angular frequency
ω	Angular frequency (rad/s)
ω_0	The term used to normalize the angular frequency
ρ	The mass density per unit volume
$\boldsymbol{\sigma}$	The Cauchy stress tensor
σ_{ij}	The components of the Cauchy stress tensor
σ_{AB}	The stress on a plane with a normal in the A direction in the direction of B
θ_0	The amplitude of the θ displacement profile for longitudinal wave propagation
θ	The local rotation field
$\ddot{\theta}$	The pointwise local rotational acceleration field
ξ	The radius of gyration of a disk
ζ^0	A dimensionless governing parameter for longitudinal wave propagation

In this chapter the ideas presented in the previous chapter are further generalized to create a two-dimensional model capable of representing a class of metamaterials with strong local rotational-translational coupling. A new set of constitutive laws for this class of materials is presented, then this model is applied to a representative 2-D discrete structure in order to prove suitability. Following this, propagation of both longitudinal and transverse harmonic waves in the new material will be studied, and the dispersion relations for these waves will presented, analyzed, and the critical frequencies will be identified.

5.2. A new material model

In previous studies of one-dimensional elastic metamaterials, it has been observed that a new type of continuum material with local rotational motion can effectively describe the dynamic properties of a class of metamaterials whose salient features cannot be captured by the classical micropolar model [36, 37]. In the current study, a general two-dimensional material model capable of accounting for the local rotational effects in these materials is developed. The new continuum model allows for the superposition of a local rotation field on top of the usual classical continuum to account for the local rotational motion. The following linear model is proposed for a class of continuum materials with local rotational deformation:

$$\sigma_{ij,j} = \rho \ddot{u}_i \tag{137}$$

$$M = i^* \ddot{\theta} \tag{138}$$

$$\sigma_{ij} = C_{ijkl}\varepsilon_{kl} + R_{ij}\theta \tag{139}$$

$$M = ptr(\boldsymbol{\varepsilon}) + q_1 \Delta\theta + q_2\theta \tag{140}$$

where C is the classical elasticity tensor, R is a new rotational stiffness tensor, q_1, q_2 and p are new elastic constants, Δ is the 2-D Laplacian operator in cartesian basis, i^* is the moment of inertia of the material per unit volume, tr is the usual trace operator and θ is the local rotation of the material, defined point-wise. These new constitutive laws represent a continuum where each mathematical point, in addition to the classical linear displacements, has ascribed to it a rotation which affects the constitutive properties of the material. The suitability of this model will be studied using a representative discrete 2-D elastic metamaterial.

5.3. A representative discrete metamaterial model

The proposed material model represents a specific class of elastic metamaterials with strong local rotational translational coupling. Consider a typical elastic metamaterial system made of rigid disks and linear Hookean springs shown in Fig. 34, forming a 2-D chiral model. A second 2-D chiral system, the mirror image of the first will be imposed on top of the first model to create a 2-D metamaterial with local rotational-translational coupling without chiral effects. The center-to-center distances between neighbouring disks are assumed to be the same and the displacement at the center of a disk is the same as that belonging to the corresponding disk in the mirror image.

For the 2-D chiral model considered, there are 12 forces acting on each disk; 6 forces, F_1, F_2, F_3, F_4, F_5, F_6 from central springs, and 6 forces, F_1', F_2', F_3', F_4', F_5', F_6' from tangential springs, as shown in Fig. 35. Superimposing the mirror image on top of the chiral model, will yield a non-chiral system. However, for simplicity of analysis the equations of motion as well as expressions for each of the forces acting on the original chiral system will be obtained, and then the mathematical addition of the system of opposite chirality will be done a posteriori. To this end, the equations of motion of the disk, representing the translational and rotational motions of the chiral system can be expressed as:

$$\begin{aligned}&\frac{-1}{2}F_1 + F_1'(\frac{1}{2}cos\alpha) + \frac{1}{2}F_2 + F_2'(\frac{1}{2}cos\alpha) + F_3 + F_3'cos\alpha \\ &+ \frac{1}{2}F_4 + F_4'(\frac{1}{2}cos\alpha) + \frac{-1}{2}F_5 + F_5'(\frac{-1}{2}cos\alpha) - F_6 - F_6'cos\alpha = m\ddot{u}\end{aligned} \tag{141}$$

$$\begin{aligned}&\frac{\sqrt{3}}{2}F_1 + F_1'(\frac{\sqrt{3}}{2}cos\alpha) + \frac{\sqrt{3}}{2}F_2 + F_2'(\frac{\sqrt{3}}{2}cos\alpha) + \frac{-\sqrt{3}}{2}F_4 \\ &+ F_4'(\frac{-\sqrt{3}}{2}cos\alpha) + \frac{-\sqrt{3}}{2}F_5 + F_5'(\frac{-\sqrt{3}}{2}cos\alpha) = m\ddot{v}\end{aligned} \tag{142}$$

$$-R(F_1' + F_2' + F_3' + F_4' + F_5' + F_6') = I\ddot{\theta} \tag{143}$$

where m and I are the mass and moment of inertia of the disk, respectively, R is the radius of the rigid disk, and α is the angle between a central spring and a corresponding tangential spring. The deformation of the springs is dominated by the linear and rotational displacements of the disks. The

deformation of a central spring is given by:

$$\Delta L = L' - L_0 = \Delta u cos\beta + \Delta v sin\beta \tag{144}$$

where ΔL is the change in central spring length, L' is the length of the central spring when the neighbouring disk is perturbed, L_0 is the initial length of the central spring and β is the angle of orientation pertaining to the central spring measured from the x axis. Without the rotation of the disks, the change in length of the tangential spring between the contact points of two neighbouring disks can be determined as:

$$\Delta d = \frac{\Delta L}{cos\alpha} \tag{145}$$

It should be noted that the Δd also contains the released length due to spring unwrapping during deformation, which is given by

$$\Delta d_{rigid} = 2R\Delta\alpha \tag{146}$$

where $\Delta\alpha$ is the change of α given by:

$$\Delta\alpha = \frac{-sin\alpha}{Lcos\alpha}(\Delta u cos\beta + \Delta v sin\beta) \tag{147}$$

The stretch of the tangential spring can then be determined as:

$$\Delta d_{spring} = \Delta d - \Delta d_{rigid} = \Delta L cos\alpha. \tag{148}$$

Making use of the deformation of the springs determined in Eqs. (145)-(148) and considering also the contribution of the rotational displacements of the disks, the 12 forces acting on the representative disk can be expressed as:

$$F_1 = k[\frac{1}{2}(u - u_1) + \frac{\sqrt{3}}{2}(v_1 - v)] \tag{149}$$

$$F_2 = k[\frac{1}{2}(u_2 - u) + \frac{\sqrt{3}}{2}(v_2 - v)] \tag{150}$$

$$F_3 = k[(u_3 - u)] \tag{151}$$

$$F_4 = k[\frac{1}{2}(u_4 - u) + \frac{\sqrt{3}}{2}(v - v_4)] \tag{152}$$

$$F_5 = k[\frac{1}{2}(u - u_5) + \frac{\sqrt{3}}{2}(v - v_5)] \tag{153}$$

$$F_6 = k[(u - u_6)] \tag{154}$$

$$F_1' = k'[(\frac{1}{2}(u - u_1) + \frac{\sqrt{3}}{2}(v_1 - v))cos\alpha + R(\theta + \theta_1] \tag{155}$$

$$F_2' = k'[(\frac{1}{2}(u_2 - u) + \frac{\sqrt{3}}{2}(v_2 - v))cos\alpha + R(\theta + \theta_2] \tag{156}$$

$$F_3' = k'[(u_3 - u)cos\alpha + R(\theta + \theta_3)] \tag{157}$$

$$F_4' = k'[(\frac{1}{2}(u_4 - u) + \frac{\sqrt{3}}{2}(v - v_4))cos\alpha + R(\theta + \theta_4)] \tag{158}$$

$$F_5' = k'[(\frac{1}{2}(u - u_5) + \frac{\sqrt{3}}{2}(v - v_5))cos\alpha + R(\theta + \theta_5)] \tag{159}$$

$$F_6' = k'[(u - u_6)cos\alpha + R(\theta + \theta_6)] \tag{160}$$

where ' denotes the quantity belongs to a tangential spring, u_i and v_i are the displacements of a disk i in the x and y directions, and u and v are the displacements of the central disk in the x and y directions, as shown in Fig. 34.

5.4. Continuum model of the discrete metamaterial

If the linear and angular displacements of the disks u_j, v_j, θ_j are represented by continuous fields u, v and θ, then u_j, v_j and θ_j can be written in terms of derivatives of u, v and θ in a unique way by employing Taylor series expansions, such that:

$$u_1 = u - \frac{1}{2}au_{,x} + \frac{\sqrt{3}}{2}au_{,y} + \frac{1}{8}a^2u_{,xx} + \frac{3}{8}a^2u_{,yy} - \frac{\sqrt{3}}{4}a^2u_{,xy} + O(a^3) \tag{161}$$

$$u_2 = u + \frac{1}{2}au_{.x} + \frac{\sqrt{3}}{2}au_{,y} + \frac{1}{8}a^2u_{,xx} + \frac{3}{8}a^2u_{,yy} + \frac{\sqrt{3}}{4}a^2u_{,xy} + O(a^3) \tag{162}$$

$$u_3 = u + au_{,x} + \frac{1}{2}a^2u_{,xx} + O(a^3) \tag{163}$$

$$u_4 = u + \frac{1}{2}au_{,x} - \frac{\sqrt{3}}{2}au_{,y} + \frac{1}{8}a^2u_{,xx} + \frac{3}{8}a^2u_{,yy} - \frac{\sqrt{3}}{4}a^2u_{,xy} + O(a^3) \tag{164}$$

$$u_5 = u - \frac{1}{2}au_{,x} - \frac{\sqrt{3}}{2}au_{,y} + \frac{1}{8}a^2u_{,xx} + \frac{3}{8}a^2u_{,yy} + \frac{\sqrt{3}}{4}a^2u_{,xy} + O(a^3) \tag{165}$$

$$u_6 = u - au_{,x} + \frac{1}{2}a^2 u_{,xx} + O(a^3) \tag{166}$$

The Taylor series expansions for v and θ are similar, with u being replaced with v or θ. Substituting the expansions for u, v, and θ into the equations of motion of the discrete model of the chiral system, one can obtain the equations of motion for the chiral system. Considering this set of equations but with the substitutions $u_{mirror} = -u$, $v_{mirror} = v$, $\theta_{mirror} = \theta$, $y_{mirror} = y$ and $x_{mirror} = -x$, the following equations of motion for the continuous non-chiral metamaterial can be obtained:

$$a^2(k + k'cos^2\alpha)(\frac{9}{8}u_{,xx} + \frac{3}{8}u_{,yy} + \frac{3}{4}v_{,xy}) + 3ak'Rcos\alpha\theta_{,x} = m\ddot{u} \tag{167}$$

$$a^2(k + k'cos^2\alpha)(\frac{9}{8}v_{,yy} + \frac{3}{8}v_{,xx} + \frac{3}{4}u_{,xy}) + 3ak'Rcos\alpha\theta_{,y} = m\ddot{v} \tag{168}$$

$$-3aRk'cos\alpha(u_{,x} + v_{,y}) - \frac{3}{2}k'R^2a^2(\theta_{,xx} + \theta_{,yy}) - 12k'R^2\theta = I\ddot{\theta} \tag{169}$$

5.5. The effective material

Making use of the classical strain-displacement relations, the derivatives in Eqs. (167)-(169) can be represented in terms of strain components as:

$$u_{,xx} = \frac{\partial\varepsilon_{xx}}{\partial x} \qquad u_{,xy} = \frac{\partial\varepsilon_{xx}}{\partial y} \qquad u_{,yy} = 2\frac{\partial\varepsilon_{xy}}{\partial y} - \frac{\partial\varepsilon_{yy}}{\partial x} \tag{170}$$

$$v_{,xx} = 2\frac{\partial\varepsilon_{xy}}{\partial x} - \frac{\partial\varepsilon_{xx}}{\partial y} \qquad v_{,xy} = \frac{\partial\varepsilon_{yy}}{\partial x} \qquad v_{,yy} = \frac{\partial\varepsilon_{yy}}{\partial y} \tag{171}$$

The equations of motion 167-169 can then be written in terms of strains as:

$$a^2(k + k'cos^2\alpha)\left(\frac{9}{8}\frac{\partial\varepsilon_{xx}}{\partial x} + \frac{3}{8}\frac{\partial\varepsilon_{yy}}{\partial x} + \frac{3}{4}\frac{\partial\varepsilon_{xy}}{\partial y}\right) + 3ak'Rcos\alpha\theta_{,x} = m\ddot{u} \tag{172}$$

$$a^2(k + k'cos^2\alpha)\left(\frac{3}{8}\frac{\partial\varepsilon_{xx}}{\partial y} + \frac{9}{8}\frac{\partial\varepsilon_{yy}}{\partial y} + \frac{3}{4}\frac{\partial\varepsilon_{xy}}{\partial x}\right) + 3ak'Rcos\alpha\theta_{,y} = m\ddot{v} \tag{173}$$

$$-3aRk'cos\alpha(\varepsilon_{xx} + \varepsilon_{yy}) - \frac{3}{2}k'R^2a^2\Delta\theta - 12k'R^2\theta = I\ddot{\theta} \tag{174}$$

where Δ is the 2-D Laplacian operator in cartesian basis.

To provide a general description of the newly developed material model, all constants and equations should be posed per unit volume. For a representative volume element (RVE), as shown in Fig. 36, the volume can be determined from the geometry to be:

$$V = \frac{\sqrt{3}}{2}a^2 b \tag{175}$$

where b is the thickness of the RVE. Normalizing Eqs. 172-174 by dividing by the volume of the RVE, the governing equations of the new material can be expressed as:

$$\frac{9}{8}E\left(\frac{\partial \varepsilon_{xx}}{\partial x} + \frac{1}{3}\frac{\partial \varepsilon_{yy}}{\partial x} + \frac{2}{3}\frac{\partial \varepsilon_{xy}}{\partial y}\right) + \lambda\theta_{,x} = \rho\ddot{u} \tag{176}$$

$$\frac{9}{8}\left(\frac{\partial \varepsilon_{xx}}{\partial y} + \frac{1}{3}\frac{\partial \varepsilon_{yy}}{\partial y} + \frac{2}{3}\frac{\partial \varepsilon_{xy}}{\partial x}\right) + \lambda\theta_{,y} = \rho\ddot{v} \tag{177}$$

$$-\lambda(\varepsilon_{xx} + \varepsilon_{yy}) - q(a^2\Delta\theta + 8\theta) = i^*\ddot{\theta} \tag{178}$$

where:

$$E = \frac{2(k + k'cos^2\alpha)}{\sqrt{3}b} \qquad \lambda = \frac{2\sqrt{3}k'Rcos\alpha}{ab} \qquad q = \frac{\sqrt{3}k'R^2}{a^2 b} \tag{179}$$

$$\rho = \frac{2m}{\sqrt{3}a^2 b} \qquad i^* = \frac{2I}{\sqrt{3}a^2 b} \tag{180}$$

Comparing Eqs. 176-178 to the governing equations of a continuum body, the equations of motion of the new material can be expressed as:

$$\frac{\partial \sigma_{xx}}{\partial x} + \frac{\partial \sigma_{xy}}{\partial y} = \rho\ddot{u} \tag{181}$$

$$\frac{\partial \sigma_{xy}}{\partial x} + \frac{\partial \sigma_{yy}}{\partial y} = \rho\ddot{v} \tag{182}$$

$$M = i^*\ddot{\theta} \tag{183}$$

in which,

$$\sigma_{xx} = \frac{E}{1-\nu^2}(\varepsilon_{xx} + \nu\varepsilon_{yy}) + \lambda\theta \tag{184}$$

$$\sigma_{xy} = \frac{E}{2(1+\nu)}2\varepsilon_{xy} \tag{185}$$

$$\sigma_{yy} = \frac{E}{1-\nu^2}(\varepsilon_{yy} + \nu\varepsilon_{xx}) + \lambda\theta \tag{186}$$

$$M = -(\lambda(\varepsilon_{xx} + \varepsilon_{yy}) + q(a^2\Delta\theta + 8\theta)) \tag{187}$$

where ν=1/3. From these expressions we can easily identify Young's Modulus to be the constant given by Eq. 179, Poisson's ratio to be $\nu = 1/3$, and the shear modulus to be the following:

$$G = \frac{E}{2(1+v)} \tag{188}$$

6. Results and discussion

6.1. Effective properties of the new material

If a more "realistic" material model is adopted, and the springs are replaced by simple bars, the spring constants k and k' can be expressed as:

$$k = \frac{E_0 A_0}{a} \tag{189}$$

$$k' = \frac{E_1 A_1}{a cos\alpha} \tag{190}$$

where E_0 and E_1 are the Young's modulii of the central and tangential bars, A_0 and A_1 are the cross-sectional areas of the respective bars. The effective material constants can then be expressed as:

$$E = \frac{2(E_0 A_0 + E_1 A_1 cos\alpha)}{\sqrt{3}ab} \tag{191}$$

$$\lambda = \frac{E_1 A_1 R}{2\sqrt{3}a^2 b} \tag{192}$$

$$q = \frac{\sqrt{3}E_1 A_1}{cos\alpha}\frac{R^2}{a^3 b} = \frac{1}{4}\lambda\frac{sin\alpha}{cos\alpha} \tag{193}$$

The constitutive relations of the new material can further be expressed in tensorial form as:

$$\boldsymbol{\sigma} = \mathbf{C}\boldsymbol{\varepsilon} + \lambda\theta \tag{194}$$

$$M = -\lambda tr(\boldsymbol{\varepsilon}) - q(a^2\Delta\theta + 8\theta) \tag{195}$$

Correspondingly, the governing equations can be written in the following form:

$$\frac{E}{1-\nu^2}\left(\frac{\partial\varepsilon_{xx}}{\partial x} + \nu\frac{\partial\varepsilon_{yy}}{\partial x}\right) + G\frac{\partial\varepsilon_{xy}}{\partial y} + \lambda\frac{\partial\theta}{\partial x} = \rho\ddot{u} \tag{196}$$

$$\frac{E}{1-\nu^2}\left(\frac{\partial\varepsilon_{yy}}{\partial y} + \nu\frac{\partial\varepsilon_{xx}}{\partial y}\right) + G\frac{\partial\varepsilon_{xy}}{\partial x} + \lambda\frac{\partial\theta}{\partial y} = \rho\ddot{v} \tag{197}$$

$$-\lambda(\varepsilon_{xx} + \varepsilon_{yy}) - q(a^2\Delta\theta + 8\theta) = i^*\ddot{\theta} \tag{198}$$

6.1.1. Comparison to Micropolar Model

The governing equations for a two-dimensional micropolar continuum with no body forces or body moments are given in Eqs. 14- 16. The similarity between Eqs. 167-169 and Eqs. 14-16 is clearly seen. Eq. 167 and Eq. 15 have the same θ terms, yet have opposite derivatives of the linear displacements u and v. This shows that this model is fundamentally different from the micropolar model. In fact, the behaviour of those terms in the new model can be clearly observed when the response of the original discrete model to the rotational motion (θ) is evaluated. This is the behaviour the new model captures but the micropolar model does not.

For one-dimensional cases where $v = 0$ and $\frac{\partial}{\partial y} = 0$ the current material model given by 167, 168 and 169 becomes the following:

$$a^2\frac{9}{8}(k + k'cos^2\alpha)u_{,xx} + 2ak'Rcos\alpha\theta_{,x} = \rho\ddot{u} \tag{199}$$

$$-\left(\frac{3}{2}kR^2a^2\theta_{,xx} + 2ak'Rcos\alpha u_{,x} + 12k'R^2\theta\right) = i^*\ddot{\theta} \tag{200}$$

which correspond to the following one-dimensional constitutive law:

$$\sigma_{xx} = E\varepsilon_{xx} + \lambda\theta \tag{201}$$

$$M = -(\lambda\varepsilon_{xx} + q(a^2\theta_{,xx} + 8\theta)) \tag{202}$$

In comparison, when reduced to one dimension, the micropolar model yields the expressions given by Eqs. 21 and 22 Clearly, in the governing equations, and subsequently in the constitutive law, the rotational effects and linear displacements are completely decoupled in the micropolar model. The current model, however, when reduced to one dimension, predicts strong local rotational-translational coupling, which is consistent with that observed from the discrete model.

6.1.2. Comparison to Previously Proposed 1-D Model with Local Rotation

A one-dimensional elastic metamaterial with local rotation, which has a different spring-disk system, has been studied [37] and the following model was developed:

$$kL^2\frac{\partial^2 u}{\partial x^2} - 2kRL\frac{\partial \theta}{\partial x} = m\ddot{u} \tag{203}$$

$$2kRL\frac{\partial u}{\partial x} - kR^2L^2\frac{\partial^2 \theta}{\partial x^2} - 4kR^2\theta = I\ddot{\theta}. \tag{204}$$

where k is a spring constant, L is a characteristic length associated with the model, and R is the radius of the rigid disks. The model furnishes the following constitutive law:

$$\sigma = E_0\varepsilon - \eta\theta \tag{205}$$

where:

$$E_0 = \frac{kL}{A} \qquad \eta = \frac{2RE_0}{L} \tag{206}$$

It is clear to see that the constitutive laws, and the governing equations of these models, when looked at in one dimension possess remarkable similitude although derived from different discrete spring-disk systems. In fact, the format of the governing equations, and as a result the format of the constitutive law is identical, and differs only by characteristic parameters of the specific discrete structures of the two materials. The current model provides a general description of a class of discrete metamaterials with local rotation.

6.1.3. 1-D harmonic transverse wave

A harmonic transverse wave propagating in the x-direction has the following displacement profile:

$$u = 0, \qquad v = V_0 e^{iK(x-ct)}, \qquad \theta = 0 \tag{207}$$

where V_0 is the amplitude, K is the wavenumber, c is wavespeed, i is the imaginary unit and t is time. This displacement profile furnishes the following stresses and strains from Eq. 184-186 and the classical definitions of strain:

$$\sigma_{xx} = \sigma_{yy} = 0, \qquad \sigma_{xy} = \frac{1}{2} V_0 i K e^{iK(x-ct)} \tag{208}$$

$$\varepsilon_{xx} = \varepsilon_{yy} = 0, \qquad \varepsilon_{xy} = i V_0 G K e^{iK(x-ct)} \tag{209}$$

Substituting Eqs. 207-209 into Eq. 182, the following equation is obtained:

$$(V_0 \omega^2 \rho - K^2 V_0 G) e^{iK(x-ct)} = 0 \tag{210}$$

which trivially returns the following dispersion relation:

$$\omega^2 \rho - K^2 G = 0 \tag{211}$$

The transverse wave is not dispersive and hence the wavespeed has the following simple expression:

$$c = \sqrt{\frac{G}{\rho}} \tag{212}$$

which is the exact same as the classical result for a shear wave.

6.1.4. 1-D harmonic longitudinal wave

A harmonic longitudinal wave propagating in the x-direction has the following displacement profile:

$$u = U_0 e^{iK(x-ct)}, \qquad v = 0, \qquad \theta = \theta_0 e^{iK(x-ct)} \tag{213}$$

where θ_0 and U_0 are the amplitudes, K is the wavenumber, and c is the wavespeed. This displacement profile furnishes the following stresses and strains from Eq. 184-186:

$$\sigma_{xx} = \frac{E}{1-\nu^2} (U_0 i K) e^{iK(x-ct)} + \lambda \theta_0 e^{iK(x-ct)} \tag{214}$$

$$\sigma_{yy} = \frac{E\nu}{1-\nu^2} (U_0 i K) e^{iK(x-ct)} + \lambda \theta_0 e^{iK(x-ct)} \tag{215}$$

$$\sigma_{xy} = 0 \tag{216}$$

$$\varepsilon_{xx} = U_0 iK e^{iK(x-ct)}, \qquad \varepsilon_{xy} = \varepsilon_{yy} = 0 \tag{217}$$

Substituting these stress-strain definitions into Eq. 181 and Eq. 174 results in the following homogeneous equations:

$$\begin{bmatrix} \omega^2\rho - \frac{K^2E}{1-\nu^2} & iK\lambda \\ iK\lambda & q(8-a^2K^2) - i^*\omega^2 \end{bmatrix} \begin{bmatrix} U_0 \\ \theta_0 \end{bmatrix} = \begin{bmatrix} 0 \\ 0 \end{bmatrix} \tag{218}$$

where $\omega = cK$ and all other quantities are as previously defined. Taking the determinant and setting it to zero, the following dispersion relation can be obtained:

$$\left(\rho\omega^2 - \frac{K^2E}{1-v^2}\right)(8q - a^2K^2q - i^*\omega^2) + K^2\lambda^2 = 0 \tag{219}$$

Defining the following normalized frequency, wavenumber and wavespeed:

$$\overline{\Omega} = \sqrt{\frac{i^*}{q}}\omega = \frac{\omega}{\omega_0} \qquad \overline{k} = Ka \qquad \overline{c} = \overline{\Omega}/\overline{k} \tag{220}$$

where:

$$\omega_0 = \sqrt{\frac{q}{i^*}} = \sqrt{\frac{\sqrt{3}E_1 A sin^2\alpha}{4\rho ab\xi^2 cos\alpha}} \tag{221}$$

and introducing the following constants:

$$E' = \frac{E}{1-\nu^2} \tag{222}$$

$$\zeta^0 = \frac{\overline{\zeta^0}}{a^2} = \frac{E'}{\rho}\frac{i^*}{a^2q} = \frac{E'}{E_1}\frac{4b\xi^2 cos\alpha}{\sqrt{3}aA_1 sin^2\alpha} \tag{223}$$

$$\eta^0 = \frac{\overline{\eta^0}}{a^2} = \frac{i^*\lambda^2}{a^2q^2\rho} = \frac{16\xi^2}{a^2 tan^2\alpha} \tag{224}$$

the dispersion relation can be expressed explicitly in the following normalized

format:

$$\overline{\Omega}^2 = \frac{-(\eta^0 - 8\zeta^0)\overline{c}^2 - 8\overline{c}^4}{\zeta^0 - (1-\zeta^0)\overline{c}^2 - \overline{c}^4} \tag{225}$$

or in the following form to obtain an explicit expression for $\overline{k}^2$:

$$\overline{k}^2 = \frac{\overline{\Omega}^2(1-\zeta^0) - (\eta^0 - 8\zeta^0)}{2\zeta^0} \pm \frac{1}{2\zeta^0}\sqrt{\left(\overline{\Omega}^2(1-\zeta^0) - (\eta^0 - 8\zeta^0)\right)^2 + 4\zeta^0\overline{\Omega}^2(\overline{\Omega}^2 - 8)} \tag{226}$$

Equations 225 and 226 both represent the general dispersion relation for a longitudinal wave in the new material. It should be mentioned that the wave is clearly dispersive. The dispersion relation is dominated by two parameters; η^0 and ζ^0.

The parameter η^0 is controlled primarily by geometry, and represents the effect of the local rotation within the material due to the intrinsic material structure, with small η^0 representing significant local rotational effects, and large η^0 representing negligible local rotational effects. The parameter ζ^0 is dominated by the ratio of the overall effective elastic modulus of the material and the modulus of the tangential bars in the physical model. This means it is a measure of the effect of local rotation with respect to the effect of translation, with moderate values of ζ^0 representing very significant rotational effects, and extremely large values of ζ^0 representing insignificant rotational effects. However, unlike η^0, this parameter is primarily controlled by material properties. The lower bound of ζ^0 is $\frac{3}{16}\eta^0$, which corresponds to the case where the central spring is removed. In the limiting case of $\eta^0 = 0$, the dispersion relation given by Eq. 225 reduces to:

$$\overline{\Omega}^2 = \frac{8\overline{c}^2\left(\omega_0^2\overline{\zeta^0} - c^2\right)}{\left(\overline{\zeta}^0\omega_0^2 - c^2\right)\left(a^2\omega_0^2 + c^2\right)} \tag{227}$$

This results in two branches:

$$\overline{k} = \overline{\Omega}/\sqrt{\zeta^0} \qquad \overline{k} = \sqrt{8 - \overline{\Omega}^2} \tag{228}$$

The first of these forms a wave without dispersion and the second is dispersive with a cutoff frequency of $\overline{\Omega} = 2\sqrt{2}$. For very high frequencies ($\overline{\Omega} \to \infty$) the

dispersion relation becomes:

$$-\left(\frac{\overline{\Omega}}{\overline{k}}\right)^4 + (\zeta^0 - 1)\left(\frac{\overline{\Omega}}{\overline{k}}\right)^2 + \zeta^0 = 0 \tag{229}$$

which results in a constant wavespeed of:

$$\frac{\overline{\Omega}}{\overline{k}} = \sqrt{\zeta^0} \tag{230}$$

When the parameter $a^2 \to 0$ the dispersion relation becomes the following:

$$\overline{\Omega}^2 = 8 - \frac{\omega_0^2 \overline{\eta}^0}{\overline{\zeta}^0 \omega_0^2 - c^2} \tag{231}$$

This indicates a wave which is certainly still dispersive, despite the "size effect" of the unit cell vanishing when $a^2 \to 0$. This means that in a perfect continuum material with no discrete structure the model still predicts new phenomena.

The general dispersion relation for the longitudinal wave given in Eq. 225 for different values of governing parameters ζ^0 and η^0 is shown in Figs. 37-42. Focusing on the properties of wave propagation, only the real part of the wavenumber is presented in these figures. Figure 37 shows the variation of $\overline{c}$ with $\overline{\Omega}$ for different values of η^0 for the case where $\zeta^0 = 0.1$. It is evident that there exists a stop-band whose width is dependent on the value of the parameter η^0, with larger values of η^0 producing a wider stop band. It can also be clearly observed that the stop-band always begins at $\overline{c} = \sqrt{\zeta^0}$, and increases in width towards $\overline{c} = 0$ with an increase in η^0. One can also observe that for large values of normalized frequency all curves tend towards one wavespeed, as predicted by Eq. 230. The limiting case where $\eta^0 \to 0$ is shown by solid lines. The branch which exhibits a constant wavespeed shown by Eq. 228 is not shown as it appears in both the numerator and denominator of the dispersion relation, however it is still a valid solution, and behaviour similar to this Is seen for the other cases, represented by the straight line at $\overline{c} \approx \sqrt{\zeta^0}$. Figures 38 and 39 show behaviour similar to that exhibited in figure 37, with larger values of η^0 corresponding to wider stop-bands. Additionally, for an increase in the parameter ζ^0 increases the value of the constant wavespeed branch of the solution, as expected. This behaviour

clearly represents new wave propagation phenomena due to the coupled local rotational effects along with translational effects, as more interesting and physically relevant phenomena such as the creation of wider stop-bands occur at moderate values of both ζ^0 and η^0.
Figure 40 shows the variation of $\overline{k}$ with $\overline{\Omega}$ for different values of ζ^0 in the case where $\eta^0 \to 0$. As previously mentioned, the constant wavespeed branch is not shown, as it cancels in the general dispersion relation when $\eta \to 0$, however it remains a valid solution. Figures 41 and 42 show the variation of $\overline{k}$ with $\overline{\Omega}$ for different values of ζ^0 in the case where $\eta^0 = 1$ and $\eta^0 = 10$, respectively. Similar to previous examples, the stop-band always begins at $\overline{c} = \sqrt{\zeta^0}$, meaning that the location of the stop-band is controlled by the value of the parameter ζ^0 alone. This is confirmed in figures 41 and 42. This combined with the fact that the width of the stop-band is controlled by the value of the parameter η^0 indicates potential for application in the field of vibration filtering via the creation of stop-bands at desired frequencies by tuning both geometric and material parameters.

6.2. Conclusions

- The traditional micropolar model is insufficient to describe all of the phenomena occurring in this class of 2-D metamaterials with strong local rotational-translational coupling
- A new constitutive law was proposed, and then ratified using a representative structure for the aforementioned class of metamaterials
- New material constants λ and q were obtained in terms of both material properties and geometric parameters
- General 2-D harmonic wave propagation was studied by investigating the dispersion relations resulting from longitudinal and transverse harmonic wave propagation
- Two controlling dimensionless parameters, η^0 and ζ^0 were found to govern longitudinal wave propagation
- η^0 represents the significance of rotational effects due to intrinsic material microstructure
- ζ^0 is a measure of the effect of local rotation with respect to that of translational motion, however unlike η^0 is controlled primarily by material modulii rather than geometric factors
- The dispersion curves with the most unique phenomena were obtained when both governing parameters are at moderate levels, highlighting the necessity to include local rotational effects as well as translational effects

- Numerical analysis indicates potential applications in the field of precise vibration elimination at a targeted frequency as well as vibration elimination for a wide range of frequencies

6.3. Figures

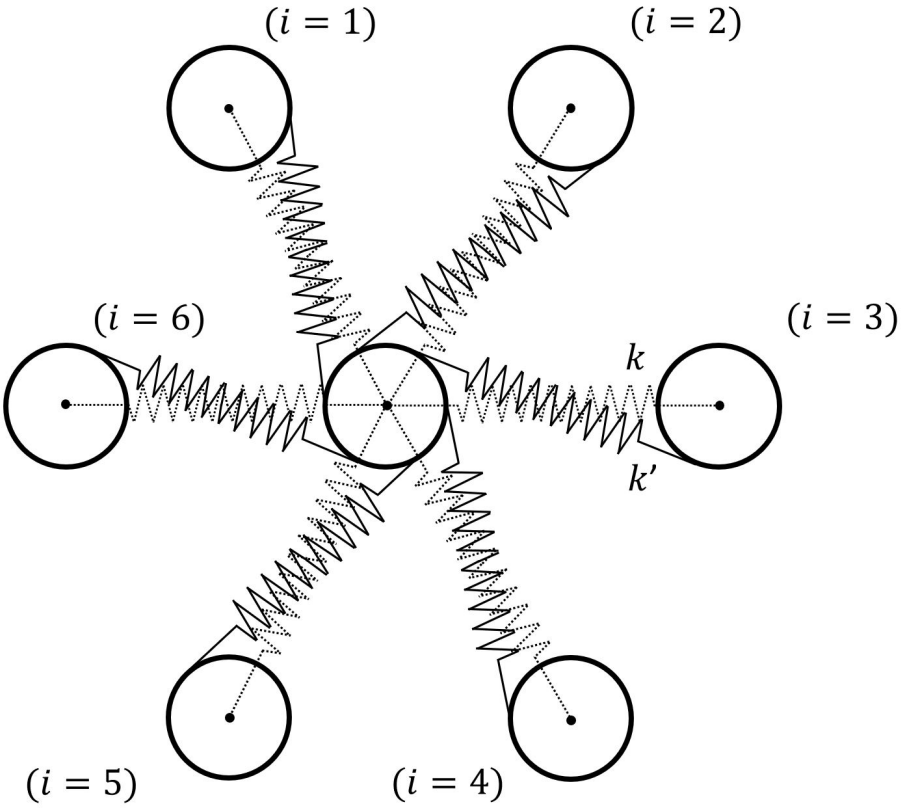

Figure 34: The fundamental unit cell for the representative metamaterial

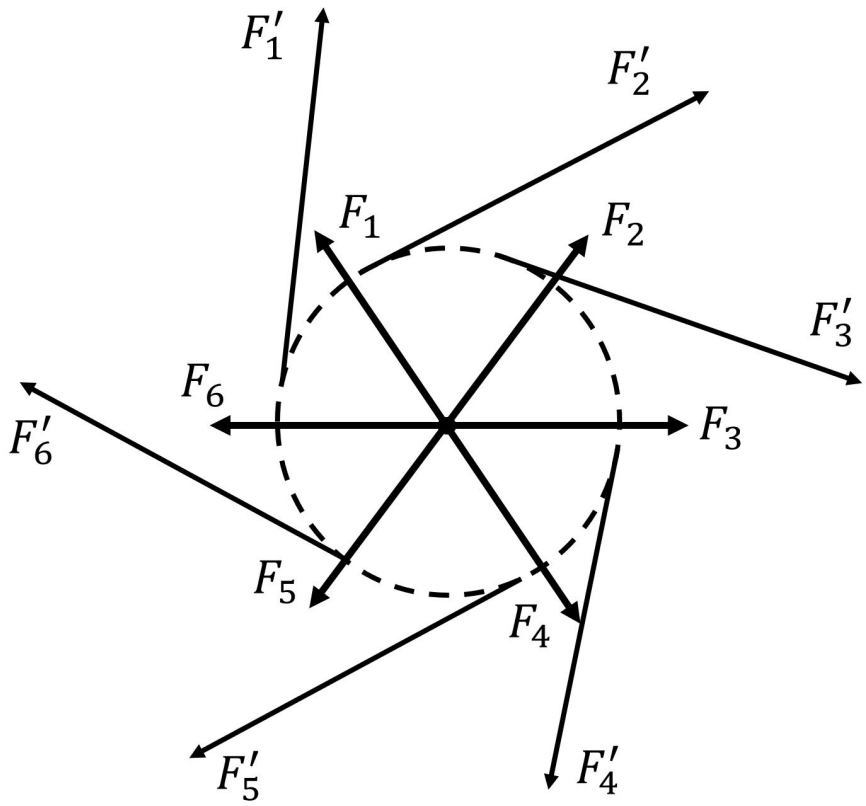

Figure 35: The forces acting on one disk in the discrete model of the metamaterial

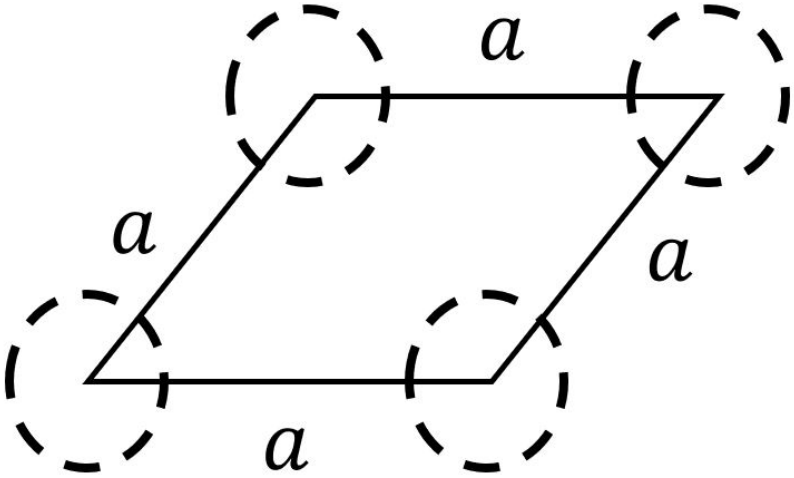

Figure 36: A representative volume element of the metamaterial

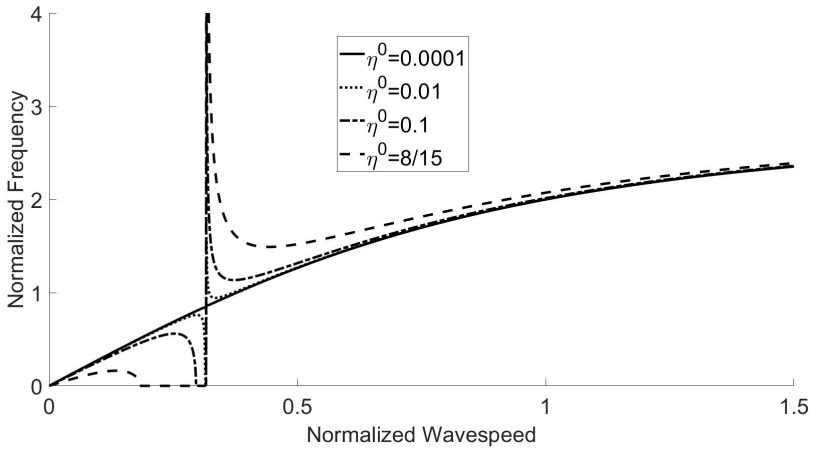

Figure 37: The dispersion curves when governing parameter η^0 is varied with $\zeta^0 = 0.1$ held constant

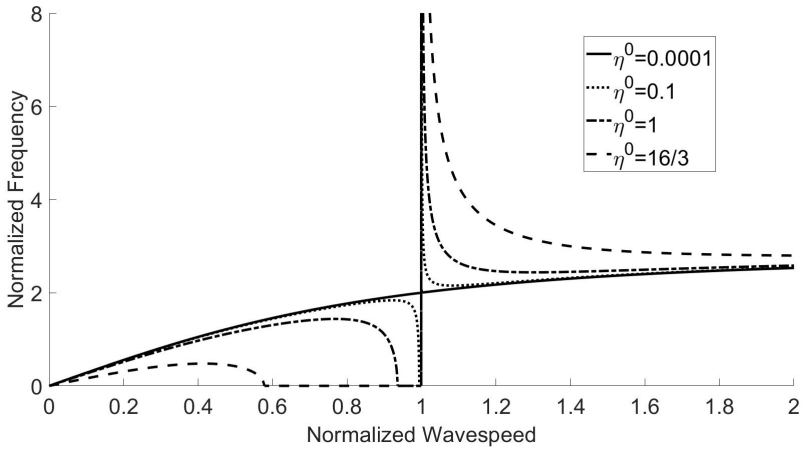

Figure 38: The dispersion curves when governing parameter η^0 is varied with $\zeta^0 = 1$ held constant

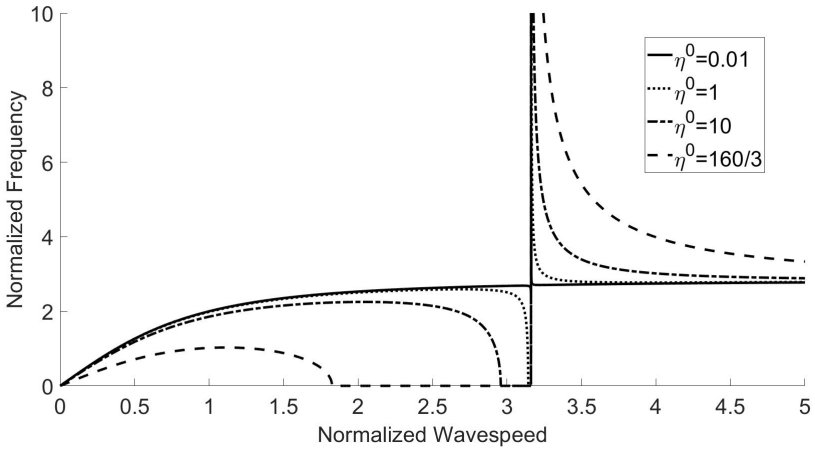

Figure 39: The dispersion curves when governing parameter η^0 is varied with $\zeta^0 = 10$ held constant

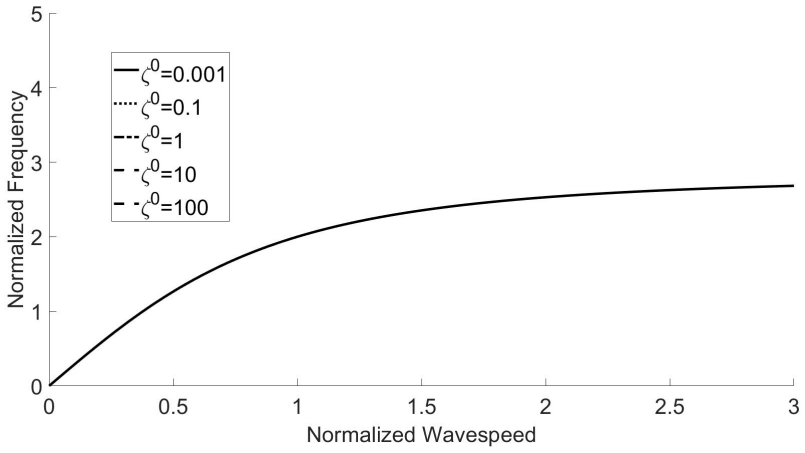

Figure 40: The dispersion curves when governing parameter ζ^0 is varied with $\eta^0 \to 0$ held constant

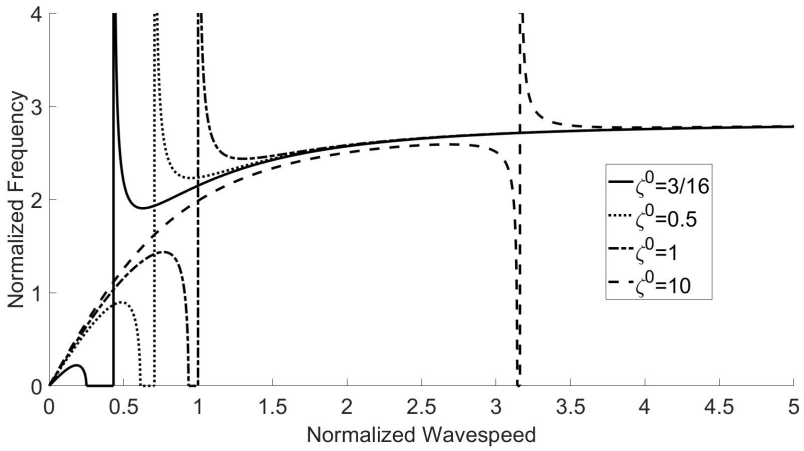

Figure 41: The dispersion curves when governing parameter ζ^0 is varied with $\eta^0 = 1$ held constant

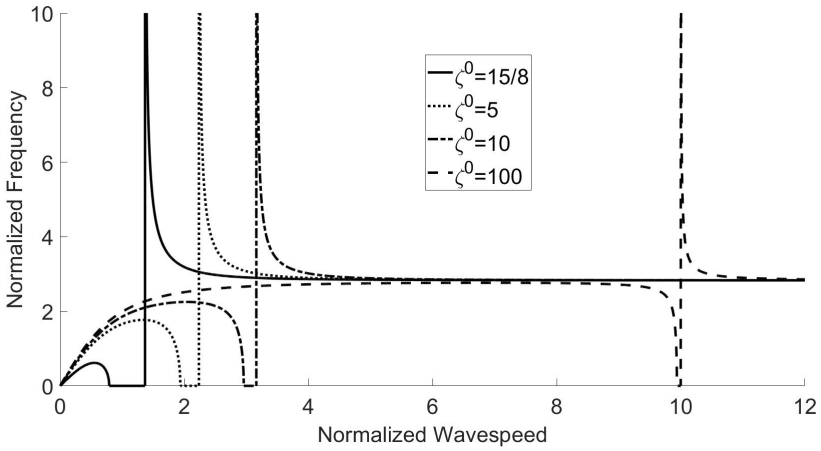

Figure 42: The dispersion curves when governing parameter ζ^0 is varied with $\eta^0 = 10$ held constant

7. Dispersive Surface Waves Propagating Through a Continuous Elastic Medium with Local Rotation

7.1. Symbols

Symbol	Meaning
e	Euler's number
a	A characteristic length scale
A	The amplitude of the x component of the displacement
$\overline{A}$	A variable related to the amplitudes A and B
A_1	The amplitude of the x component of the displacement resulting from b_1
$\overline{A}_1$	A variable related to the amplitudes A and B resulting from b_1
A_2	The amplitude of the x component of the displacement resulting from b_2
$\overline{A}_2$	A variable related to the amplitudes A and B resulting from b_2
B	The amplitude of the y component of the displacement
$\overline{B}$	A variable related to the amplitudes A and B
B_1	The amplitude of the y component of the displacement resulting from b_1
$\overline{B}_1$	A variable related to the amplitudes A and B resulting from b_1
B_2	The amplitude of the y component of the displacement resulting from b_2
$\overline{B}_2$	A variable related to the amplitudes A and B resulting from b_2
b	A damping parameter
b_1	The first solution for the damping parameter
b_2	The second solution for the damping parameter
C	The amplitude of the local rotational displacement field
C_1	The amplitude of the local rotational displacement field resulting from b_1
C_2	The amplitude of the local rotational displacement field resulting from b_2
c	The wavespeed of the surface wave
c_T	The transverse wavespeed
c_L	A constant resembling a wavespeed
$\overline{c}_L$	A constant representing the modified longitudinal wavespeed
c_R	The Rayleigh wavespeed
E	Young's Modulus
f	A parameter governing surface wave propagation
G	Shear modulus
g	A parameter governing surface wave propagation
i^*	The volumetric moment of inertia of the continuum
i	The imaginary unit
k	The wavenumber

$\overline{k}$	The normalized wavenumber
k_0	The quantity used to normalize k
M	The local moment
q	A rotational elastic constant
t	Time
u	The x component of the displacement field
u_1	The x component of the displacement field resulting from b_1
u_2	The x component of the displacement field resulting from b_2
$\ddot{u}$	The x component of the acceleration field
v	The y component of the displacement field
v_1	The y component of the displacement field resulting from b_1
v_2	The y component of the displacement field resulting from b_2
$\ddot{v}$	The y component of the acceleration field
x	The direction along the free surface of the half-plane
y	The direction perpendicular to the free surface
z	The out-of-plane direction
Δ	The 2-D Laplacian operator
ε_{AB}	The strain on a plane with normal in the A direction in the direction of B
λ	A rotational coupling constant
ν	Poisson's Ratio
ω	Angular frequency
ω_0	A constant used to normalize ω in the general dispersion relation
ρ	The volumetric mass density of the continuum
σ_{AB}	The stress on a plane with normal in the A direction in the direction of B
θ	The local rotation field
θ_1	The local rotation field resulting from b_1
θ_2	The local rotation field resulting from b_2
$\ddot{\theta}$	The angular acceleration of the local rotational field

In this chapter the model developed in the previous chapter is used to investigate the propagation of surface waves in a continuous medium with local rotation, and by extension, the class of 2-D metamaterials discussed in the previous chapter. Necessary conditions for the decay parameters b_1 and b_2 were obtained, as well as a general dispersion relation. The dispersive character of the surface waves was investigated in both simplified cases, as well as in the most general case. The motion of the particles residing on the surface of the elastic continuum was also investigated. This chapter showcases some unique phenomenon that occur as a result of the local rotational effects, highlighting the usefulness of the model developed in the previous chapter.

7.2. Statement of the Problem and Governing Equations

The problem envisaged is the propagation of surface waves along the free surface of a two-dimensional continuous elastic half-plane. The continuous medium is modelled from an elastic metamaterial system and assumed to be homogeneous, isotropic, and linear elastic, but with local rotation, which stems from the internal rotation inside the unit cell of the metamaterial. A Cartesian coordinate system (x, y, z) is used to describe the half-plane with the x-axis being along the free surface of the half-plane, the y-axis being perpendicular to the free surface with the outer normal in the negative y-direction, and the z-axis being in the out-of-plane direction. The half-plane is traction free in the out-of-plane direction. As a result, the plane stress condition can be used. In the following study it is assumed that the surface wave propagates in the positive x-direction.

A representative unit cell for a material belonging to this class of metamaterials is shown in Fig. 34. As in the previous chapter, this unit cell the mass-spring system generates the overall inertia and modulus from the mass of the disk and the spring constants. The rigid disk is allowed to rotate and the local rotation of the disk will affect and be affected by the deformation of the cell. This discrete system, superimposed with its mirror image, can be modelled as a continuous elastic medium, as shown in the previous chapter. The new elastic medium containing local rotation is assumed to have the following constitutive relations under the plane stress condition:

$$\sigma_{xx} = \frac{E}{1-\nu^2}(\varepsilon_{xx} + \nu\varepsilon_{yy}) + \lambda\theta \tag{232}$$

$$\sigma_{yy} = \frac{E}{1-\nu^2}(\varepsilon_{yy} + \nu\varepsilon_{xx}) + \lambda\theta \tag{233}$$

$$\sigma_{xy} = \frac{E}{2(1+\nu)}2\varepsilon_{xy} \tag{234}$$

where σ_{ij} and ε_{ij} are the stress and strain components in the i direction on a plane with normal in the j direction respectively, θ is the local rotational displacement, λ is a coupling parameter which represents the influence of local rotation, E is Young's Modulus, and ν is Poisson's ratio.
The equations of motion are given by:

$$\frac{\partial\sigma_{xx}}{\partial x} + \frac{\partial\sigma_{xy}}{\partial y} = \rho\ddot{u} \tag{235}$$

$$\frac{\partial\sigma_{xy}}{\partial x} + \frac{\partial\sigma_{yy}}{\partial y} = \rho\ddot{v} \tag{236}$$

where ρ is the mass density, and u and v are the displacements in the x and y directions, respectively. For the discrete system shown in Fig. 34, the local rotation will be governed by the following equation, which has been developed previously:

$$M = i^*\ddot{\theta} \tag{237}$$

$$M = -(\lambda(\varepsilon_{xx} + \varepsilon_{yy}) + q(a^2\Delta\theta + 8\theta)) \tag{238}$$

where M is the local moment, i^* is the moment of inertia per unit volume of the material, a is a characteristic length scale, q is a constant representing the local rotational stiffness, and Δ is the Laplacian operator in Cartesian basis. It should be mentioned that λ and q depend on the geometry and material properties of the unit cell of the particular material. For the specific unit cell geometry shown in Fig. 34, λ and q are given in the previous chapter.

7.3. Surface Waves with Local Rotational Effects

Consider a surface wave in the current continuous medium. Similar to a classical Rayleigh wave, the following displacement profile is assumed

$$u(x,y,t) = Ae^{-by}e^{ik(x-ct)}, \qquad v(x,y,t) = Be^{-by}e^{ik(x-ct)} \tag{239}$$

where c is the phase velocity of the wave given by $c = \omega/k$. ω and k are the circular frequency and wavenumber, respectively, A and B are the amplitudes of each of the displacement components, i is the imaginary unit, x and y are

the planar Cartesian coordinates, t is time, and b is a unknown coefficient with its real part, $Re(b)$, representing the decay of the field away from the free surface. The local rotational displacement θ, which depends directly on u and v, will have a similar displacement profile, given by

$$\theta(x, y, t) = Ce^{-by}e^{ik(x-ct)} \tag{240}$$

where C is the amplitude of θ.
The general solution of the surface wave can be built by superimposing all possible waveforms, of which the format is given by Eqs. 239 and 240. The decay parameter b has multiple solutions, and the general solution of the displacement field is obtained by taking the superposition of each of these solutions.
For a surface wave propagating in the x-direction along the free surface, the following traction-free boundary conditions should be satisfied:

$$\sigma_{yy}(x, 0, t) = 0 \qquad \sigma_{yx}(x, 0, t) = 0. \tag{241}$$

7.3.1. The general form of the surface wave

For the waveform given by Eqs. 239 and 240 to be valid, the decay parameter b must be in a specific form to satisfy the equations of motion. To determine the decay parameter b, substituting the displacement profiles given by Eq. 239 and 240 into the governing equations given by Eqs. 235-237 and using the constitutive relations given by Eqs. 232-234 and Eq. 238, the following system of equations can be obtained:

$$\frac{E}{1-\nu^2}\left(\frac{1-\nu}{2}b^2 - k^2\right)A - \frac{E}{2(1-\nu)}ikbB + ik\lambda C = -\omega^2\rho A \tag{242}$$

$$\frac{E}{1-\nu^2}\left(b^2 - \frac{1-\nu}{2}k^2\right)B - \frac{E}{2(1-\nu)}ikbA - b\lambda C = -\omega^2\rho B \tag{243}$$

$$\lambda(ikA - bB) + a^2q(b^2 - k^2 + 8q)C = i^*\omega^2 C \tag{244}$$

To simplify these equations, parameters A and B will be replaced by $\overline{A}$ and $\overline{B}$ using the following relations:

$$A = ik\overline{A} + b\overline{B} \qquad B = -b\overline{A} + ik\overline{B} \tag{245}$$

Making use of the newly defined $\overline{A}$ and $\overline{B}$, after some algebraic manipulation, Eqs. 242 and 243 can be decoupled and the following equation containing only $\overline{B}$ can be obtained:

$$\frac{E}{1-\nu^2}\frac{1-\nu}{2}(k^2-b^2)^2\overline{B} = -\rho\omega^2(b^2-k^2)\overline{B} \tag{246}$$

which can be simplified to:

$$\left(b^2-k^2+\frac{\omega^2}{c_T^2}\right)\overline{B} = 0 \tag{247}$$

by using the relations

$$c_T^2 = \frac{G}{\rho}, \qquad G = \frac{E}{2(1+\nu)} \tag{248}$$

where c_T is the transverse wavespeed. After some further algebraic manipulation using Eqs. 242 and 243, the following simplified equation for only $\overline{A}$ and C is obtained:

$$\frac{E}{1-\nu^2}(k^2+b^2)\left(k^2-b^2-\frac{\omega^2}{c_L^2}\right)\overline{A} - \lambda(k^2+b^2)C = 0 \tag{249}$$

where c_L is given by:

$$c_L^2 = \frac{E}{(1-\nu^2)\rho} \tag{250}$$

In addition, Eq. 244 becomes:

$$\lambda(b^2-k^2)\overline{A} + q(a^2(b^2-k^2)+8)C = i^*\omega^2 C \tag{251}$$

Collecting Eqs. 246, 249 and 251, the following system of equations is formed:

$$\begin{bmatrix} 0 & k^2-b^2-\frac{\omega^2}{c_T^2} & 0 \\ \frac{E}{1-\nu^2}(k^2+b^2)\left(k^2-b^2-\frac{\omega^2}{c_L^2}\right) & 0 & -\lambda(k^2+b^2) \\ \lambda(b^2-k^2) & 0 & q(a^2(b^2-k^2)+8)-i^*\omega^2 \end{bmatrix} \begin{bmatrix} \overline{A} \\ \overline{B} \\ C \end{bmatrix} = \begin{bmatrix} 0 \\ 0 \\ 0 \end{bmatrix} \tag{252}$$

Making the determinant zero, the following necessary condition for wave propagation is obtained:

$$\left(k^2 - b^2 - \frac{\omega^2}{c_T^2}\right)(k^2+b^2)\left(\frac{E}{1-\nu^2}\left(k^2 - b^2 - \frac{\omega^2}{c_L^2}\right)\left(q(a^2(b^2-k^2)+8) - i^*\omega^2\right) + \lambda^2(b^2-k^2)\right) = 0 \tag{253}$$

One possible solution from this equation is $b = \pm ik$. However, this furnishes a two-dimensional wave propagating in both the x and y directions without decaying with y. This is clearly not a surface wave, so this solution will be considered extraneous for the purposes of this study. Clearly, a value of b^2 that satisfies this equation is given by Eq. 247. So for the current problem, two solutions b_1 and b_2 are considered, which correspond to two different waveforms and satisfy the equations of motion given by:

$$b_1^2 = k^2 - \frac{\omega^2}{c_T^2} \qquad with \qquad \overline{B}_1 \neq 0, \overline{A}_1 = 0 \tag{254}$$

and

$$\frac{E}{1-\nu^2}\left(k^2 - b_2^2 - \frac{\omega^2}{c_L^2}\right)\left[q(a^2(b_2^2-k^2)+8) - i^*\omega^2\right] + \lambda^2(b_2^2-k^2) = 0 \tag{255}$$

with $\overline{A}_2 \neq 0$ and $\overline{B}_2 = 0$.

7.3.2. Dispersion Relation of the Surface Wave with Local Rotation

There are two groups of solutions; one of which is characterized by variables b_1, $\overline{A}_1$, $\overline{B}_1$ and C_1 with b_1 given by Eq. 254 and the other is characterized by variables b_2, $\overline{A}_2$, $\overline{B}_2$ and C_2 with b_2 given by Eq. 255. Making use of the system of equations in Eq. 252 we can determine the relations between the constants of each solution to be the following:

$$\overline{A}_1 = C_1 = 0 \tag{256}$$

$$\overline{B}_2 = 0 \tag{257}$$

$$C_2 = -\frac{\lambda(b_2^2 - k^2)}{q(a^2(b_2^2-k^2)+8) - i^*\omega^2}\overline{A}_2 \tag{258}$$

Accordingly, the original amplitudes of the displacements for the two solutions, A_1, A_2, B_1 and B_2 can be expressed in terms of $\overline{A_1}$ and $\overline{B_2}$ as:

$$A_1 = b_1\overline{B}_1 \qquad B_1 = ik\overline{B}_1 \tag{259}$$

$$A_2 = ik\overline{A}_2 \qquad B_2 = -b_2\overline{A}_2 \tag{260}$$

The general solution of the displacements u, v, and θ can then be determined as:

$$u(x,y,t) = u_1 + u_2 \qquad v(x,y,t) = v_1 + v_2 \qquad \theta(x,y,t) = \theta_1 + \theta_2. \tag{261}$$

Making use of the displacement profiles defined by Eqs. 239 and 240 the following expressions for the displacements are obtained:

$$u(x,y,t) = b_1\overline{B}_1 e^{-b_1 y} e^{ik(x-ct)} + ik\overline{A}_2 e^{-b_2 y} e^{ik(x-ct)} \tag{262}$$

$$v(x,y,t) = ik\overline{B}_1 e^{-b_1 y} e^{ik(x-ct)} - b_2\overline{A}_2 e^{-b_2 y} e^{ik(x-ct)} \tag{263}$$

$$\theta(x,y,t) = -\frac{\lambda(b_2^2 - k^2)}{q(a^2(b_2^2 - k^2) + 8) - i^*\omega^2}\overline{A}_2 e^{-b_2 y} e^{ik(x-ct)}. \tag{264}$$

The stresses can be obtained using the constitutive relations given by Eqs. 233 and 234 as:

$$\sigma_{yy}(x,y,t) = -\frac{\lambda^2(b_2^2 - k^2)}{q(a^2(b_2^2 - k^2) + 8) - i^*\omega^2}\overline{A}_2 e^{-b_2 y} e^{ik(x-ct)} \tag{265}$$

$$\sigma_{xy}(x,y,t) = G\left(-(b_1^2 + k^2)\overline{B}_1 e^{-b_1 y} - 2ikb_2\overline{A}_2 e^{-b_2 y}\right) e^{ik(x-ct)}. \tag{266}$$

The traction free boundary conditions given in Eq. 241 yield the following two equations:

$$\frac{E}{1-\nu^2}ikb_1(\nu-1)\overline{B}_1 + \left(\frac{E}{1-\nu^2}(b_2^2 - \nu k^2) - \frac{\lambda^2(b_2^2 - k^2)}{q(a^2(b_2^2 - k^2) + 8) - i^*\omega^2}\right)\overline{A}_2 = 0 \tag{267}$$

$$(b_1^2 + k^2)\overline{B}_1 + 2ikb_2\overline{A}_2 = 0. \tag{268}$$

which, after some algebraic manipulation, yield the following dispersion relation:

$$(b_1^2 + k^2)^2 - 4k^2 b_1 b_2 = 0 \tag{269}$$

It is interesting to mention that Eq. 269 presents itself the exact same format as that for the classical Rayleigh wave, with the only divergence in the two dispersion relations coming from the expression for b_2.

7.4. Results and Discussion

In this section the properties of the surface waves are investigated, with particular interest given to the dispersion relation of the waves. The dispersion relation can be normalized by multiplying Eq. 269 by $1/k^4$ and making use of the definition of c, as well as b_1 given by Eq. 254. The following expression for wavespeed c is obtained:

$$\left(2-\frac{c^2}{c_T^2}\right)^2-4\left(1-\frac{c^2}{c_T^2}\right)^{1/2}\left(\frac{b_2}{k}\right)=0 \tag{270}$$

Similarly, Eq. 255 becomes:

$$\frac{E}{1-\nu^2}\left(1-\frac{b_2^2}{k^2}-\frac{c^2}{c_L^2}\right)\left[q\left(a^2\left(\frac{b_2^2}{k^2}-1\right)+\frac{8}{k^2}\right)-i^*c^2\right]+\frac{\lambda^2}{k^2}\left(\frac{b_2^2}{k^2}-1\right)=0 \tag{271}$$

from which b_2 can be obtained.

7.4.1. Wave propagation when $q << 1$

The situation where $q << 1$ corresponds to the case where the effect of the local rotational motion is relatively weak when compared to that of the translational motion. In this case, Eq. 271 becomes:

$$\frac{E}{1-\nu^2}\left(1-\frac{b_2^2}{k^2}-\frac{c^2}{c_L^2}\right)\left(\frac{8q}{k^2}-i^*c^2\right)+\frac{\lambda^2}{k^2}\left(\frac{b_2^2}{k^2}-1\right)=0 \tag{272}$$

which can be rearranged to obtain the following expression:

$$\left(\frac{b_2^2}{k^2}-1\right)=\frac{c^2}{c_L^2}\frac{8q-i^*c^2k^2}{\frac{\lambda^2(1-\nu^2)}{E}-(8q-i^*c^2k^2)}. \tag{273}$$

For $k\to\infty$,

$$\left(\frac{b_2^2}{k^2}-1\right)=-\frac{c^2}{c_L^2} \tag{274}$$

predicting a wavespeed identical to that of the classical Rayleigh wave.
For $k \to 0$,

$$\left(\frac{b_2^2}{k^2} - 1\right) = \frac{c^2}{c_L^2\left(\frac{\lambda^2(1-\nu^2)}{8qE} - 1\right)} \tag{275}$$

indicating a wave corresponding to a different c_L (or different Poisson's ratio). Substituting Eq. 273 into Eq. 272, the following dispersion relation can be obtained:

$$\overline{k}^2 = \frac{c_T^2}{c^2}\left[f + \frac{\left[\left(2 - \frac{c^2}{c_T^2}\right)^4 - 16\left(1 - \frac{c^2}{c_T^2}\right)\right]}{16\left(1 - \frac{c^2}{c_T^2}\right)\left(1 - \frac{c^2}{c_L^2}\right) - \left(2 - \frac{c^2}{c_T^2}\right)^4}\right]. \tag{276}$$

where:

$$\overline{k} = \frac{k}{k_0}, \qquad f = \frac{8qE}{\lambda^2(1-\nu^2)} \tag{277}$$

with

$$k_0 = \frac{\lambda}{c_T}\sqrt{\frac{1-\nu^2}{Ei^*}} \tag{278}$$

It is clearly shown that, even for the case of $q << 1$, surface waves propagating through this novel continuous medium are dispersive.
For the limiting case where $\lambda \to 0$, indicating no rotational effects, Eq. 276 reduces to

$$16\left(1 - \frac{c^2}{c_T^2}\right)\left(1 - \frac{c^2}{c_L^2}\right) - \left(2 - \frac{c^2}{c_T^2}\right)^4 = 0 \tag{279}$$

which, when solved will produce the wavespeed from classical Rayleigh wave propagation, c_R.

7.4.2. Behaviour when $k \to \infty$
When $k \to \infty$, Eq. 271 becomes:

$$\frac{E}{1-\nu^2}\left(1 - \frac{b_2^2}{k^2} - \frac{c^2}{c_L^2}\right)\left(qa^2\left(\frac{b_2^2}{k^2} - 1\right) - i^*c^2\right) = 0. \tag{280}$$

This equation has two solutions, the first solution is:

$$b_2^2 = k^2 - \frac{\omega^2}{c_L^2} \tag{281}$$

which, along with Eqs. 254 and 269, furnish the solution to the classical Rayleigh wave problem. This means one of the two waves that propagates at very large wavenumbers is the classical Rayleigh wave. The second solution is given by:

$$b_2^2 = k^2 + \frac{i^* \omega^2}{qa^2} \tag{282}$$

This is a solution which depends entirely on the local rotational parameters, and does not exist as a solution in classical Rayleigh wave problems. The existence of this second wave is entirely due to the presence of the local rotational elements in the new continuous medium, highlighting a key difference between Rayleigh wave propagation in a classical material, and surface wave propagation in a metamaterial with local rotational effects.

7.4.3. Behaviour when $k \to 0$

When $k \to 0$, Eq. 271 becomes:

$$\frac{E}{1-\nu^2}\left(1 - \frac{b_2^2}{k^2} - \frac{c^2}{c_L^2}\right)\frac{8q}{k^2} + \frac{\lambda^2}{k^2}\left(\frac{b_2^2}{k^2} - 1\right) = 0 \tag{283}$$

which, when rearranged gives the following expression for b_2^2:

$$b_2^2 = k^2 - \frac{\omega^2}{\bar{c}_L^2} \tag{284}$$

where

$$\bar{c}_L^2 = c_L^2\left(1 - \frac{\lambda^2(1-\nu^2)}{8Eq}\right) \tag{285}$$

This is a non-dispersive wave, and takes a very similar format to the classical Rayleigh wave, with the only difference lying in the modified longitudinal wave speed, $\bar{c}_L$. This shows that although surface wave propagation in this representative 2-D metamaterial may follow the same general framework as is observed in traditional materials, the local rotational structure of the continuous field will act to change the physical phenomena.

7.4.4. General Dispersion Curves

To determine the general dispersion curves, Eq. 271 can be rearranged to yield the following explicit dispersion relation:

$$\frac{\omega^2}{\omega_0^2} = -\left(\frac{c^2}{c_T^2}\right)\frac{\left(1-\frac{c^2}{c_L^2}-\frac{b_2^2}{k^2}\right)f+\left(\frac{b_2^2}{k^2}-1\right)}{\left(1-\frac{c^2}{c_L^2}-\frac{b_2^2}{k^2}\right)\left(g\left(\frac{b_2^2}{k^2}-1\right)-\frac{c^2}{c_T^2}\right)} \tag{286}$$

in which b_2/k is obtained by rearranging Eq. 270:

$$\frac{b_2^2}{k^2} = \frac{\left(2-\frac{c^2}{c_T^2}\right)^4}{16\left(1-\frac{c^2}{c_T^2}\right)}, \tag{287}$$

with f given previously in Eq. 277 the rest of the constants given by:

$$\omega_0^2 = \frac{\lambda^2(1-\nu^2)}{Ei^*} \qquad g = \frac{qa^2}{i^* c_T^2} \tag{288}$$

The parameters f and g given by Eqs. 277 and 288 are clearly important in defining the general dispersive nature of this wave. It is important to discuss their physical relevance before analyzing the dispersion relation. The parameter f represents the effect of local rotation on the wave propagation, with higher values of f corresponding to weaker local rotational effects in the material. The parameter g represents the size effect of the unit cell, combined with the rotational effect, with a decrease in the size of the unit cell corresponding to a decrease in g.

The dispersion relation is illustrated in Figs. 43 - 45 for $f = 0.01, 1, 10$, respectively. For lower values of f (0.01 and 1), the phase velocity is limited to values between c_R and c_T. However, for $f = 10$, Fig. 45 shows surface waves with speeds lower than c_R. In all cases two peaks between c_R and c_T are observed, the first one close to c_R and the second close to c_T. It is apparent that the parameter g controls the location of the second peak of the dispersion curve, with higher values of g resulting in a second peak further away from $c/c_T = 1$, and smaller values of g resulting in a second peak closer to the first peak, which is close to the classical Rayleigh wavespeed in the material. This observation is consistent with the result obtained when $k \to \infty$ that shows a second surface wave controlled by the rotation exists, as given in Eq. 282.

Figures 46 - 48 show the dispersion relation for $g = 0.01, 1, 10$, respectively. From these figures it is clear that the value of f controls the existence of surface waves slower than c_R, as well as the behaviour in between the first and second peaks, but does not change the location of the peaks. This again indicates that the location of the second peak is controlled by the parameter g. Similarly, for relatively high values of f, $f = 1.2$ for example, surface waves with speeds lower than c_R exist. In this case the wavespeed is very sensitive to the frequency. From these figures it is apparent that f controls the heights of both the first and second peaks, with a larger f corresponding to a higher peak. In all these figures only wave propagation with $c/c_T < 1$ is considered. There are possible solutions for $c/c_T > 1$, but since b_1 and b_2 will be imaginary, they cease to be surface waves. These waves are not the focus of this paper, and will not be considered here.

7.4.5. Particle Motion

It is well known that in a classical Rayleigh wave the path of particle motion at the free surface is an ellipse. To investigate particle motion at the free surface of this specific continuous medium, consider Eqs. 262 and 263 with $y = 0$:

$$u(x, 0, t) = \left(b_1 \overline{B}_1 + ik\overline{A}_2\right) e^{ik(x-ct)} \tag{289}$$

$$v(x, 0, t) = \left(ik\overline{B}_1 - b_2\overline{A}_2\right) e^{ik(x-ct)} \tag{290}$$

From Eq. 268 we have the following relation between $\overline{A}_2$ and $\overline{B}_1$:

$$\overline{A}_2 = \frac{i\left(b_1^2 + k^2\right)}{2kb_2}\overline{B}_1. \tag{291}$$

Substituting Eq. 291 into Eqs. 289 and 290, the following expressions can be found for the displacements:

$$u(x, 0, t) = \left(b_1 - \frac{b_1^2}{2b_2} - \frac{k^2}{2b_2}\right)\overline{B}_1 e^{ik(x-ct)} \tag{292}$$

$$v(x, 0, t) = \frac{i\omega^2}{2kc_T^2}\overline{B}_1 e^{ik(x-ct)} \tag{293}$$

If $\overline{B}_1 \in \mathbb{R}$, without loss of generality, then the displacements have the following real components:

$$Re(u) = \left(b_1 - \frac{b_1^2}{2b_2} - \frac{k^2}{2b_2}\right)\overline{B}_1 cos(kx - \omega t) \tag{294}$$

$$Re(v) = -\frac{\omega^2}{2kc_T^2}\overline{B}_1 sin(kx - \omega t) \tag{295}$$

which means that the particle motion takes the following form:

$$\left(\frac{Re(u)}{b_1 - \frac{b_1^2}{2b_2} - \frac{k^2}{2b_2}}\right)^2 + \left(\frac{Re(v)}{\frac{\omega^2}{2kc_T^2}}\right)^2 = \overline{B}_1^2 \tag{296}$$

indicating that the path of motion is elliptic.

7.5. Conclusions

- Surface waves propagating through an elastic medium with local rotation are dispersive in nature
- The dispersion relation for surface waves in this material is the same format as for classical Rayleigh waves, differing only by the formula for b_2
- For the case where the effect of local rotation is small compared to that of translational motion, the surface waves are still dispersive
- For the limiting case $k \to \infty$ there are two solutions; one corresponding to the classical Rayleigh wave, and a second wave which depends purely on the local rotational parameters
- The general dispersion curve was found to have two peaks of frequency between c_R, the classical Rayleigh wavespeed, and c_T, the classical shear wavespeed
- Two parameters g and f were found to govern the general dispersion characteristics of the surface waves
- The parameter g controls the location of the second peak in the dispersion curve, with higher values of g corresponding to a peak further away from $c = c_T$
- The parameter f controls the height of each peak
- For values of $f \approx 1$ or greater, surface waves with phase velocities significantly slower than c_R are observed, a phenomena unique to this continuum
- The motion of the particles on the traction free surface is elliptic during surface wave propagation, similar to classical Rayleigh wave propagation

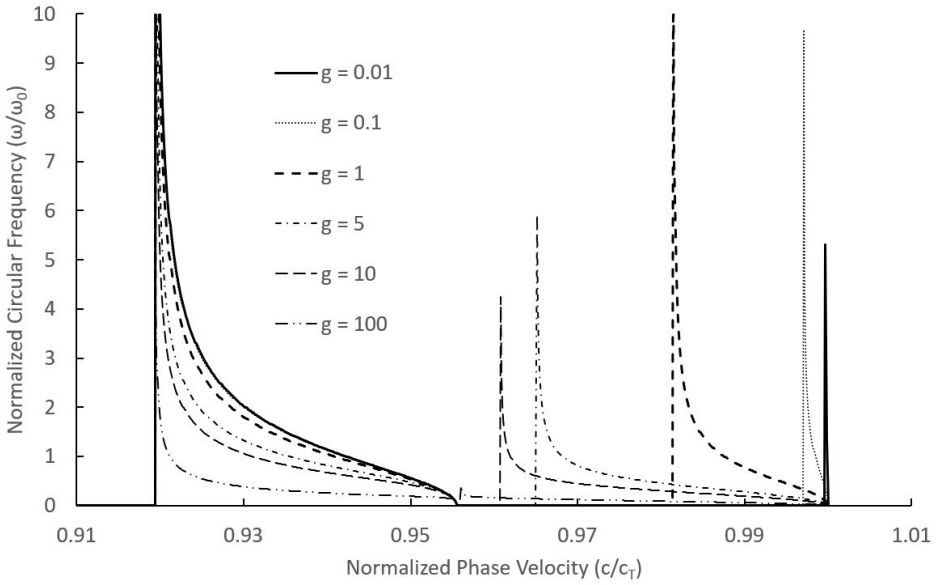

Figure 43: A graphical representation of the general dispersion relation when the parameter g is varied and the parameter f is fixed at a value of 0.01

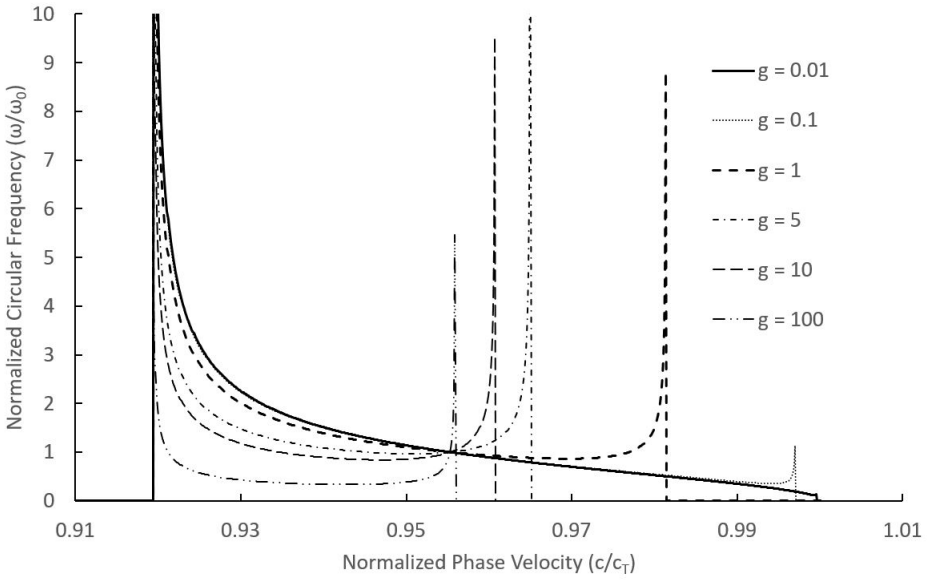

Figure 44: A graphical representation of the general dispersion relation when the parameter g is varied and the parameter f is fixed at a value of 1

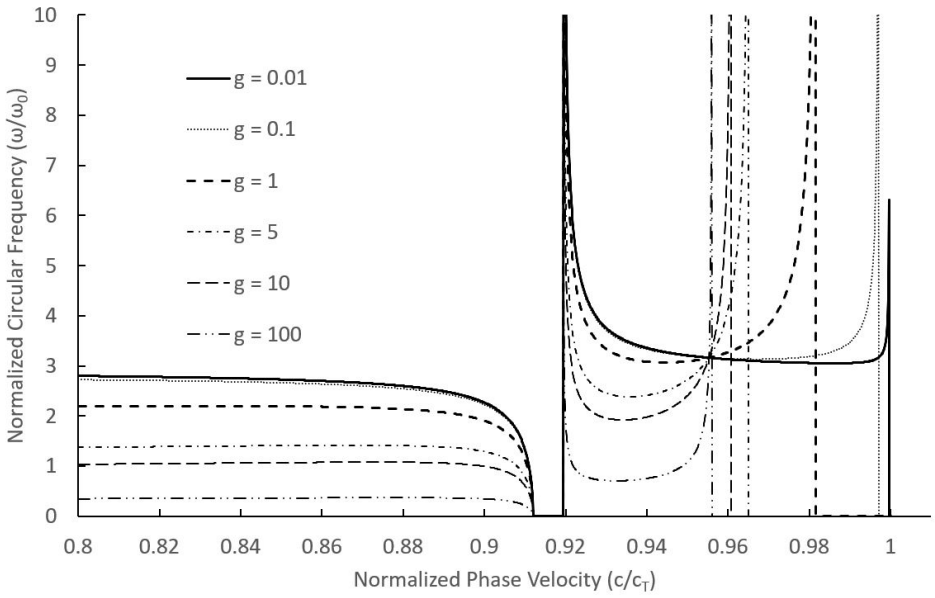

Figure 45: A graphical representation of the general dispersion relation when the parameter g is varied and the parameter f is fixed at a value of 10

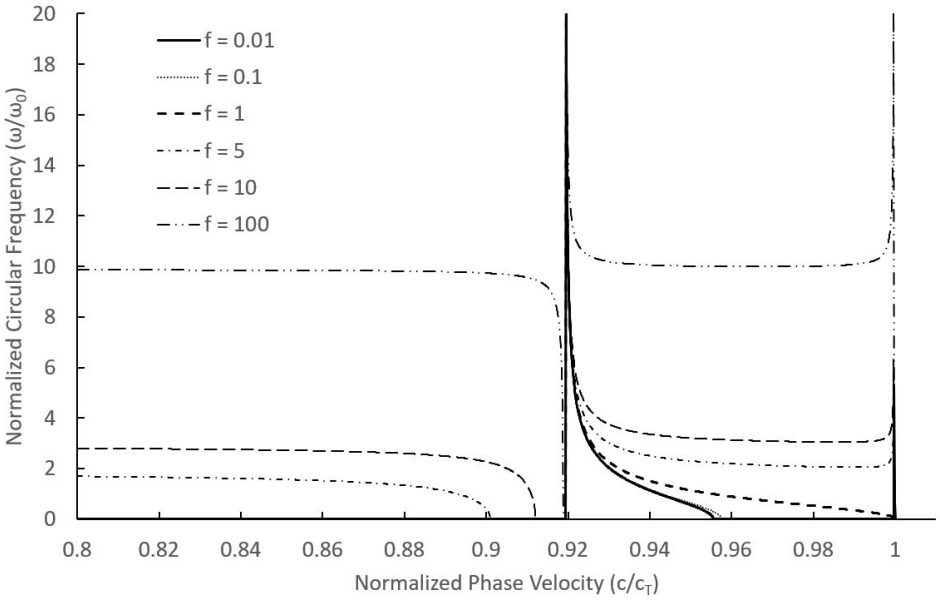

Figure 46: A graphical representation of the general dispersion relation when the parameter f is varied and the parameter g is fixed at a value of 0.01

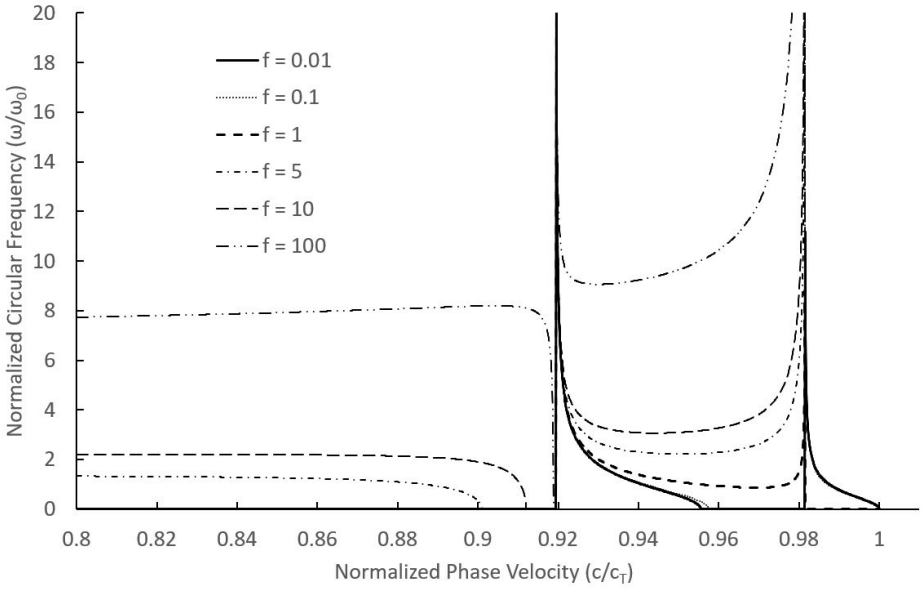

Figure 47: A graphical representation of the general dispersion relation when the parameter f is varied and the parameter g is fixed at a value of 1

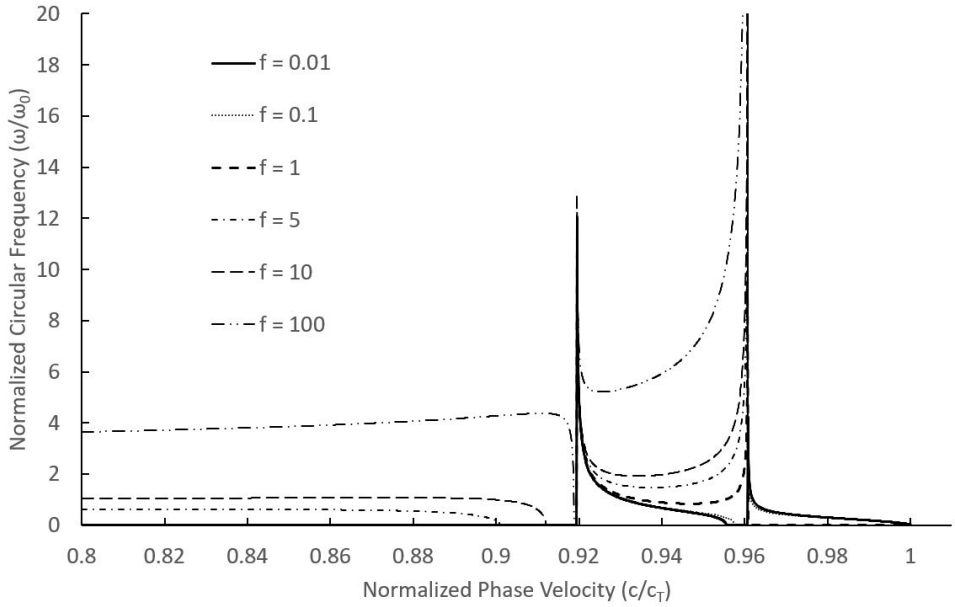

Figure 48: A graphical representation of the general dispersion relation when the parameter f is varied and the parameter g is fixed at a value of 10

8. Conclusions and Future Work

This thesis has focused on the formulation of various different continuum models of a class of elastic metamaterials in both one and two dimensions in a variety of different loading cases. The main findings from each chapter will be summarized in the subsections to follow, after which suggestions and ideas for future work will be presented. As Chapter 1 was an introductory chapter, and Chapter 2 was dedicated to notation and an overview of microcontinuum theories, conclusions will start from the third chapter.

8.1. Summary of Findings

8.1.1. Findings from Chapter 3

Chapter 3 introduced a micropolar-type continuum model of a particular 1-D double negative elastic metamaterial. This was done by first modelling it first as a periodic system of rigid disks and linear Hookean springs, from which a continuum approximation was made using Taylor series expansions. It is important to note here that this model does not include a second order derivative of the local rotational variable θ, hence it is dubbed the "lower order model". Upon comparison with the traditional 1-D micropolar model it was found that the newly developed continuum model had a remarkably similar framework, but with a few extra coupling terms between the local rotational and translational motions. This motivated the classification of this model as a micropolar-type continuum model.

Due to the decreased complexity afforded to this model by the absence of the second order local rotational term, an analytic solution for a transient loading problem involving impact was generated. In this problem an especially important governing parameter $\overline{\lambda} = (ct_0)^2\lambda$ was identified. This governing parameter takes into account the importance of rotational effects, wave speed, as well as impact time and characteristic length. Comparing the numerical solution from the newly developed micropolar-type continuum model to both the actual material response generated from the discrete model, and the response of an equivalent bar model generated using finite element analysis it was determined that for values of $\lambda < 1$, the behaviour predicted by the new micropolar-type model showed very good agreement to those predicted by the equivalent bar model, and those predicted by the discrete model. Additionally, it was determined that for all values of λ the wave speed and pulse length can be accurately determined using the new micropolar-type model. The work presented in this chapter serves as a novel way to model a double

negative elastic metamaterial in order to capture more salient features than would be possible with the traditional micropolar model.

8.1.2. Findings From Chapter 4

Chapter 4 introduced a brand new "higher order" continuum model of a class of elastic metamaterials with local rotational-translational effects. This model was made in a similar fashion to the first, except a representative 1-D metamaterial is modelled rather than one specific double negative metamaterial. After the continuum model is developed for the representative material, it is generalized to the entire class of materials and two new constitutive laws are proposed. A stark difference between this model and the one presented previously is the existence of a higher order derivative of the local rotational variable, θ. At first glance the inclusion of just one more term may seem like a trivial matter, however when applying general transient boundary conditions to this problem, the complexity rears its ugly head. With this in mind, rather than investigating the general transient problem, the harmonic loading problem was investigated instead.

An expression for the dispersion relation of the same particular 1-D metamaterial investigated previously subject to harmonic wave propagation was obtained, and the stop and passing bands were determined. Comparisons were made between the new continuum model and the lower order continuum model presented in the third chapter, as well the discrete model. It was further determined that wave propagation was controlled by just one dimensionless governing parameter, ζ/R. This parameter was varied, and it was found that the location of the stop and passing bands could be changed simply by varying this one parameter.

It was determined retroactively that the new continuum model was capable of predicting the same critical frequency p_2 and the same stop bands as the discrete model, highlighting the usefulness of this model. It was also observed that the new continuum model captured the wave propagation for frequency ranges $p > p_2$ when the governing parameter $\zeta/R < 1$, which was not possible using the model presented in the third chapter, reinforcing the importance of the higher order θ derivative. The work in this chapter provides a more general novel continuum model for a class of one-dimensional elastic metamaterials which possess strong local rotational-translational coupling. This will prove to be a valuable tool for those looking to predict the behaviour of these materials, as this new model captures more salient features than the traditional micropolar model.

8.1.3. Findings From Chapter 5

Chapter 5 introduced a two-dimensional extension of the continuum model presented in Chapter 4 suitable for modelling an analogous two-dimensional class of elastic metamaterials with strong local rotational-translational coupling. This model was derived in a different fashion than the previous two; first a set of constitutive laws was proposed, and then a representative discrete structure from the general class of two-dimensional metamaterials of interest was analyzed to determine the model's suitability.

Expressions for the usual elastic constants, as well as new material constants related to the local rotational-translational coupling were obtained in terms of both material and geometric parameters. General two-dimensional harmonic wave propagation through a representative elastic metamaterial was then studied by evaluating the dispersion relations associated with both longitudinal and transverse harmonic waves. Two parameters, η^0 and ζ^0 were identified as the parameters governing wave propagation. The parameter η^0 represents the rotational effects which derive purely from material structure, whereas ζ^0 is an indicator of the relative strength of the local rotational effects in comparison to that of the translational effects, and is controlled primarily by material modulii rather than geometric parameters. A key point to note is that the dispersion curves with the most unique phenomena occurred when local rotational and translational effects were both at moderate levels, reinforcing the necessity of capturing the local rotational effects in these materials. This chapter presents a novel two-dimensional continuum model with local rotational effects. This model captures salient features of these materials that the traditional micropolar model in two dimensions cannot, and will prove extremely useful to researchers attempting to incorporate surfaces of elastic metamaterial onto their structures for applications such as wave guiding.

8.1.4. Findings From Chapter 6

Chapter 6 utilized the new two-dimensional model developed in Chapter 5 to study surface wave propagation in a continuous medium with local rotation. Expressions for the decay parameters b_1 and b_2 were obtained, as well as an expression for the dispersion relation.

Some simplified cases were analyzed with special attention being given to the dispersion relation in each case. It was found that even for the case where the effect of local rotational motion is very small compared the effect of translational motion, the surface waves are dispersive. It was also found

that for very large values of the wavenumber there are two waves that propagate; the first is the classical Rayleigh wave, and the second is a new wave with wavespeed governed entirely by the local rotational parameters.
The general dispersion relation was also analyzed, and two governing parameters, f and g were determined. The dispersion curve possesses two frequency peaks between c_R, the classical Rayleigh wavespeed, and c_T, the shear wavespeed. The parameter f control the height of each of these frequency peaks, with higher values of f resulting in higher peaks. Additionally, for values of $f \approx 1$ and greater, surface waves with phase velocities significantly slower than c_R were observed, a phenomenon unique to this continuum. The parameter g controls the location of the second peak, with higher g values corresponding to a peak further from $c = c_T$.
Finally, the motion of the particles residing on the surface of the continuum was determined to be elliptic, similar to classical Rayleigh wave propagation. This chapter clearly demonstrates the effect of local rotation on the properties of surface wave propagation, emphasizing the need to model such effects properly.

8.2. Future Work

This thesis has pioneered the use of continuum models in modelling elastic metamaterials with strong local rotational effects in one and two dimensions, in both transient and harmonic loading cases. Since these models are the first of their kind, there are plenty of areas for future work, in fact, some of these areas I am currently working on developing myself. The following are some, but certainly not all of the most promising ideas for future work:

- Modelling of Three-Dimensional Materials

Since one and two-dimensional continuum models incorporating local rotational effects have been developed in this thesis, a natural next step would be to create a three-dimensional analogue. This however, presents its own challenges, as in three dimensions there are many different structures which can exist; much more than in one or two dimensions. There are countless ways to stack two-dimensional layers of elastic metamaterial on top of each other to create unique three-dimensional structures, each would need a model of its own. A starting point for three-dimensional modelling would be a structure with a cubic unit cell. The relatively simple geometry of this three-dimensional structure would serve as a good "first step" into full three-dimensional modelling as the relative simplicity of the geometry would

be reflected in the governing equations, making the model development less algebraically taxing.

- **More Complicated Geometries**

In thesis infinite and semi-infinite materials have been considered exclusively. These are very mathematically idealized ideas which do not typically exist naturally unless the phenomena of interest is much smaller than the size of the structure being analyzed. It would be useful to be able to model these metamaterials in more realistic geometries with finite boundaries, or even non-euclidean geometries for applications such as helmets or coatings on aerodynamic surfaces with non-trivial curvatures. For this reason, the unification of shell theory with the existing mathematical models would be incredibly useful. This would involve leaving the realm of Cartesian coordinates, and instead using a system of convected coordinates to describe the position of material points within the elastic metamaterial. In addition to this, chiral geometries may interesting to model as well, as many elastic metamaterials possess chiral characteristics.

- **Transient Problems**

In this thesis, apart from the third chapter, only harmonic loading has been considered. This is because it is much more convenient to find an analytical solution for the harmonic problem than the transient problem. The transient problem could be approached by doing a Fourier transform on the governing equations, as well as the boundary conditions and attempting to solve the resulting problem in the frequency domain. After this the transform must be inverted, either analytically or numerically, in order to produce a displacement profile. This is an important extension, as it can allow for the study of transient phenomenon in metamaterials such as shockwave propagation.

- **Modelling of an Interfacial Crack in an Elastic Metamaterial**

The model developed in Chapter 5 can model any two-dimensional elastic metamaterial with local rotational effects belonging to the pertinent class of materials, in a variety of different loading cases. The only loading case that was explicitly explored in Chapter 5 was general harmonic wave propagation. An especially relevant scenario which lends itself to two-dimensional analysis is that of crack propagation along an interface. If one were to employ a thin layer of elastic metamaterial to create a so-called "metasurface" for an application such as wave attenuation, an important scenario to understand would be that of an interfacial crack. This is a situation which could easily happen in many practical applications, and hence is important to look in to so

that the material behaviour of a damaged structure is known. A good place to start with this analysis would be applying the classical crack boundary conditions to the governing equations presented in Chapter 5, and working through to find an analytical solution.

- **Consideration of Thermal Effects**

The particular group of elastic metamaterials investigated in this thesis has great promise for application in the field of vibration mitigation, as well as precise vibration elimination. Many situations which require such vibration control would involve machines operating significantly above room temperature. For this reason, it is important to find some way to include thermal effects in the existing mathematical model to aid in the uptake of these elastic metamaterials in such applications.

9. Bibliography

References

[1] Silin, R. A., 2012, "On the History of Backward Electromagnetic Waves in Metamaterials", Metamaterials, **6**(1-2), pp. 1-7

[2] Moghbeli, E. et al., "The Effect of Geometric Parameters of a Single-Gap SRR Metamaterials on Its Electromagnetic Properties As a Unit Cell of Interior Invisibility Cloak in the Microwave Regime". Optic. Laser Technol., **108**, pp. 626-633

[3] Zhao, G. et al., 2019, "A Zero Refraction Metamaterial and Its Application in Electromagnetic Stealth Cloak", Mater. Today Commun. **21**, p. 100603

[4] Chen, Z. et al., 2016, "3D Printing of Piezoelectric Element for Energy Focusing and Ultrasonic Sensing"., Nano Energy, **27**, pp. 78-86

[5] Pan, C. T. et al., 2014, "Ultrasonic Sensing Device with ZNO Piezoelectric Nanorods by Selectively Electrospraying Method", Sens. Actuators. A. **216**. pp. 318-327

[6] Li, D. et al., 2020, "A Novel 3D Re-Entrant Unit Cell Structure With Negative Poisson's Ratio and Tunable Stiffness", Smart Mater. Struct., **29**(4), p. 045015

[7] Ren, C. et al.,2020, "Mechanical Performance of Multidirectional Buckling-Based Negative Stiffness Metamaterials: An Analytical and Numerical Study", Materials, **11**(7), p.1078

[8] Zhakatayev, A. et al., 2020, "Analytical Modelling and Design of Negative Stiffness Honeycombs", Smart Mater. Struct. **29**(4) p. 045024

[9] Tan, X. et al., 2019, "Novel Multidirectional Negative Stiffness Mechanical Metamaterials", Smart Mater. Struct., **29**(1), p. 015039

[10] Jaberzadeh, M. et al., 2019, "Wave Propagation in an Elastic Metamaterial With Anisotropic Effective Mass Density", Wave Motion, **89**, pp. 131-141

[11] Shaat, M. and El Dhaba, A. R., 2019, "On the Equivalent Shear Modulus of Composite Metamaterials", Compos. Part B: Engin., **172**, pp. 506-515

[12] Wang. W. et al., 2020, "Elastic Stubbed Metamaterial Plate With Torsional Resonances", Ultrasonics, **106**, p. 106142

[13] Dudek, K. et al., 2020, "3D Composite Metamaterial With Magnetic Inclusions Exhibiting Negative Stiffness and Auxetic Behaviour", Mater. Des. **187** p. 108403

[14] Li, Z. and Wang, X.D., 2018, "On the Dynamic Behaviour of a Two-Dimensional Elastic Metamaterial System", Int. J. Solids. Struct., **78-79**, pp. 174-181

[15] Li, Z. et al., 2018, "A New Two-dimensional Elastic Metamaterial System With Multiple Local Resonances", Inter. J. Mech. Sci., **149**, pp. 273-284

[16] Li, Z. et al., 2019, "Modelling of Elastic Metamaterials With Negative Mass and Modulus Based on Translational Resonance", Int. J. Solids. Struct., **162**, pp. 271-284

[17] Oyelade, A.O., et al., 2019, "On the Dynamic Properties of Metamaterials in Civil Engineering Structures", IOP Conf. Ser.: Mater. Sci. Eng., **640**, p. 012045

[18] Wu, I. and Li, Y.M., 2020, "A Locally Resonant Elastic Metamaterial Based on Coupled Vibration of Internal Liquid and Coating Layer", J. Sound. Vib., **468** p. 115102

[19] Xu, X. et al., 2019, "A Nonlinear Dissipative Elastic Metamaterial for Broadband Wave Mitigation", Int. J. Mech. Sci., **164**, p. 105159

[20] Wu, L. et al., 2020, "Mechanical Metamaterials for Full-Band Mechanical Wave Shielding", Appl. Mater. Today, **20**, p. 100671

[21] Li, Z. et al., 2020, "Dual-Functional Metamaterial With Vibration Isolation and Heat Flux Guiding", F. Sound. Vib., **469**, p. 115122

[22] Zhong, R. et al., 2019, "A Novel Three-Dimensional Mechanical Metamaterial With Torsional Resonances", Compos. Struct., **226**, p. 111232

[23] Chen, X. et al., 2020, "Light-Weight Shell-Lattice Metamaterials for Mechanical Shock Absorption" Int. J. Mech. Sci. **169**, p. 105288

[24] Tan, X. et al., 2019, "Novel Multi-S Mechanical Metamaterials for Trapping Energy Through Shear Deformation", Int. J. Mech. Sci., **164**, p. 105168

[25] Hu, J. et al., 2019,"Low-Speed Impact Mitigation of Recoverable DNA-Inspired Double Helical Metamaterials", Int. J. Mech. Sci., **161-162**, p. 105050

[26] Kumar, S. et al., 2020, "Ventilated Acoustic Metamaterial Window Panels for Simultaneous Noise Shielding and Air Circulation". Appl. Acoust., **159**, p. 107088

[27] Wang, X. et al., 2018, "Acoustic Perfect Absorption and Broadband Insulation Achieved by Double-Zero Metamaterials", Appl. Phys. Lett., **112**(2), p. 021901

[28] Liao, Y. et al.,2018, "Adaptive Metamaterials for Broadband Sound Absorption At Low Frequencies", Smart Mater. Struct., **28**(2), p. 025005

[29] Yang, H. et al., 2009, "Asymptotic Homogenization of Composite Materials and Structures", ASME Appl. Mech. Rev., **62**(3), p. 030802

[30] Pernas-Salomón, R. and Shmuel, G., 2020, "Symmetry breaking creates electro-momentum coupling in piezoelectric metamaterials", J. Mech. Phys. Solids, Vol. 134, p. 103770.

[31] Yang, H. et al., 2019, "Determination of metamaterial parameters by means of a homogenization approach based on asymptotic analysis", Continuum Mech. Thermodyn., Vol. 32, pp. 1251–1270.

[32] Robert W. Soutas-Little, "History of Continuum Mechanics", Encyclopedia of Life Support Systems (EOLSS)

[33] Eugster, S.R. et al., 2019, "Continuum Theory For Mechanical Metamaterials With A Cubic Lattice Substructure", Mathematics and Mechanics of Complex Systems, Vol. 7, pp. 75-98

[34] Porubov, A.V., Grekova E.F., 2020, "On nonlinear modeling of an acoustic metamaterial", Mech. Res. Commun., Vol. 103, p. 103464.

[35] Chen, Y. et al., 2020, "Mapping acoustical activity in 3D chiral mechanical metamaterials onto micropolar continuum elasticity", J. Mech. Phys. Solids, Vol. 137, p. 103877

[36] Schiavone, A. et al., 2021, "Modeling and Analysis of the Transient Behaviour of an Elastic Metamaterial as a Generalized Cosserat Continuum", ASME J. Appl. Mech., Vol. 88, Issue 9, p. 091003

[37] Schiavone, A. and Wang, X.D., 2021, "Continuous Modelling of a Class of Periodic Elastic Metamaterials with Local Rotation", Z. Angew. Math. Phys., Volume 73, Issue 29

[38] P. Chadwick, *Continuum Mechanics Concise Theory and Problems*, Dover Publications, 1999

[39] A. Cemal Eringen, *Microcontinuum Field Theories I: Foundations and Solids*, Springer, 1999

[40] Hasanpour, S. and Heppler, G. R., 2017, "Micropolar elasticity theory: a survey of linear isotropic equations, representative notations, and experimental investigations", Math. Mech. Solids, Volume 22, Issue 2, pp. 224-242